Master's thesis

NTNU
Norwegian University of Science and Technology
Faculty of Information Technology and Electrical Engineering
Department of Engineering Cybernetics

Martha Halvorsen

Robust Estimation of Blood Glucose Level Based on Subcutaneous Sensors and Analysis of Blood Samples

Master's thesis in Cybernetics and Robotics
Supervisor: Professor Anders Lyngvi Fougner
Co-supervisor: PhD candidate Karim Davari Benam, PhD candidate Hasti Khoshamadi

June 2022

NTNU
Norwegian University of Science and Technology

Martha Halvorsen

Robust Estimation of Blood Glucose Level Based on Subcutaneous Sensors and Analysis of Blood Samples

Master's thesis in Cybernetics and Robotics
Supervisor: Professor Anders Lyngvi Fougner
Co-supervisor: PhD candidate Karim Davari Benam, PhD candidate Hasti Khoshamadi
June 2022

Norwegian University of Science and Technology
Faculty of Information Technology and Electrical Engineering
Department of Engineering Cybernetics

NTNU
Norwegian University of
Science and Technology

Preface

This master's thesis is submitted as a part of the requirements for the master degree at the Department of Engineering Cybernetics at the Norwegian University of Science and Technology (NTNU). The work presented in this thesis has been carried out under the supervision of Prof. Anders Lyngvi Fougner, PhD candidate Karim Davari Benam and PhD candidate Hasti Khoshamadi at the Department of Engineering Cybernetics, NTNU, and is written in collaboration with the cross-disciplinary research group Artificial Pancreas Trondheim (APT), NTNU.

This master's thesis is a continuation of a specialization project I conducted during the autumn of 2021, see [1], referred to as the *term project*. As is customary, the specialization project is not published. This means that important background theory from the project report will be restated in full throughout this thesis to provide the best reading experience. A pending approval conference paper, based on the term project, was written during the development of this thesis, hence some sections from this paper will also be restated. The paper can be found in Appendix D. Below, a complete list of the material included from the term project and the conference paper, is listed.

- Term project: Section 1.7, Section 2.1.2, specifically the part about BGA, Section 2.2.1 with some changes, Section 2.2.6, Section 2.3.1 and Section 2.3.2, both with some changes, and Section 2.4.4.
- Conference paper: Chapter 4.

During the project, I have been provided multiple tools by my supervisors. Data sets used for code simulations, are based on previous animal experiments, performed by APT and the animal faculty of NTNU. Theory related to system identification, Matlab code for retrieving information from the data sets, as well as additional information regarding the data sets and experiments were kindly given to me by PhD candidate Karim Davari Benam and PhD candidate Hasti Khoshamadi at the Department of Engineering Cybernetics, NTNU.

During the master´s project I have developed methods for estimating blood glucose level based on subcutaneous glucose level measurements, obtained by a continuous glucose monitoring sensor, using provided data sets and Matlab code. This includes modeling of the pharmacodynamics between blood plasma and subcutaneous tissue, modeling of the blood glucose dynamics, choice of estimation method, and additional estimate enchantment method for achieving more robust blood glucose estimates.

Unless otherwise stated with references in figure captions, all figures and illustrations have been created by the author.

I am profoundly grateful to my supervisor Prof. Anders Lungvi Fougner, as well as my co-supervisors PhD candidate Karim Davari Benam and PhD candidate Hasti Khoshamadi for valuable guidance, and much appreciated support. I thank you for your expertise and feedback, as well as words of encouragement. You have introduced me to an incredibly interesting topic of research.

I also want to thank the professors who have educated me throughout these five years at NTNU, as well as other staff at the Department of Engineering Cybernetics. Thank you for creating an inspiring work environment, and for investing time in educating me.

Lastly, I want to thank my family, for always believing in me and for the unconditional support. A special thanks also goes out to my friends and classmates for making these five years so special. The memories we share will always stay very dear to me.

Martha Halvorsen

Trondheim, June 2022

Abstract

Diabetes mellitus is a metabolic disorder, or disease, that affects millions of people around the globe. The disease is divided into three main types: type 1, type 2 and gestational, and is characterized by insufficient, or defect insulin secretion, insulin action, or both, resulting in chronic hyperglycemia. In order to manage the disease, patients need tight blood glucose control, achieved by sensing blood glucose levels, and exogenous insulin injections. The currently most common form of measuring glucose level for people with type 1 diabetes is continuous glucose monitoring systems, which measures the glucose level in the interstitial fluid, in the subcutaneous tissue in the body.

Interstitial fluid glucose is known to have different dynamics from blood glucose, hence measuring glucose in subcutaneous tissue does cause some inconveniences, most notably a time lag between interstitial fluid glucose and corresponding blood glucose level. In addition CGM sensors are not perfect, being exposed to several sensor errors and disturbances. Such issues in combination with slow dynamics between blood and interstitial fluid compartments reduces quality of blood glucose control when utilizing CGM systems, which may result in avoidable hyper- and hypoglycemic events. One way to combat these issues, is through blood glucose level estimation.

In this work four filters, and three models have been tested, in order to achieve blood glucose estimates, using CGM sensor readings only: Finite difference approximation of a rearranged Steil-Rebrin model of the interstitial fluid glucose dynamics, robust two stage Kalman filter with unknown inputs using the Steil-Rebrin model with blood glucose level as the unknown input, a standard Kalman filter using an inputless rate-only model in combination with the Steil-Rebrin model, and a M-robust Kalman filter, using the same model as the standard Kalman filter. Their respective estimates are observed and inspected, and their performance evaluated. Enhancement methods, such as moving average smoothing, weighted least squares linear regression, and low pass filtering of measurements, are implemented to enhance the estimates ability to tackle sudden changes in CGM measurements, not part of the glucose dynamics, and ensure estimate robustness. Performance is measured by statistical accuracy scores mean squared error and mean absolute percentage error, as well as observing estimate standard deviation, where it relevant. The designed structures are evaluated on data conducted from four animal experiments performed on pigs. The data sets consist of CGM measurements, transmitted every 1.2 sec, and sporadic blood glucose measurement obtained by a blood gas analyzer.

Results indicate that finite difference filter, as well as robust two stage Kalman filter with unknown inputs, are insufficient in estimating blood glucose level based on CGM measurement only. Kalman filter and M-robust Kalman filte results show sufficient compensation of slow blood to interstitial fluid dynamics, and manages to accurately estimate blood glucose level, which is evident when both considering mean squared error, mean absolute percentage error, and estimate standard deviation. Estimate robustness is further improved when utilizing the proposed enhancement methods, which

is reflected in statistical scores, as well as figures.

Successfully compensating of time lag between blood and interstitial fluid glucose levels will ensure tighter blood glucose control, and promising results for achieving this are presented. Further research is, however, still needed, seen as both Kalman filter and M-robust Kalman filter suffers from overestimation of glucose peaks, and overreacts to sudden changes, not part of the actual blood glucose dynamics, in the CGM measurements, which will lead to incorrect decision making in a control algorithms, or by users themselves.

Sammendrag

Diabetes mellitus er en sykdom, som påvirker millioner av mennesker rundt om i verden. Sykdommen er delt inn i tre hovedtyper: type 1, type 2 og svangerskaps diabetes, og er karakterisert ved utilstrekkelig eller defekt insulinsekresjon, insulinvirkning, eller begge deler, som resulterer i kronisk hyperglykemi. For å håndtere sykdommen trengs tett blodsukkerkontroll, oppnådd ved måling av blodsukkernivåer og eksogene insulininjeksjoner. Den vanligste formen for måling av glukosenivå for personer med type 1 diabetes er kontinuerlige glukoseovervåkingssystemer, som måler glukosenivået i interstitialvæsken, i underhudsvevet i kroppen.

Interstitiell væskeglukose er kjent for å ha forskjellig dynamikk fra blodsukker, og måling av glukose i subkutant vev inkluderer dermed noen problemer, blant annet en tidsforsinkelse mellom interstitiell væskeglukose og tilsvarende blodsukkernivå. I tillegg lider CGM-sensorer av flere typer sensor feil og forstyrrelse. Slike problemer i kombinasjon med langsom dynamikk mellom blod- og interstitielle væskerom reduserer kvaliteten på blodsukkerkontrollen ved bruk av CGM-systemer, noe som kan føre til unngåelige hyper- og hypoglykemiske hendelser. En måte å bekjempe disse problemene på, er gjennom estimering av blodsukkernivå.

I dette arbeidet har fire filtre og tre modeller blitt testet, for å oppnå et blodsukkerestimat, ved bruk av kun CGM-sensoravlesninger: Finitt forskjellstilnærming av en omorganisert Steil-Rebrin-modell av interstitiell væskeglukosedynamikk, robust totrinns Kalman-filter med ukjente pådrag som bruker Steil-Rebrin-modellen med blodsukkernivå som ukjent pådrag, et standard Kalman-filter som bruker en pådragsfri hastighetsmodell i kombinasjon med Steil-Rebrin-modellen, og et M-robust Kalman-filter, som bruker samme modell som standard Kalman-filteret. Deres respektive estimat har blitt observert og inspisert, og deres ytelse evaluert. Forbedringsmetoder, som glidende gjennomsnittlig utjevning, vektet minste kvadraters lineær regresjon og lavpassfiltrering av målinger, er implementert for å forbedre estimatens evne til å takle plutselige endringer i CGM-målinger, som ikke utgjør en del av glukosedynamikken, samt for å sikre estimat robusthet. Ytelsen måles ved hjelp av statistiske nøyaktighetsskårer som gjennomsnitt kvadratisk feil og gjennomsnittlig absolutt prosentvis feil, samt observasjon av estimat standardavvik, der det er relevant. De utformede strukturene er evaluert basert på data fra fire dyreforsøk utført på griser. Datasettene består av CGM-målinger, overført hver 1.2 sek, og sporadisk blodsukkermåling målt av en blodgassanalysator.

Resultatene indikerer at finitt forskjellsfilter samt robust totrinns Kalman-filter med ukjente pådrag er utilstrekkelige til å estimere blodsukkernivået, basert kun på CGM-måling. Kalman-filter og M-robuste Kalman-filterresultater viser tilstrekkelig kompensasjon av langsom blod- til interstitiell væskedynamikk, og klarer å estimere blodsukkernivået nøyaktig, noe som er tydelig når man både vurderer gjennomsnittlig kvadratfeil og gjennomsnittlig prosentvis feil, og estimatenes standardavvik. Estimatets robusthet forbedres ytterligere ved å bruke forbedringsmetoder, noe som gjenspeiles i statistiske skårer, så vel som i figurer.

Vellykket kompensasjon for tidsforskyvning mellom blod- og interstitiell væskeglukosenivå vil sikre tett blodsukkerkontroll, og lovende resultater for å oppnå dette, presenteres. Ytterligere forskning er imidlertid fortsatt nødvendig, grunnet at både Kalman-filter og M-robust Kalman-filter lider av overestimering av glukosetopper, og viser egenskaper som ekstreme reaksjoner på plutselige endringer i CGM-målinger, noe som vil føre til feil beslutningstaking i en kontrollalgoritme , eller av brukerne selv.

Nomenclature

Abbreviations

AP - Artificial Pancreas

APT - Artificial Pancreas Trondheim

BG - Blood Glucose

BGA - Blood Gas Analyzer

BMI - Body Mass Index

CGM - Continuous Glucose Monitoring

EBD - Euler Backward Differentiation

FD - Finite Difference

ISF - Interstitial Fluid

KF - Kalman Filter

LPF - Low Pass Filter

LR - Linear Regression

MA - Moving Average

MAE - Mean Absolute Error

MAPE - Mean Absolute Percentage Error

MSE - Mean Squared Error

NTNU - Norwegian University of Science and Technology

OTSKF - Optimal Two-Stage Kalman Filter

PISA - Pressure Induced Sensor Attenuation

RSS - Residual Sum of Squares

RTSKF-UI - Robust Two Stage Kalman Filter with Unknown Inputs

SD - Standard Deviation

SMBG - Self Monitoring of Blood Glucose

T1D - Type 1 Diabetes

T2D - Type 2 Diabetes

WLS LR - Weighted Least Squares Linear Regression

WRSS - Weighted Residuals Sum of Squares

Medical Terms

Blood Plasma - Fluid containing blood-cells, consisting of water, plasma protein, amino acid, hormones and metabolites [2].

Interstitial fluid - Fluid found in the space around cells in multi-celled organisms, such as humans, consisting of water and nutrition from the bodies capillaries [3].

Subcuntanous tissue - Deepest layer of the skin, made up of cells and connective tissue [4].

Contents

*

Figures

Tables

Chapter 1

Introduction

1.1 Background and motivation

Diabetes mellitus is a metabolic disorder, which currently affects 387 million people worldwide, and this number is predicted to increase with 205 million people by 2035 [5]. In the USA diabetes is the seventh leading cause of death.

For centuries the only available treatment for diabetes was starvation [6]. The cause of the illness was not discovered until in the early twentieth century, when it was suggested that the illness was in fact a disorder resulting from lack of the hormone insulin. In 1920, this theory was confirmed when insulin was successfully extracted from a dog, and the regulatory role of the hormone was registered [5]. The team that discovered insulin and it's regulatory role was awarded a Nobel Prize in 1923 [6].

Their discovery paved the way for advancements in diabetic treatments, and devices for injecting exogenous insulin was soon after developed. However, in order to achieve tight blood glucose (BG) control, dosage of exogenous insulin has to correspond to actual BG level. Hence, methods for measuring BG level also received popularity among researches, due to the consensus of it being an essential part of maintaining homeostasis of the insulin-glucose regulatory loop, in the body.

In early experiments, blood glucose was continuously measured using invasive methods [6]. Invasive methods are not fitted for usage over a long period of time, inflicting both pain and discomfort to the patient, hence, manual blood glucose level control using intermittent sampling was researched, and eventually developed. This method is commonly known as self-monitoring of blood glucose (SMBG), and involves pricking the finger, extracting capillary blood, and place it on a glucose meter, which determines the glucose level. Since the 1980 self-monitoring of BG has been the dominating method for achieving BG control [7].

Due to the manual requirement of the measurement process of using SMBG, the measuring system is prone to user specific errors, which ultimately affects the measurement accuracy. Accuracy may also be affected by sparse sensor readings, seen as the sample rate of sensor readings are dependent on the number of finger-prick blood samples the user is willing to perform [8]. Spares SMBG readings provide only current snapshots of BG levels, hence information about fluctuations and trends are lacking.

In 1999 a minimally invasive method for glucose monitoring was approved by the Food and Drug Administration in the US [9], namely the continuous glucose monitoring (CGM) system. CGM systems measure glucose levels in interstitial fluid (ISF) in the subcutaneous adipose tissue, and not directly from the blood [10]. A small measuring needle size, as well as the measuring technique also allows for the sensor to stay in place over long periods of time, without causing much discomfort to users. This ability allows for continuous glucose monitoring, and characterises the CGM system as a minimal-invasive measuring technique, which have revolutionized the daily management of diabetes.

The most notable benefit of using CGM is the possibility of achieving a time-series of glucose data, which gives information about trends, patterns and fluctuations of the ISF glucose level [10]. This is achieved by the sensor through small sampling time, resulting in rapid sensor readings, varying of about 1 min to 5 min [9]. This provides users with valuable information, which can help in making decisions, both about exogenous insulin dosages and food intake. With this improved amount of glucose information, threshold detectors are also given attention, allowing for early detection of possible hypo- and hyperglycemic events, which will give users better time for taking action.

Although CGM sensors are the preferred glucose monitoring method among relevant users, the technique has it's limitations. The technique is based on the assumption that a correlation exists between the subcutaneous glucose level and the BG level, which is only valid to an extent [6]. Although the dynamics between the BG level and subcutaneous glucose level are similar, there are some dynamical differences which, if not addressed, could lead to sub-optimal glucose control. Sub-optimal control can lead to false interpretation of the current glucose level, as well as false alarms for hypo- and hyperglycemia, which may be both frustrating and upsetting for the users [8].

1.2 Artificial pancreas

Artificial pancreas (AP) is a type of system which aims to automate insulin delivery in people with diabetes. An AP system achieves this by automating insulin pump operations through the use of a closed loop controller, that is provided information about the glucose level in the body by glucose monitoring sensors [5]. The sensors, and their transmitters, computes the optimal amount of insulin needed to be infused, based on the current measurement, or the most recent measurement window, and manipulates the infusion rate of the insulin pump.[5]. A diagram showcasing the loop-structure of an AP system is displayed in Figure 1.1.

Such a system requires, ideally, no action from the user, which would greatly improve the lives of people with diabetes mellitus. Many current AP systems are, however, not fully automated, yet, hence the challenge of safe technologies for measuring BG level and insulin delivery are not solved [5].

Current AP systems are developed for usage of CGM measurements only [5]. A delay in glucose level sensing is introduced by the diffusion process from the blood compartment to the subcutaneous tissue compartment, when CGM measurements are used. This could lead to sub-optimal control of the insulin pump, seen as action might not be initiated fast enough during rapid glucose changing events, such as exercise induced hypoglycemia [5]. Sudden changes in the CGM measurements, due to sensor error, may also cause AP systems to overdoes insulin [5], which could cause harm to the user.

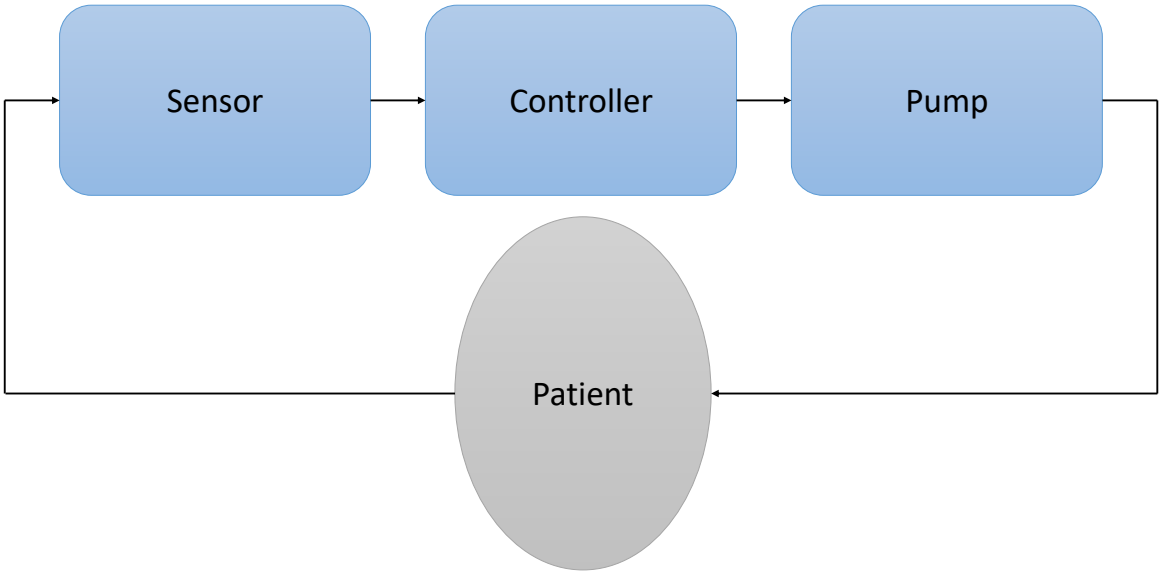

Figure 1.1: AP system loop.

1.3 Thesis Objectives

The main goal of this thesis is to develop a method that can use subcutaneous glucose measurement, obtained by a CGM sensor, and estimate BG levels, without the need of calibration using BG samples, in real time. Such an aim includes modelling of the sensor dynamics and the pharmacodynamics between blood plasma and subcutaneous tissue, as well as BG dynamics, and utilize the resulting model, or models, in estimation algorithms. Estimation algorithm performances are evaluated through standard accuracy assessment scores, as well as estimate standard deviation evaluations, with added emphasizes on estimate robustness.

1.4 Related Work

Several attempts of estimating BG level, based on ISF glucose level measurements exists in the literature. [11] presents BG level reconstruction trough deconvolution, while in [12] the same is attempted trough finite difference approximation. KFs have also gained popularity among researchers in topic of BG level estimation. In [12] a step- and ramp-disturbance model are used by a KF in BG level estimation, while [13] uses a dual-rate KF in estimating BG level, as well as sensor gain, using BG level measurements for re-calibrating the filter. Offline estimation of BG level is done in [14], where a smoothing KF is used, utilizing both SMBG and CGM measurements, while real-time estimation of BG level using an extended KF is done in [15]. These examples cover only a small area of the research related to BG level estimation in the field of diabetes research, indicating that the issue is very much relevant, and improvements are continuously made.

1.5 Contributions

This thesis contributes to the field of diabetes research by investigation of further improvements of CGM sensor accuracy, through elimination of time lag between BG level and ISF glucose level measurements, as well as dynamical differences, by modeling the pharmacodynamics between BG and ISF glucose, and use of estimation filtering algorithms. In regards to the collaborating research group APT, a method for estimating BG level, using only CGM sensor readings, with optional smoothing, regression and low pass filtering methods, as well as methods for evaluating BG level estimate in real time, is implemented, for use in future experiment settings.

First half of the thesis, time was primarily spent on a literature search, regarding the modeling part of this thesis objectives for estimating BG level using ISF glucose level measurements, deciding upon potential models, identification of model parameters and investigating potential filter algorithms, and corresponding code implementations in Matlab. The second half was spent on investigating missing robustness of robust-promising filters, which included thorough investigation of the CGM sensor readings. Based upon the investigation, enhancement methods, in the form of smoothing, regression and low pass filtering of measurements, were decided implemented, due to real-time qualities.

1.6 Outline

In Chapter 2 relevant theory is presented. The theory includes relevant background theory covering areas such as the glucose-regulatory system and relevant sensor systems, a more in depth presentation of different estimation algorithms, theory relating to estimate accuracy assessment and glucose dynamics, and finally, system identification. In Chapter 3 the aim of this thesis will be stated, in addition to putting the aim into context considering the term project. Provided data sets are explained in Chapter 4. Description of the literature search and code-implementation are given in Chapter 5, while results are displayed in Chapter 6. Discussion based on the theory, the aim, the method and the results can be found in Chapter 7, and concluding remarks, in addition to suggestions for future work, are given in Chapter 8.

1.7 Artificial Pancreas Trondheim

This thesis is written in collaboration with Artificial Pancreas Trondheim (APT). The artificial pancreas Trondheim research group was established in 2013 at The Norwegian University of Science and Technology, in Trondheim. APT is a cross-disciplinary group of researchers with high competence in the fields of control engineering, biomedical engineering, biosensors, applied clinical research, endocrinology, anesthesia and intensive care medicine, pharmacology, biotechnology, mathematical modelling, biochemistry and chemometrics, as well as collaboration with relevant biosensor industry [16]. The long term goal of APT is to develop a robust closed-loop glucose control system for patients with type 1 diabetes (T1D) and type 2 diabetes (T2D).

Chapter 2

Theory

This section will present theory which is considered essential in understanding the thesis' work and aim. Basic knowledge about diabetes mellitus, as well as relevant sensors, will first be introduced. This will ensure the reader about the motivation, as well as the context of the thesis. The next part is dedicated to explain various estimation algorithms. Following the estimation algorithms, a introduction to accuracy assessment is given, which will present selected accuracy measures, as well as problems concerning bias and variance. The next part is dedicated to glucose dynamics, which will serve as the foundation in constructing the mathematical models used by the estimation algorithms. Lastly, a section is devoted to address the structure and process of system identification.

2.1 Essential Background Knowledge

2.1.1 Diabetes mellitus

Diabetes mellitus is characterized by chronic hyperglycemia in response to ingestion of carbohydrates, fat, and protein, resulting from defects of insulin secretion, insulin action, or both [5]. Glucose is a form simple carbohydrate, and counted to be the most widespread form of sugar in the plant kingdom [17]. In an averaged diet, glucose is commonly considered the most essential form of energy.

In a healthy individual, BG level is narrowly controlled through the use of two hormones, insulin and glucagon, both of which are produced in the pancreas [18]. These hormones are components of the negative feedback glucose regulatory loop, described by Figure 2.1. Insulin secretion makes the glucose level in the blood decrease, while glucagon secretion increases the BG level [5]. Insulin increases the muscles and fat cells uptake of glucose from the blood, and increases the livers ability to remove glucose from the blood and store it in the body's glycogen storage, while glucagon breaks down this stored glycogen, so that glucose is again released into the blood, as well as limits the muscles and fat cells ability to take up glucose [19].

Failure of this regulatory loop will cause the BG level to go too low, *hypoglycemia*, or too high, *hyperglycemia*, both of which can be life threatening. Hyperglycemia occurs most often if diabetes is not treated, while hypoglycemia is usually a side-effect of exogenous insulin treatment [20].

There are three main types of diabetes; T1D, T2D and gestational diabetes [21]. Only T1D will be explained here, since these patients are the most frequent users of CGM systems. In T1D, the pancreas does not produce insulin due to an autoimmune destruction of beta cells, which are insulin producing cells found in the pancreas [21]. As a result, insulin must be administered from an external source [5], hence people with T1D require daily insulin treatment, regular BG monitoring, and a healthy lifestyle in order to manage their condition effectively [22].

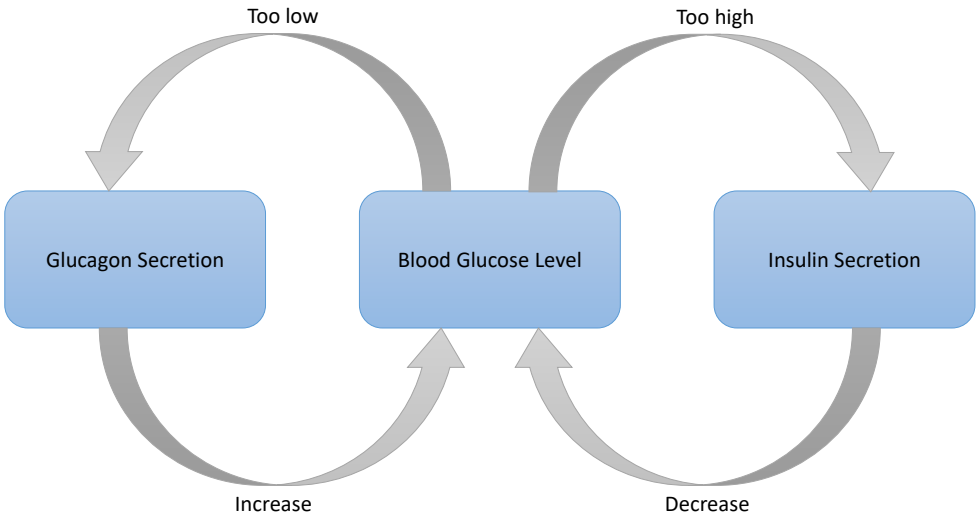

Figure 2.1: The negative feedback glucose regulatory loop.

2.1.2 Sensor systems

For individuals with diabetes, there are two primary methods for measuring the BG levels in everyday life: capillary BG measurement, also known as self-monitoring of blood glucose, and continuous glucose monitoring. Both SMBG and CGM systems are what is called minimal invasive sensor techniques [23]. Blood gas analyzing (BGA) of BG is an invasive measurement technique, mostly used in a hospital setting [23]. This thesis will focus on the CGM and BGA sensor systems.

All mentioned sensors in the above, uses what is called an amperometric sensing technique, in order to achieve readable glucose level measurements [23]. The amperometric glucose sensing technique is based on a chemically-based method of glucose sensing [6]. The sensor estimates glucose by measuring an electrical current generated by the reaction of glucose, either with oxygen or with an immobilized redox mediator [24].

Continous Glucose Monitoring

A CGM system consists of a minimally invasive sensor implantable in subcutaneous tissue, which measures the glucose level in the interstitial fluid, in real time [5]. The minimally invasive structure

of the sensor system allows for continuous glucose measurements [9] and zero need for extraction of fluids for measuring [6].

Due to transportation of glucose between the blood and interstitial fluid (ISF), CGM measurements are delayed, compared to measurements taken directly from the blood, during rapid changes of BG levels [10]. This is because of the plasma-to-ISF glucose dynamics, which refers to the glucose diffusion across capillaries and through the interstitial space where the sensor is located [10]. Please keep in mind that onward, whenever it is referred to *plasma*, it naturally entails *blood plasma*. The slow dynamics between these two compartments, together with sensor processing time, causes a time lag of approximately 4 − 10 min, in CGM sensors, from actual BG levels [5].

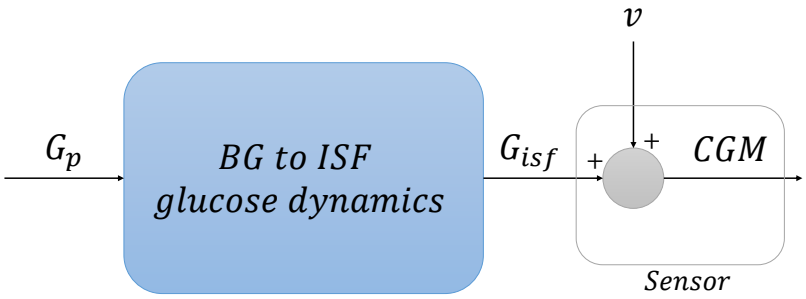

Figure 2.2: Block diagram describing how the a CGM sensor signal is obtained.

A block diagram, found in Figure 2.2, describes how a CGM measurement is obtained. First the the BG, G_p, diffuses into the ISF, where it is transformed into ISF glucose, G_{isf}. As the ISF is being measured, some additive measurement noise, v, is added to the sensor signal, which results in the final output signal, CGM.

Implantable sensors, like the CGM, does entail some disadvantages. Among the most mentioned disadvantages is the problem of membrane biofouling. Bioufouling is a phenomenon describing the adhesion of proteins and other biological matter on sensor surfaces, which will result in sensor drift and diminishing of sensor signal [6]. The biofouling process starts immediately upon contact between the sensor and body [6], and develops over time. Other concerns relating to the CGM sensor are inflammation, corrosion of the electrodes and noise originating from movement [6].

Due to such circumstances, CGM sensors must uphold certain ISO standards in order to be approved for commercial use. ISO stands for the International Organization for Standardization, and is an international standardization organisation which provides common standards among nations, in various areas, such as healthcare [25]. ISO 15197:2015 is used for *in-vitro* diagnostics test systems, which includes BG monitoring systems for managing diabetes [26].

Given this, the ISO standard can be used for modeling of measurement error v, see Figure 2.2, of CGM sensors. A sensor following ISO 15197:2015 should have an error within ± 0.83 [mmol/L] when the BG level is below 5.55 [mmol/L], and less than ±15% error when the BG level rises above this limit

[14]. The requirement from the standard is that 95 % of all measurements fall within this limit. This correspond to roughly two standard deviations (SD), given a normal distribution, when interpreting the limit as a 95 % confidence interval, and the approximated measurement variance is then given by $\sigma^2 = 0.172$ [mmol^2/L^2] when BG level is recorded below 5.55 [mmol/L] and $\sigma^2 = 0.0056y^2$ [mmol^2/L^2] for BG levels above this limit, where y describes recorded BG level [14].

Bloood Gas Analyzer

Blood gas analyzers are used to measure blood gas, pH, electrolytes and a selection of metabolites in whole blood specimens [27]. Among the selection of metabolites, it can measure the level of glucose in the blood, hence the analyzer can help determine abnormal glucose levels. The blood used in the analysis is most commonly drawn from the radial artery [28]. This makes the measuring technique an invasive measuring method, which entails enhanced accuracy in measuring glucose in the blood [6].

2.2 Estimation Algorithms

An estimate is an approximation of an unknown value, calculated based on collected data [29]. Considering a quantitative response Y, and p predictors, X_1,X_2...X_p, an assumed relationship between the quantitative response and the predictors is written on the form:

$$Y = f(X) + \epsilon, \tag{2.1}$$

where f is some fixed but unknown function of the predictors that represents the systematic information that X provides about Y, and ϵ is a random error term [30]. Estimating $f(X)$ then yields an estimate of the quantitative response Y. There are two main reasons for wanting to estimate f: *prediction* and *inference* [30]. Considering prediction, since the error term will average to zero [30], the resulting prediction of Y equals:

$$\hat{Y} = \hat{f}(X), \tag{2.2}$$

where $\hat{f}$ now represents an estimate of f, and $\hat{Y}$ is the prediction of Y [30].

Inference on the other hand is about understanding the connections between the predictors and the quantitative responses. Meaning that the interests of estimating f originate in the wish of understanding how Y is affected by X [30].

From this point on, when discussing or referring to the word *estimation*, it will be related to *prediction*, and will not include *inference*, the reason being that prediction is considered the goal of estimation in this thesis.

2.2.1 Observability

Before delving into the topic of estimation algorithms, observability is explained, due to it being an essential part of estimation processes considering systems. Observability is a concept describing how well it is possible to observe a system. More formally explained, a discrete time system is observable if for any initial state x_0, and some final time k, the initial state x_0 can be uniquely determined by knowledge of the inputs and outputs for all $i \in [0, k]$ [31].

Consider the time-invariant system in Equation (2.3)-Equation (2.4).

$$x_{k+1} = F_d x_k + B_d u_k \tag{2.3}$$
$$y_k = H_d x_k + D_d u_k, \tag{2.4}$$

The n-state system is has the observability matrix O defined by:

$$O = \begin{bmatrix} C \\ CA \\ \vdots \\ CA^{n-1} \end{bmatrix}, \tag{2.5}$$

and is said to be observable if, and only if, $\rho(O) = n$ [31], where ρ refers to the rank of O.

2.2.2 Lowpass Filter

A low-pass filter (LPF) is a type of filter that let signals below a cutoff frequency pass and attenuates signals above the cutoff frequency [32], cutoff frequency being a boundary in a system's frequency response. One such filter is the Butterworth filter, and the continuous-time transfer function of the filter of order n is [33]:

$$H(s) = \frac{\omega_c^n}{(s-\lambda_1)(s-\lambda_2)...(s-\lambda_n)}, \tag{2.6}$$

where ω_c^n is the cut-off frequency of order n and $\lambda_1, \lambda_2 ... \lambda_n$ are the n poles of the filter.

By setting $n = 1$ in Equation (2.6), the first order continuous-time transfer function is obtained:

$$H(s) = \frac{y(s)}{u(s)} = \frac{\omega_c}{s-\lambda_1} = \frac{\frac{1}{T}}{s-(-\frac{1}{T})} = \frac{1}{Ts+1}, \tag{2.7}$$

where $u(s)$ is the filter input, $y(s)$ is the filter output, $\omega_c = \frac{1}{T}$, T being the time constant.

In order to obtain the discrete-time low-pass filter, one may use Euler backward differentiation (EBD) [34].

The first step is to cross-multiply Equation (2.7), which gives

$$\begin{aligned}(Ts+1)y(s) &= u(s)\\ Tsy(s)+y(s) &= u(s).\end{aligned} \tag{2.8}$$

Now, using the inverse Laplace transform the following is obtained:

$$T\dot{y}(t)+y(t)=u(t). \tag{2.9}$$

In order to present a certain point in discrete time, t is now changed to t_k. This gives:

$$T\dot{y}(t_k)+y(t_k)=u(t_k). \tag{2.10}$$

Now the EBD is substituted for the time derivative of $y(t)$. This will given the following approximation:

$$\dot{y}(t_k)\approx\frac{y(t_k)-y(t_{k-1})}{h}, \tag{2.11}$$

where h denotes the step size. Inserting Equation (2.11) into Equation (2.10) gives

$$T\frac{y(t_k)-y(t_{k-1})}{h}+y(t_k)=u(t_k). \tag{2.12}$$

Solving for $y(t_k)$ gives [34]:

$$y(t_k)=\frac{T}{T+h}y(t_{k-1})+\frac{h}{T+h}u(t_k) \tag{2.13}$$

Hence the discrete time first order low-pass filter is given by [35]:

$$y(t_k)=(1-b)y(t_{k-1})+bu(t_k), \tag{2.14}$$

where

$$b=\frac{h}{T+h}. \tag{2.15}$$

2.2.3 Moving Average Smoothing

Moving average filter is a type of LPF [32], where the estimate consists of several averages spanning over different subsets of a full data set. The moving average (MA) filter is an excellent method for

achieving an overall idea about trends of data sets [36], and is frequently used on time series data, to smooth out short-term fluctuations [37]. The MA formula is given by:

$$\bar{y}_k = \frac{y_k + y_{k-1} + ... + y_{k-n-1}}{n}, \tag{2.16}$$

where y is the data, k is the current iteration, or period, and n is the total number of iterations or periods considered in the current subset.

2.2.4 Linear Regression

Linear regression (LR) is an approach for predicting a quantitative response Y based on predictor variable X, assuming a linear relationship between Y and X [30]. Mathematically it is formulated as the following:

$$y_i \approx \beta_0 + \beta_1 x_i + \epsilon_i, \tag{2.17}$$

where β_0 and β_1 are unknown constants representing the *intercept* and the *slope*, respectively. The response y_i is in Equation (2.17) being regressed on the predictor x_i, while ϵ is the error term, for an i'th observation.

Letting $i = 1, ..., n$ then gives:

$$y_1 = \beta_0 + \beta_1 x_1 + \epsilon_1 \tag{2.18}$$
$$y_2 = \beta_0 + \beta_1 x_2 + \epsilon_2 \tag{2.19}$$
$$\vdots \tag{2.20}$$
$$y_n = \beta_0 + \beta_1 x_n + \epsilon_n, \tag{2.21}$$

which can be reformulated into matrix-form:

$$\begin{bmatrix} y_1 \\ y_2 \\ \vdots \\ y_n \end{bmatrix} = \begin{bmatrix} 1 & x_1 \\ 1 & x_2 \\ \vdots & \vdots \\ 1 & x_n \end{bmatrix} \begin{bmatrix} \beta_0 \\ \beta_1 \end{bmatrix} + \begin{bmatrix} \epsilon_1 \\ \epsilon_2 \\ \vdots \\ \epsilon_n \end{bmatrix} \tag{2.22}$$
$$Y = X\beta + \epsilon. \tag{2.23}$$

Now X is the design matrix, β is the vector of regression coefficients ϵ is the vector of error terms and Y is the vector of responses.

Now, in the problem of estimation, Equation (2.23) is rewritten:

$$\hat{Y}(\beta) = X\beta, \tag{2.24}$$

which leads to:

$$\epsilon(\beta) = Y - \hat{Y}(\beta) = Y - X\beta, \tag{2.25}$$

where $\epsilon(\beta)$ is the β dependent residuals.

One way of obtaining the optimal vector of coefficients, β, is to minimize the residual sum of squares (RSS) [30]:

$$\begin{aligned} \text{RSS}(\beta) &= \sum_{i=1}^{n} \epsilon_i^2(\beta) && (2.26)\\ &= \epsilon(\beta)^T \epsilon(\beta) && (2.27)\\ &= (Y - X\beta)^T (Y - X\beta) && (2.28)\\ & && (2.29) \end{aligned}$$

To find the minimum of RSS(β), the derivative with respect to β is computed:

$$\begin{aligned} \frac{d}{d\beta} RSS(\beta) &= \frac{d}{d\beta}(Y - X\beta)^T (Y - X\beta) && (2.30)\\ &\vdots && (2.31)\\ &= -2X^T (Y - X\beta), && (2.32) \end{aligned}$$

Setting Equation (2.32) equal to 0 and solving for β then gives the least squares estimator for the coefficients [30]:

$$\beta = (X^T X)^{-1} X^T Y. \tag{2.33}$$

Weighted Least Squares Linear Regression

The weighted linear regression, also known as weighted least squares linear regression (WLS LR), is a generalization of the ordinary linear regression, or ordinary least squares, in which variance of the observations are incorporated into the regression [38]. Recall that in linear regression the goal is to minimize the RSS of the estimation error, see Equation (2.26), which results in Equation (2.33). In WLS LR the goal is to minimize the weighted RSS (WRSS):

$$\text{WRSS}(\beta) = \sum_{i=1}^{n} w_i \epsilon_i^2, \tag{2.34}$$

where ϵ is the estimation error, and w are the weights. Setting $w_i = 1$ results in the ordinary least squares solution to the regression problem. The minimization problem in Equation (2.34) can be solved similarly to how it was done for ordinary least squares, see Equation (2.32):

$$\text{WRSS}(\beta) = (Y - X\beta)^T W (Y - X\beta) \tag{2.35}$$
$$= (Y^T WY - Y^T WX\beta - \beta^T X^T WY + \beta^T X^T WX\beta). \tag{2.36}$$

Differentiating with respect to β then gives:

$$\frac{d}{d\beta}\text{WRSS}(\beta) = -2(X^T WY - X^T WX\beta). \tag{2.37}$$

Setting the above equal to zero, and solving for β results in [39]:

$$\beta = (X^T WX)^{-1} X^T WY, \tag{2.38}$$

where W is a symmetrical matrix in which the individual weights lie along the diagonal, and is defined by the variance of the observations:

$$W_{ii} = \frac{1}{\sigma_i^2}. \tag{2.39}$$

However, the variances may not always be known, hence the weight are in many cases found by weight functions. Such a weight function is the tricube weight function [40]:

$$W(u) = \begin{cases} (1-u^3)^3 & \text{if } 0 \leq u \leq 1 \\ 0 & \text{otherwise} \end{cases} \tag{2.40}$$

where

$$u = \frac{x_0 - x_i}{d}, \tag{2.41}$$

for $i = 1...N$, where x_0 is a constant value of x. d is the order of the polynomial that is locally fit to each point of x_i, and $d = 1$ most always provide adequate smoothed points, while also being computational feasible [40].

2.2.5 Finite Differences Approximation

The finite difference (FD) approximation approach proceeds by substituting derivatives in a differential equation with finite difference approximations [41].

The derivative of a function, f, at a point, x, is defined by the following limit:

$$f'(x) = \frac{df(x)}{d\Delta x} = \lim_{\Delta x \to 0} \frac{f(x+\Delta x) - f(x)}{\Delta x}, \tag{2.42}$$

which can be said to be an exact approximation of $f'(x)$ if h is small, but finite [42]. There are three basic types of finite differences approximation: *forward*, *backward* and *central*. They are given by Equation (2.43), Equation (2.44), Equation (2.45), respectively, see also Figure 2.3 for visual description. Only backward finite differences approximation is relevant in this thesis, due to the method's usage for approximating derivatives when future data is unavailable.

$$\frac{f(x+\Delta x) - f(x)}{\Delta x} = \frac{\Delta_\Delta x f(x)}{\Delta x} = \frac{f(x+1) - f(x)}{\Delta x} \tag{2.43}$$

$$= \frac{\nabla_\Delta x f(x)}{\Delta x} = \frac{f(x) - f(x-1)}{\Delta x} \tag{2.44}$$

$$= \frac{\delta_\Delta x f(x)}{\Delta x} = \frac{f(x+\frac{\Delta x}{2}) - f(x-\frac{\Delta x}{2})}{\Delta x}. \tag{2.45}$$

For analyzing the errors of the backward approximation, the function value of f is expanded using Taylor series, about the point x [41], which results in the following error:

$$\frac{f(x) - f(x-\Delta x)}{\Delta x} - f'(x) = O(\Delta x), \tag{2.46}$$

where $O(h) \to 0$ when $\Delta x \to 0$ [42]. From this point on, backward finite difference approximation will be referred to as FD approximation.

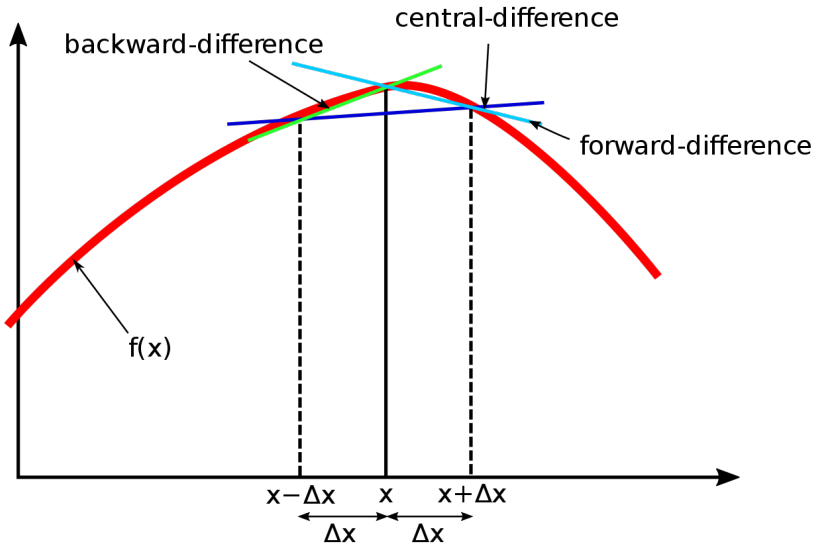

Figure 2.3: The three types of the finite difference approximations, retrieved from [43].

2.2.6 Kalman Filter

The Kalman Filter (KF) is an optimal estimator that provides a recursive computational methodology for estimating the state of a discrete-data controlled process from measurements, while also providing an estimate of the uncertainty of the estimates [44]. A figure describing KF, in combination with an actual system may be found in Figure 2.4.

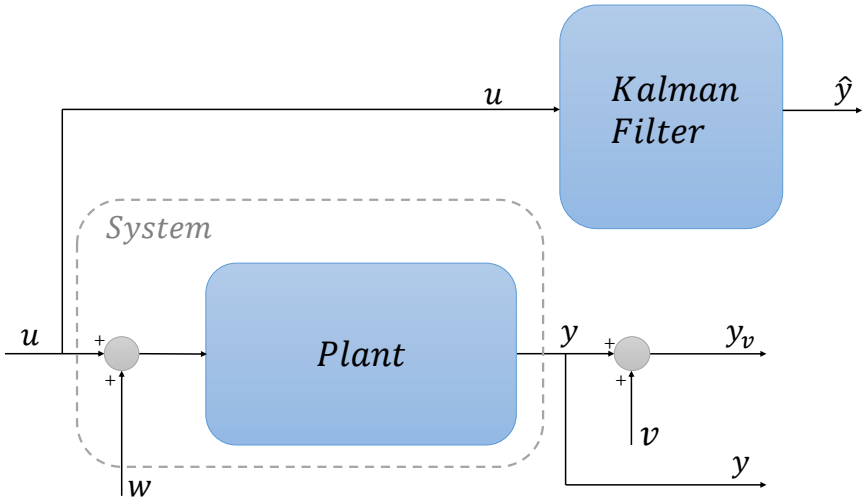

Figure 2.4: The complete system with included Kalman filter for state estimation diagram.

Given the linear discrete-time system

$$x_{k+1} = F_k x_k + B_k u_k + w_k \tag{2.47}$$
$$y_k = H_k x_k + v_k \tag{2.48}$$

where $x_k \in \mathbb{R}^n$ are the system states, $u_k \in \mathbb{R}^p$ is the system input and $y_k \in \mathbb{R}^m$ is the system output. F_k is the state transition matrix, B_k is the input transition matrix and H_k is the measurement matrix. Assume that the system matrices all have appropriate dimensions.

The noise processes w_k and v_k are considered white, zero-mean, uncorrelated and have known covariance matrices Q_k and R_k, respectively:

$$w_k \sim (0, Q_k) \tag{2.49}$$
$$v_k \sim (0, R_k) \tag{2.50}$$
$$E[w_k w_j^T] = Q_k \delta_{k-j} \tag{2.51}$$
$$E[v_k v_j^T] = R_k \delta_{k-j} \tag{2.52}$$
$$E[v_k w_j^T] = 0 \tag{2.53}$$

where δ_{k-j} is the Kronecker delta function. The Kronecker delta function gives $\delta_{k-j} = 1$ if $k = j$,

and $\delta_{k-j} = 0$ if $k \neq j$ [31]. Q_k is the process noise covariance at time k, and R_k is the measurement noise covariance at time k.

The goal of the standard KF is then to estimate the state x_k based on the knowledge of the system dynamics and the availability of measurements, y_k.

The KF manages this by combining *a posteriori* and *a priori* estimates of the state x_k. The *a posteriori* estimate is the expected value of x_k conditioned on all of the measurements up to and including time k.

$$\hat{x}_k = E[x_k | y_1, y_2, ..., y_k] = a\ posteriori \text{ estimate.} \tag{2.54}$$

The *a priori* estimate on the other hand is the expected value of x_k conditioned on all of the measurements prior to time k.

$$\bar{x}_k = E[x_k | y_1, y_2, ..., y_{k-1}] = a\ priori \text{ estimate.} \tag{2.55}$$

The estimation error covariance matrix of the *a posteriori* estimate at time k is denoted by P_k, while the *a priori* estimation error covaraince matrix at time k is denoted by $\bar{P}_k$.

$$P_k = E[(x_k - \hat{x}_k)(x_k - \hat{x}_k)^T] \tag{2.56}$$
$$\bar{P}_k = E[(x_k - \bar{x}_k)(x_k - \bar{x}_k)^T]. \tag{2.57}$$

Assuming a prior estimate $\bar{x}$, the aim is to use the measurement y_k to improve the posterior estimate:

$$\hat{x}_k = \bar{x}_k + K_k(y_k - H_k\bar{x}_k), \tag{2.58}$$

where K_k is the Kalman gain. In order to determine K_k the minimum mean-square error is used as the performance criterion [45]. Consider the covariance matrix of the estimate, which now can be rewritten using Equation (2.47) and Equation (2.48) and Equation (2.58):

$$P_k = E[(x_k - \hat{x}_k)(x_k - \hat{x}_k)^T] \tag{2.59}$$
$$P_k = E[((x_k - \bar{x}_k) - K_k(H_k x_k + v_k - H_k\bar{x}_k)) \tag{2.60}$$
$$((x_k - \bar{x}_k) - K_k(H_k x_k + v_k - H_k\bar{x}_k))^T]. \tag{2.61}$$

Recognize that $(x_k - \bar{x}_k)$ is the *a priori* estimation error, and that it is uncorrelated with the measurement error v_k. Performing the indicated expectation then yields:

$$P_k = (I - K_k H_k)\bar{P}_k(I - K_k H_k)^T + K_k R_k K_k^T. \tag{2.62}$$

Now this expression is expanded into:

$$P_k = \bar{P}_k - K_k H_k \bar{P}_k - \bar{P}_k H_k^T K_k^T + K_k (H_k \bar{P}_k H_k^T + R_k) K_k^T, \tag{2.63}$$

The goal is then to minimize the trace of P, since it is the sum of the mean squared error in the estimates of all the elements of the state vector [45]. This is done by differentiating the trace of P_k with respect to K_k. Note that the trace of $\bar{P}_k H_k^T K_k^T$ is equal to the trace of it's transpose $K_k H_k \bar{P}_k$. This gives:

$$\frac{d(\text{trace} P_k)}{dK_k} = -2(H_k \bar{P}_k)^T + 2K_k (H_k \bar{P}_k H_k^T + R_k). \tag{2.64}$$

Setting the derivative equal to zero and solving for the optimal gain gives:

$$K_k = \bar{P}_k H_k^T (H_k \bar{P}_k H_k^T + R_k)^{-1}. \tag{2.65}$$

By routine substitution of the optimal gain in Equation (2.65) into Equation (2.63) the following result is obtained:

$$P_k = (I - K_k H_k) \bar{P}_k. \tag{2.66}$$

As the first measurement is taken at time $k = 1$, the initial value of the *a posteriori* estimate, $\hat{x}_0$, is set equal to the expected value of the initial state x_0.

$$\hat{x}_0 = E[x_0]. \tag{2.67}$$

Now, given all of the above, the algorithm of the standard KF can be formulated.

The dynamical system is described by the following equations [31]:

$$x_{k+1} = F_k x_k + B u_k + w_k \tag{2.68}$$
$$y_k = H_k x_{k+1} + v_k \tag{2.69}$$
$$E[w_k w_j^T] = Q_k \delta_{k-j} \tag{2.70}$$
$$E[v_k v_j^T] = R_k \delta_{k-j} \tag{2.71}$$
$$E[v_k w_j^T] = 0 \tag{2.72}$$

The KF is initialized as follows:

$$\hat{x}_0 = E[x_0] \tag{2.73}$$
$$P_0 = E[(x_0 - \hat{x_0})(x_0 - \hat{x_0})^T] \tag{2.74}$$

For time step $k = 1, 2, \ldots$ the standard KF is given by the following equations:

Prediction:

$$\begin{aligned}\bar{x}_k &= F_k \hat{x}_{k-1} + Bu_{k-1} \\ \bar{P}_k &= F_k P_{k-1} F_k^T + Q_k\end{aligned} \tag{2.75}$$

Correction:

$$\begin{aligned}K_k &= \bar{P}_k H_k^T (H_k \bar{P}_k H_k^T + R_k)^{-1} \\ \hat{x}_k &= \bar{x}_k + K_k (y_k - H_k \bar{x}_k) \\ P_{k+1} &= (I - K_k H_k) \bar{P}_k.\end{aligned}$$

The Kalman filter recursions in Equation (2.75) are summarized in the block diagram found in Figure 2.5.

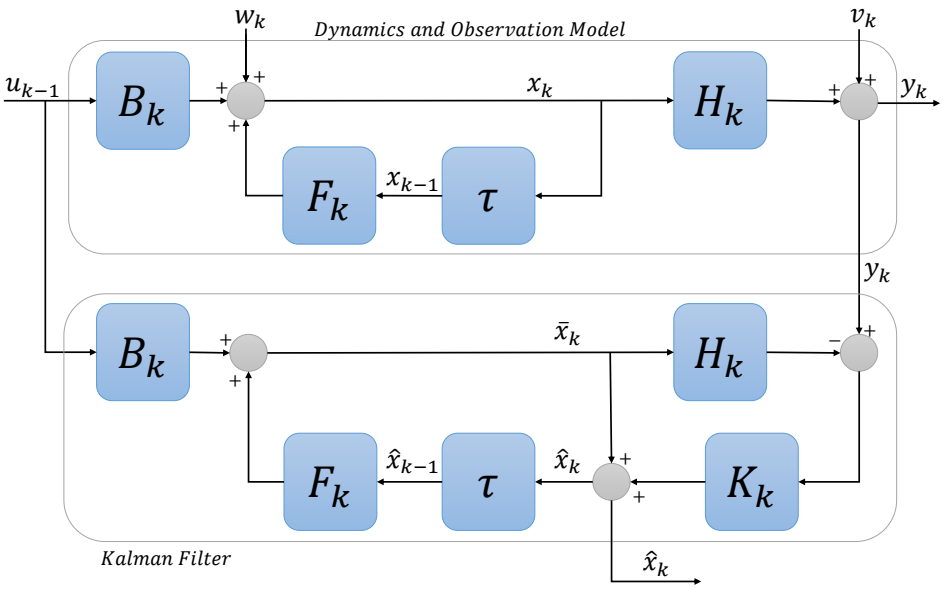

Figure 2.5: Block diagram of a dynamics and observation model and a KF.

2.2.7 Robust Two-Stage Kalman Filter with Unknown Inputs

A problem that often appears in the field of state estimation is the effect of unknown inputs. In some cases an unknown input is treated as a stochastic process with known statistics or as a constant bias. However, due to the input being unknown, such treatments are based solely on assumptions of the model. Any invalid assumption about the model may have a major effect on the filter performance, hence should be avoided if possible.

In [46] a filter for dealing with unknown inputs is presented. In [46] a unbiased minimum-variance filter [47] is re-derived, using the structure of an optimal two-stage Kalman filter (OTSKF) [48]. The resulting filter is named the robust two-stage Kalman filter with unknown inputs (RTSKF-UI). A diagram of the RTSKF-UI in combination with an actual system can be found in Figure 2.6, and a block diagram of the filter itself is shown in Figure 2.7.

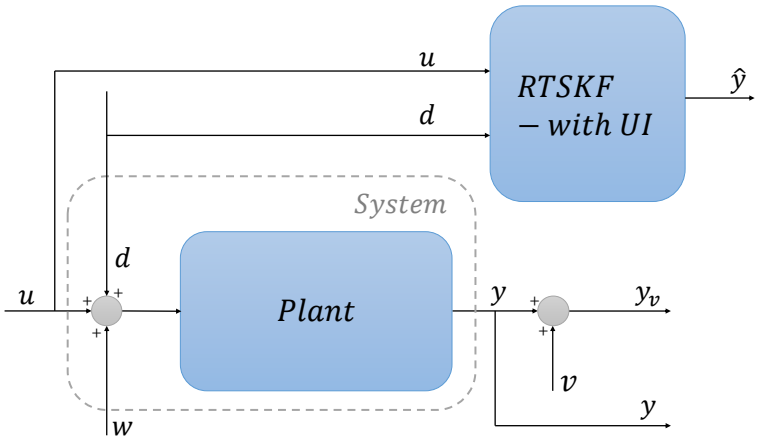

Figure 2.6: The complete system with included robust two-stage Kalman filter with unknown inputs for state estimation diagram.

First, consider the following linear discrete stochastic system with unknown inputs:

$$\begin{aligned} x_{k+1} &= F_k x_k + E_k d_k + w_k \\ y_k &= H_k x_k + v_k, \end{aligned} \tag{2.76}$$

where $x_k \in \mathbb{R}^n$ are the system states, $d_k \in \mathbb{R}^p$ is the unknown system input and $y_k \in \mathbb{R}^m$ is the system output. F_k is the state transition matrix, E_k is the unknown input transition matrix and H_k is the measurement matrix. Assume that the system matrices all have appropriate dimensions. The process noise w_k and measurement noise v_k follow the same assumptions as was made for the standard KF, see Equation (2.51) and Equation (2.52).

The main idea of RTSKF-UI is to make the state estimates unaffected by the unknown input. This way the computational burden of augmenting the system equations with the unknown inputs is avoided, as well as compromised optimality by poor choice of input noise characteristics [46].

In the augmented system case, the unknown input d_k is modeled as a stochastic process with a wide-sense representation.

$$d_{k+1} = d_k + w_k^d, \tag{2.77}$$

where w_k^d is zero-mean white noise with covariances $E[w_k^d (w_j^d)^T] = Q_k^d \delta_{k-j}$ and $E[w_k (w_j^d)^T] = Q_k^{xd} \delta_{k-j}$.

The OTSKF corresponds to the augmented system Equation (2.76)-Equation (2.77) and is given by:

$$x_{k+1} = \bar{x}_{k|k} + V_k d_{k|k} \tag{2.78}$$

$$P_{k|k}^x = P_{k|k}^{\bar{x}} + V_k P_{k|k}^d V_k^T, \tag{2.79}$$

where $\bar{x}_{k|k}$ is given by

$$\bar{x}_{k|k-1} = F_{k-1}\bar{x}_{k-1|k-1} + \bar{u}_{k-1} \tag{2.80}$$
$$\bar{x}_{k|k} = \bar{x}_{k|k-1} + K_k^{\bar{x}}(y_k - H_k\bar{x}_{k|k-1}) \tag{2.81}$$
$$P_{k|k-1}^{\bar{x}} = F_{k-1}P_{k-1|k-1}^{\bar{x}}F_{k-1}^T + \bar{Q}_{k-1} \tag{2.82}$$
$$K_k^{\bar{x}} = P_{k|k-1}^{\bar{x}}H_k^T(H_kP_{k|k-1}^{\bar{x}}H_k^T + R_k)^{-1} \tag{2.83}$$
$$P_{k|k}^{x} = (I - K_k^{\bar{x}}H_k)P_{k|k-1}^{\bar{x}}, \tag{2.84}$$

and d_k is given by

$$d_{k|k-1} = d_{k-1|k-1} \tag{2.85}$$
$$d_{k|k} = d_{k|k-1} + K_k^d(y_k - H_k\bar{x}_{k|k-1} - S_kd_{k|k-1}) \tag{2.86}$$
$$P_{k|k-1}^d = P_{k-1|k-1}^d + Q_{k-1}^d \tag{2.87}$$
$$K_k^d = P_{k|k-1}^dS_k^T(H_kP_{k|k-1}^{\bar{x}}H_k^T + R_k + S_kP_{k|k-1}^dS_k^T)^{-1} \tag{2.88}$$
$$P_{k|k}^d = (I - K_k^dS_k)P_{k|k-1}^d, \tag{2.89}$$

where

$$\bar{u}_k = (\bar{U}_{k+1}) - U_{k+1}d_{k|k} \tag{2.90}$$
$$\bar{Q}_k = Q_k - Q_k^{xd}\bar{U}_{k+1}^T - U_{k+1}(Q_k^{xd} - \bar{U}_{k+1}Q_k^d)^T \tag{2.91}$$
$$\bar{U}_k = F_{k-1}V_{k-1} + E_{k-1} \tag{2.92}$$
$$S_k = H_kU_k. \tag{2.93}$$

U_k and V_k are the two-stage blending matrices, given by

$$U_k = \bar{U}_k + (Q_{k-1}^{xd} - \bar{U}_kQ_{k-1}^d)(P_{k|k-1}^d)^{-1} \tag{2.94}$$
$$V_k = U_k - K_k^{\bar{x}}S_k. \tag{2.95}$$

A standard Kalman filter is divided in two steps. Namely the prediction step and the correction step. Considering the fact that the prediction step is obtained by the reliability of the system model, one should disregard the prediction of d_k when the unknown input model is unreliable. The remaining steps in order to achieve the suggested filter is then to modify the correction step to eliminate $d_{k|k-1}$ and $P_{k|k-1}^d$. This can be done by substituting Equation (2.85) into Equation (2.86) and combining Equation (2.88) and Equation (2.89), respectively. The modified correction step of the unknown inputs is then given by

$$d_{k|k} = (I - K_k^d H_k U_k) d_{k-1|k-1} + K_k^d (y_k H_k \bar{x}_{k|k-1}) \tag{2.96}$$
$$K_k^d = P_{k|k}^d U_k^T H_k^T (H_k P_{k|k-1}^{\bar{x}} H_k^T + R_k)^{-1}. \tag{2.97}$$

First consider the covariance $P_{k|k}^d$. In order to achieve that the unknown input filter is free from the underlying model, K_k^d is chosen to satisfy the following constraint:

$$I - K_k^d H_k U_k = 0. \tag{2.98}$$

This leads to

$$d_{k|k} = K_k^d (y_k - H_k \bar{x}_{k|k-1}). \tag{2.99}$$

Substituting Equation (2.97) into Equation (2.98) and solving for the covariance gives

$$P_{k|k}^d = (U_k^T H_k^T C_k^{-1} H_k U_k)^{-1}, \tag{2.100}$$

where

$$C_k = H_k P_{k|k-1}^{\bar{x}} H_k^T + R_k. \tag{2.101}$$

Next the U_k is considered. First, in order to give a heuristic derivation, Equation (2.80) and Equation (2.82) are rewritten, respectively, as follows

$$\bar{x}_{k|k-1} = F_{k-1} x_{k-1|k-1} + \boldsymbol{Z}_1 \tag{2.102}$$
$$P_{k|k-1}^{\bar{x}} = F_{k-1} P_{k-1|k-1}^x F_{k-1}^T + Q_{k-1} + \boldsymbol{Z}_2, \tag{2.103}$$

where

$$\boldsymbol{Z}_1 = (E_{k-1} - U_k) d_{k-1|k-1} \tag{2.104}$$
$$\boldsymbol{Z}_2 = (E_{k-1} - U_k) P_{k-1|k-1}^d (E_{k-1} - U_k)^T - U_k (Q_{k-1}^{xd})^T - Q_{k-1}^{xd} U_k^T + U_k Q_{k-1}^d U_k^T. \tag{2.105}$$

For Equation (2.102) and Equation (2.103) to be robust against the unknown input model, the following choice is made:

$$\boldsymbol{Z}_1 = 0, \qquad \boldsymbol{Z}_2 = 0. \tag{2.106}$$

This gives

$$U_k = E_{k-1}. \tag{2.107}$$

Having modified U_k, the robust two-stage Kalman filter, which is free from the unknown input model can be defined. Replacing Equation (2.102), Equation (2.103), Equation (2.99), Equation (2.97) and Equation (2.100) into Equation (2.80), Equation (2.82), Equation (2.86), Equation (2.88) and Equation (2.89), respectively, and using Equation (2.106), Equation (2.107), Equation (2.78) and Equation (2.79), the following is obtained:

$$\hat{x}_{k|k} = \bar{x}_{k|k} + V_k d_{k|k} \tag{2.108}$$
$$\hat{P}^x_{k|k} = P^{\bar{x}}_{k|k} + V_k P^p_{k|k} V_k^T, \tag{2.109}$$

where $\bar{x}_{k|k}$ is given by

$$\bar{x}_{k|k-1} = F_{k-1}\hat{x}_{k-1|k-1} \tag{2.110}$$
$$\bar{x}_{k|k} = \bar{x}_{k|k-1} + K^{\bar{x}}_k(y_k - H_k\bar{x}_{k|k-1}) \tag{2.111}$$
$$P^{\bar{x}}_{k|k-1} = F_{k-1}\hat{P}^x_{k-1|k-1}F^T_{k-1} + \bar{Q}_{k-1} \tag{2.112}$$
$$K^{\bar{x}}_k = P^{\bar{x}}_{k|k-1}H^T_k C^{-1}_k \tag{2.113}$$
$$P^x_{k|k} = (I - K^{\bar{x}}_k H_k)P^{\bar{x}}_{k|k-1}, \tag{2.114}$$

and d_k is given by

$$d_{k|k} = K^d_k(y_k - H_k\bar{x}_{k|k-1}) \tag{2.115}$$
$$K^d_k = P^d_{k|k}E^T_{k-1}H^T_k C^{-1}_k \tag{2.116}$$
$$P^d_{k|k} = (E^T_{k-1}H^T C^{-1}_k H_k E_{k-1})^{-1}, \tag{2.117}$$

where

$$V_k = (I - K^{\bar{x}}_k H_k)E_{k-1} \tag{2.118}$$
$$C_k = H_k P^{\bar{x}}_{k|k-1}H^T_k + R_k. \tag{2.119}$$

2.2.8 M-Robust Kalman Filter

As stated in Section 2.2.6 the noise processes which are involved in the standard Kalman Filter, are assumed to be white Gaussian noise processes. However, in a real system the distribution of noise

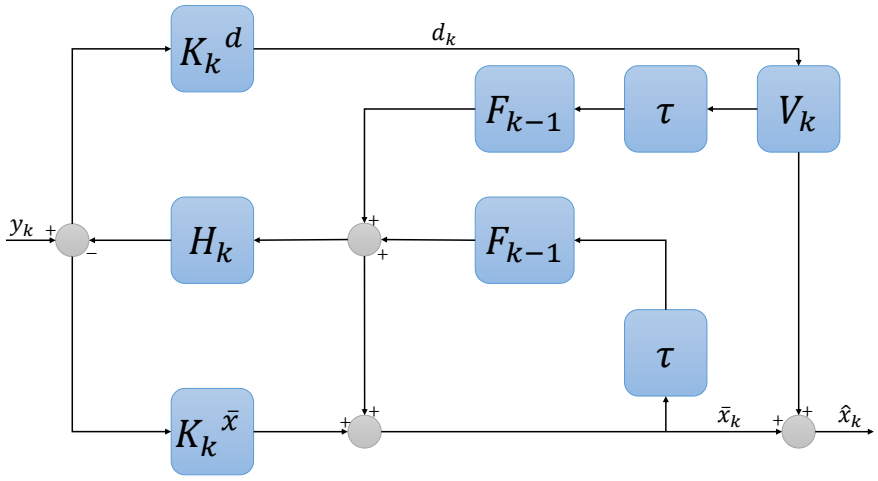

Figure 2.7: Block diagram of the RTSKF-UI, inspired by [46], where y_k is the current measurement, see Figure 2.5.

frequently deviates from the assumed Gaussian model, often bearing more resemblance to heavier tailed distributions. High intensity noise realizations, often referred to as outliers, are also common, and contradicts the assumption of clean white noise. In the presence of these phenomenons, the performance of the standard Kalman Filter will degrade. The solution to these issues are robust filters. Robust statistical procedures deals with deviations from ideal models, and remain reliable and reasonably efficient under small deviations from the models in question [49].

One way of accomplishing a robust filter is to re-formulate the Kalman Filter into a regression problem, and use M-estimation to solve it. This is the proposed solution in [50], where the regression problem is solved using weighted least squares approximation, see Section 2.2.4, of M-robust state estimates, where M referrers to *maximum likelihood*.

Regression Formulation of Standard Kalman Filters

Consider the discrete-time linear state-space model

$$x_{k+1} = F_k x_k + G_k w_k \tag{2.120}$$
$$y_k = H_k x_k + v_k \tag{2.121}$$

Now, remember the Kalman filter initialization in Equation (2.73) and Equation (2.74), and recursions in Equation (2.75). The Kalman filter can be thought of as a solution to a particular weighted least squares problem. Reformulating the problem given in Equation (2.120) and Equation (2.121) then gives

$$\begin{bmatrix} I \\ H_k \end{bmatrix} x_k = \begin{bmatrix} F_{k-1}\hat{x}_{k-1|k-1} \\ y_k \end{bmatrix} + \varepsilon_k, \tag{2.122}$$

where I is the identity matrix and

$$\varepsilon_k = \begin{bmatrix} F_{k-1}(x_{k-1} - \hat{x}_{k-1|k-1}) + G_{k-1}w_{k-1} \\ -v_k \end{bmatrix} \tag{2.123}$$

with

$$E\{\varepsilon_k \varepsilon_k^T\} = \begin{bmatrix} P_{k|k-1} & 0 \\ 0 & R_k \end{bmatrix} = S_k S_k^T. \tag{2.124}$$

S_k may be obtained through Cholesky decomposition [50].

Multiplying Equation (2.122) with S_k^{-1} then gives

$$Y_k = X_k \beta_k + \zeta_k, \tag{2.125}$$

which is now in the form of a linear least squares regression problem, with $E\{\zeta_k \zeta_k^T\} = I$, and where

$$Y_k = S_k^{-1} \begin{bmatrix} x_{k|\hat{k-1}} \\ y_k \end{bmatrix} \tag{2.126}$$

$$X_k = S_k^{-1} \begin{bmatrix} I \\ H_k \end{bmatrix} \tag{2.127}$$

$$\beta_k = x_k \tag{2.128}$$

$$\zeta_k = -S_k^{-1} \varepsilon_k. \tag{2.129}$$

The solution to Equation (2.125) is given by

$$\hat{\beta}_k = (X_k^T X_k)^{-1} X_k^T Y_k \tag{2.130}$$

$$E\{(\beta_k - \hat{\beta}_k)(\beta_k - \hat{\beta}_k)^T\} = (X_k^T X_k)^{-1}. \tag{2.131}$$

That is

$$\hat{\beta}_k = \hat{x}_{k|k} \tag{2.132}$$

$$P_{k|k} = E\{\hat{\beta}_k \hat{\beta}_k^T.\} \tag{2.133}$$

The Kalman filter recursions in Equation (2.75) will then be the solutions Equation (2.130) to the linear regression problem given by Equation (2.125), which is the least squares solution [50].

Robustifying the Kalman Filter

The least squares solution to the regression problem is only optimal if the underlying noise probability density function follows a Gaussian distribution [50]. However, in regression problems uncontrollable inhomogenicity of variance in the noise, and long-tailed noise distributions, will impair

the efficiency of the estimates [51]. Hence, there is need for robustifying the regression estimates, for which M-estimators are used, which are a maximum likelihood type estimators. The regression problem is therefore reformulated into a minimization problem:

$$\hat{\beta}_k = \arg\min_\beta J_n(\beta), \qquad J_n(\beta) = \sum_{i-1}^{n} \rho(y_{i,k} - x_{i,k}^T \beta), \tag{2.134}$$

where $y_{i,k}$ is the i-th element of Y_k, n is the dimension of Y_k, and where $x_{i,k}$ is the i-th row of X_k and ρ is the loss function. In the case where ρ is a quadratic function the estimate in Equation (2.134) reduces to the least squares solution, which also is the standard Kalman filter solution in Equation (2.130).

M-estimation reduces the influence of outliers by replacing the quadratic function in the ordinary least squares solution, by a piece-wise, usually convex [51], loss function:

$$\sum_{i=1}^{n} e_i^2 \rightarrow \min \sum_{i=1}^{n} \rho(e_i), \tag{2.135}$$

where $e_i = y_{i,k} - x_{i,k}^T \beta$ is the residual for the ith observations, and ρ is given by [51]:

$$\rho(z) = \begin{cases} \Delta|z| - \frac{\Delta}{2} & \text{if } |z| \geq \Delta \\ \frac{z^2}{2} & \text{if } |z| < \Delta, \end{cases} \tag{2.136}$$

which is called the Huber loss function. Δ is chosen to give the desired efficiency at the Gaussian model.

The Huber score function also provides an influence function $\Psi = \dot{\rho}$, that is bounded and continuous. Boundedness ensures that no single observation have large influence on the estimate, and continuity ensures that many rounding or quantization errors will have minimal effects.

Equating the first partial derivatives with respect to the elements of $\hat{\beta}_k$, that is $\hat{\beta}_{j,k}$, $j = 1...p$ equal to zero, the equivalent for finding the solution associated with the p equations is obtained

$$\sum_{i=1}^{n} x_{i,j,k} \Psi(y_{i,k} - x_{i,k}\hat{\beta}_k) = 0 \qquad j = 1...p, \tag{2.137}$$

where $x_{i,j,k}$ is the element in the i-th row and the j-th column of X_k. Observe that Ψ is nonlinear, hence Equation (2.137) can approximated as a weighted least squares expression

$$\sum_{i=1}^{n} x_{i,j,k} \omega_{i,k-1} (y_{i,k} - x_{i,k}\hat{\beta}_k) \approx 0 \qquad j = 1...p, \tag{2.138}$$

where the weights $\omega_{i,k-1}$ are given by

$$\omega_{i,k-1} = \begin{cases} \Psi(y_{i,k} - x_{i,k}^T \hat{\beta}_{k-1})(y_{i,k} - x_{i,k}^T \hat{\beta}_{k-1})^{-1} & \text{if } y_{i,k} \neq x_{i,k}^T \hat{\beta}_{k-1} \\ 1 & \text{if } y_{i,k} = x_{i,k}^T \hat{\beta}_{k-1}. \end{cases} \tag{2.139}$$

The solution to Equation (2.138) can then be formulated as

$$\hat{\beta}_k = (X_k^T \Omega_{k-1} X_k)^{-1} X_k^T \Omega_{k-1} Y_k, \tag{2.140}$$

where Ω_{k-1} is symmetrical, and the individual weights lie along its diagonal.

Now, the updated estimate from the standard Kalman filter recursion in Equation (2.75) is replaced by the estimate updating formula in Equation (2.140), based on Huber's score function in Equation (2.136), at each iteration of the filter. Updating the error covariance matrix can be dealt with trough use standard Kalman filter recursions [50], see Equation (2.75), and thus the M-robust Kalman filter derivation is complete.

2.3 Assessing Accuracy

The accuracy of an estimate depends on two quantities, the *reducible error* and the *irreducible error* [30]. Recall Equation (2.1) and Equation (2.2). The reducible error is the error introduced by the estimate $\hat{f}$, and is dependent on the estimation procedure used, while the irreducible error is a result of the error term ϵ. That is, even though $\hat{f}$ is a perfect estimate of f, there will still be error in the estimate $\hat{Y}$, since Y is also dependent on ϵ [30]. Achieving the best possible accuracy then entails minimization of the reducible error, since the irreducible error will provide an upper bound on the obtainable accuracy of the estimate.

Consider the estimation error, consisting of both the reducible and the irreducible error, given by

$$e_i = y_i - \hat{y}_i, \tag{2.141}$$

where y_i is the actual real value at iteration number i, and $\hat{y}_i$ is the estimate at time iteration number i.

In the subsequent sections different methods for evaluating accuracy, utilizing the estimation error, are presented.

2.3.1 Mean Squared Error

The mean squared error (MSE) measures the accuracy by squaring the estimation error. This results in that the MSE will be small if the estimated response is close to the true response, and large for when the estimate and true responses differ to a high degree [30]. Hence the goal of an estimate is to achieve the smallest possible MSE obtainable. MSE is given by:

$$\text{MSE} = \frac{1}{n}\sum_{i=1}^{n}(e_i)^2, \tag{2.142}$$

where n is the number of samples used, and e_i is the estimation error for sample number i.

2.3.2 Mean Absolute Error and Mean Absolute Percentage Error

Mean absolute error measures an average magnitude of all errors in a set of forecasts, ignoring the direction of the errors [35], hence all errors are assigned equal wights. The closer the MAE is to zero, the better the method evaluated fits the past time series. If MAE is shown to have a larger value, it would indicate that the method evaluated is a poor fit for the past time series [35].

$$\text{MAE} = \frac{1}{n}\sum_{i=1}^{n}|e_i|, \tag{2.143}$$

The mean absolute percentage error corresponds relatively to the MAE, but gives the accuracy a percentage and expresses the relative error [35]. If the MAPE value is less than 10% the estimate is considered to be very accurate. As the percentage increases, the accuracy worsens. MAPE is given by:

$$\text{MAPE} = \frac{1}{n}\sum_{i=1}^{n}\frac{|e_i|}{y_i}100\%. \tag{2.144}$$

2.3.3 Bias-Variance Trade-off

Consider Equation (2.142). For a given value x_0 it is possible to show that the MSE can be decomposed into the sum of three fundamental quantities [30]. That is

$$E[y_0 - \hat{y}_0]^2 = \text{Var}(\hat{f}(x_0)) + [\text{Bias}(\hat{f}(x_0))]^2 + \text{Var}(\epsilon), \tag{2.145}$$

where the three fundamental quantities are the variance of $\hat{f}(x_0)$, the squared bias of $\hat{f}(x_0)$, an the irreducible variance of the error term ϵ [30]. Hence, minimizing the reducible error, is achieved by minimizing both the variance and the bias of the estimate.

If an estimation method has high variance then small changes to the data, will result in large changes in the estimate, while high bias will introduce error by approximation [30]. Another way to interpret variance and bias is that high variance is related to over-fitting the data, while high bias results in under-fitting the data.

Assessing accuracy of an estimate is by that deducted into finding the estimate which has the lowest possible variance, while also having the lowest possible squared bias, which will insure neither over- nor under-fitting of the data. The trade-off relates to the dilemma of introducing one, to lower the other.

2.4 Glucose Dynamics

2.4.1 Steil–Rebrin model

In 1999 it was proposed by Rebrin *et. al* [52] that the relationship between blood plasma and interstitial fluid glucose were characterized by a gradient and a delay between plasma and interstitial fluid [52], described by a diffusion process. The proposed model will in this project be referred to as the *Steil-Rebrin model*, and describes the BG to ISF glucose dynamics block from Figure 2.2. The Steil-Rebrin model is a two compartmental model, where interstitial fluid glucose level and plasma glucose level are assumed convoluted [53]:

$$G_{isf}(t) = h(t) * G_p(t), \tag{2.146}$$

where G_{isf} is the glucose level in the ISF, also known as the second compartment, G_p is the glucose level in the blood plasma, also referred to as BG level, and is considered the first compartment, while $h(t)$ is the impulse response of the BG-to-IG system [54]:

$$h(t) = \frac{1}{\tau} e^{-\frac{t}{\tau}}. \tag{2.147}$$

This relationship can be formulated into a first order differential equation as given below:

$$\frac{dG_{isf}}{dt}(t) = -(k_{02} + k_{12})G_{isf}(t) + k_{21}\frac{V_1}{V_2}G_p(t), \tag{2.148}$$

where k_{02} represents a rate constant for the uptake of glucose in ISF in the subcutaneous tissue, k_{12} and k_{21} are rate constants for diffusion between the plasma and the ISF compartments, V_1 and V_2 are the volumes of the plasma and ISF glucose compartments, respectively [12]. The relationship described in Equation (2.148) is also visually described in Figure 2.8.

The relationship between the plasma glucose concentration and the ISF glucose concentration can then be transformed into:

$$\frac{dG_{isf}}{dt}(t) = -\frac{1}{T_{isf}}G_{isf}(t) + \frac{g}{T_{isf}}G_p(t), \tag{2.149}$$

where

$$g = \left(k_{21}\frac{V_1}{V_2}\right)T_{isf} \tag{2.150}$$

$$T_{isf} = \frac{1}{k_{02} + k_{12}}. \tag{2.151}$$

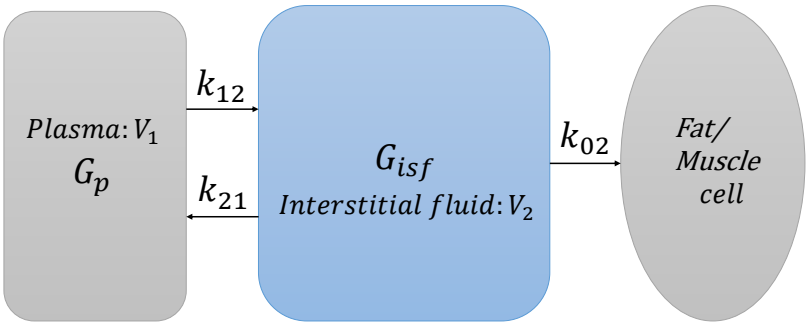

Figure 2.8: Compartmental representation of blood glucose and ISF glucose diffusion process dynamics, inspired by [12].

T_{isf} is the diffusion process time constant, hence may be recognized as τ from Equation (2.147). When the system in Equation (2.149) is at steady state, g equals the ratio $\frac{G_{isf}}{G_p}$ of the steady state concentrations. Physiologically this means that one can expect $g = 1$ [11]. Hence the expression from Equation (2.149) can be simplified:

$$\frac{dG_{isf}}{dt}(t) = -\frac{1}{T_{isf}}G_{isf}(t) + \frac{1}{T_{isf}}G_p(t). \tag{2.152}$$

2.4.2 Rearranging the Steil Rebrin Model

In [52] it is developed an intuitive approach for estimating the plasma glucose using Equation (2.152), where the diffusion process equation is rearranged in order to solve for BG level, given the ISF glucose level [31].

First consider Equation (2.152), this can be rewritten into the following:

$$\frac{dG_{isf}(t)}{dt} = aG_{isf}(t) + bG_p(t), \tag{2.153}$$

with

$$a \triangleq -\frac{1}{T_{isf}} \tag{2.154}$$

$$b \triangleq \frac{g}{T_{isf}} \tag{2.155}$$

Solving for $G_p(t)$ to achieve $\hat{G}_p(t)$ then yields:

$$\hat{G}_p(t) = \frac{\frac{dG_{isf}(t)}{dt} - aG_{isf}(t)}{b}. \tag{2.156}$$

In order to achieve a discrete formulation of the derivative, a FD approximation is used, which is explained in Section 2.2.5. This gives the following:

$$\hat{G}_{p,k} = \frac{\frac{G_{isf,k} - G_{isf,k-1}}{\Delta t} - aG_{isf,k}}{b} \tag{2.157}$$

$$\hat{G}_{p,k} = \left(\frac{1}{b\Delta t} - \frac{a}{b}\right) G_{isf,k} + \left(-\frac{1}{b\Delta t}\right) G_{isf,k-1}, \tag{2.158}$$

where Δt is the discrete time step.

2.4.3 Rate-only Model

The rate-only model is an inputless two state model for describing BG dynamics, developed in [14]. The first state is the BG level, G_p, and the second state is the blood glucose level rate of change, ΔG_p. ΔG_p is set to change by a gain of an observed rate of change a, and the derivative of G_p is only set to change according to ΔG_p. The system equations are:

$$\frac{dG_p(t)}{dt} = \Delta G_p(t) \tag{2.159}$$

$$\frac{d\Delta G_p(t)}{dt} = a\Delta G_p(t) + w(t). \tag{2.160}$$

For large values of a, ΔG_p will decay faster towards zero, while setting a equal to zero allows an observed rate of change to continue indefinitely [14].

The mathematical system given by Equation (2.159) and Equation (2.160) is combined with Equation (2.152), in order to obtain an observable system, with only ISF glucose level measurements.

$$\frac{dG_{isf}(t)}{dt} = -\frac{1}{T_{isf}} G_{isf}(t) + \frac{1}{T_{isf}} G_p(t). \tag{2.161}$$

$$\frac{dG_p(t)}{dt} = \Delta G_p(t), \tag{2.162}$$

$$\frac{d\Delta G_p(t)}{dt} = a\Delta G_p(t) + w(t). \tag{2.163}$$

From here on, ΔG_p will be denoted dG_p.

Expanding the system in such a way result in the block diagram given in Figure 2.9, in presence of noise and having CGM sensor signals as outputs, where the rate only model describes the BG dynamics block, while the Steil-Rebrin model describes the BG to ISF glucose dynamics.

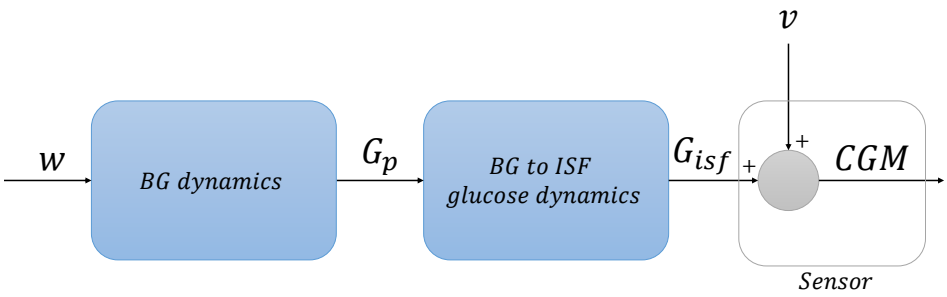

Figure 2.9: Block diagram describing the glucose dynamics of blood and the diffusion into ISF.

2.4.4 Central-Remote Rate Model

One way of achieving a dynamical model of blood glucose is to divide the glucose rate from Equation (2.160) into two new states, a central and a remote compartment, referred to as C_c and C_r, respectively. Inputs affecting the BG level, such as meals or insulin, will first affect the remote compartment, and then by a first order delay diffuse over to the central compartment, and finally it will take effect on the BG level [14]. Such inputs are modeled as disturbances to the system , hence the model is considered inputless. The state-space equations are as followings:

$$\frac{dG_p}{dt}(t) = C_r(t) \tag{2.164}$$

$$\frac{dC_c}{dt}(t) = -\frac{1}{T_d}C_c(t) \tag{2.165}$$

$$\frac{dC_r}{dt}(t) = \frac{1}{T_d}(C_c(t) - C_r(t)) + w(t), \tag{2.166}$$

where T_d is a time constant, describing the diffusion rate between the central and remote compartments [14].

The system equations given by Equation (2.164), Equation (2.165) and Equation (2.166) is combined with Equation (2.152), in order to obtain an observable system.

$$\frac{dG_{isf}(t)}{dt} = -\frac{1}{T_{isf}}G_{isf}(t) + \frac{1}{T_{isf}}G_p(t). \tag{2.167}$$

$$\frac{dG_p}{dt}(t) = C_r(t) \tag{2.168}$$

$$\frac{dC_c}{dt}(t) = -\frac{1}{T_d}C_c(t) \tag{2.169}$$

$$\frac{dC_r}{dt}(t) = \frac{1}{T_d}(C_c(t) - C_r(t)) + w(t). \tag{2.170}$$

This system is also described by Figure 2.9, in the equal manners as the rate-only model.

2.5 System Identification

System identification is the problem of building a mathematical model of a dynamic system using measurements of the input and output signals of that system [55]. A system is in this work considered to be an object in which different variables interact at all kinds of time and space scales, and observable signals are produced. These variables usually consists of input u, disturbance w, state x, disturbance v and output y. The way these variables interact within a system and a sensor is described in Figure 2.10. In system theory there are four problem areas that can be distinguished: *modeling*, *analysis*, *estimation* and *control* [56]. The system identification problem directly involve the modeling and estimation areas.

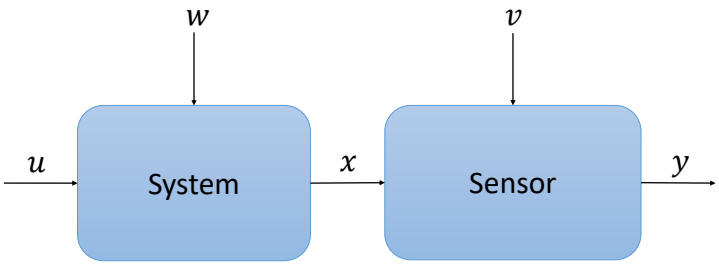

Figure 2.10: General system representation.

Modeling is the critical step of finding a mathematical model which adequately describes the physical process of the relevant system. Both the system boundaries and the system variables have to be specified. The relationship between the variables is then based upon prior knowledge, and assumptions about the uncertainties are made. These steps will together define the model structure [56].

When a model is set, the problem of estimating the unknown variables is the next step. The estimates will be based upon a given set of input and output signals. This estimation step may be divided

into three sub-steps: State estimation, parameters estimation and parameter, also called system, identification [56].

The process of system identification can be summarized by the following steps [55]:

- Obtain observable input and output signals of the system.
- Select a model structure.
- Apply an estimation method to estimate the parameters in the candidate model structure.
- Evaluate the estimated model to assure it adequate for the relevant application.

These steps can be formulated into a loop, where if the model is not evaluated to be appropriate, the procedure starts over again. The system identification loop is visualized in Figure 2.11.

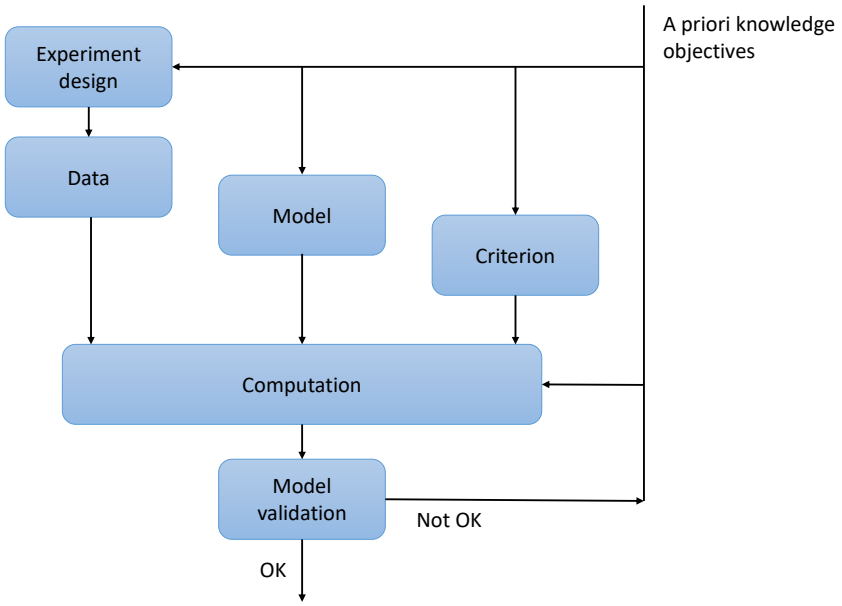

Figure 2.11: System identification loop, inspired by [56].

The data, or input and output signals, are often collected based on prior knowledge of the system. This again allows for an appropriate experiment design for the collection of data. The model candidate can be chosen through three different ways: white-box modeling, black-box modeling and grey-box modeling [55]. Only the latter is relevant in this paper. In grey-box modeling the model structure can be deduced by physical principles, while the model parameters are less known and needs to be estimated from relevant data.

Once a model candidate is settled, an evaluation of the fit to the data is the next step. The quality of the model is measured by [55]:

- Compare Model Response to Measured Response
- Analyze Residuals
- Analyze Model Uncertainty

Comparing the model to measured data is a way of assuring that the model in question is reliable and will produce responses equal or at least similar to relevant measured data. The potential error between the measured data and the model in question is called a residual, hence the residual is the portion of output data that cannot be explained by the model [55], and this needs to be evaluated in order to asses the model accuracy. One common way of analyzing the residuals is by looking at the RSS, and try to minimize this sum. This will ensure a *least-squares* estimate of the model parameters [56].

Validation is the final step of one iteration of the system identification loop. In this step the model is evaluated and decided to be good enough, or not good enough. If the case is the latter, then the loop has to be repeated.

Chapter 3

Project Aim

The aim of this thesis is estimation of BG level, and other states within the body, using only interstitial fluid glucose level measurements, obtained by a CGM sensor, in real time. Such aim involves modeling of sensor dynamics, as well as pharmacodynamics between blood and subcutaneous tissue, and investigation of estimation algorithms, with real-time qualities. This aim is a continuation of the aim of the term project, and builds upon the work done during that project.

In the term project a four state central-remote rate model was used to model blood glucose dynamics, while the Steil-Rebrin model was used to model diffusion of glucose between blood and subcutaneous tissue compartments. A Kalman filter was used to produce estimates, while an unknown input Kalman filter was attempted, but not successfully implemented. For measuring the fit of the estimate to BG level measurement obtained by a BGA, accuracy measures such as MAE, MSE, RMSE and MAPE were utilized.

Concluding remarks of the term project are thus considered essential building blocks in achieving the aim of this thesis. It was concluded the Kalman filter is a suitable method for achieving estimation in real time. However, estimate robustness was a lacking quality of the filter, hence should be investigated and improved upon in future work. Unknown input filters were still considered a possibility, seen as minimal results of such a filter was obtained during the term project. Using MSE, MAE, RMSE and MAPE, with BGA measurements as the comparing value, was also considered too thin of an analysis of the estimation algorithms fit for estimating BG level, hence improvements should be made in this area. Feedback regarding the model was also given in the aftermath of the term project, stating that it being too complex, given the purpose.

Based on these concluding remarks, some specific goals, in addition to the overlying aim, for the master thesis were constructed. Different forms of Kalman filters and models should be tested, and their performance of estimating BG level be evaluated, with added emphasis on estimate robustness and reducing model complexity, as well as improving upon the estimate accuracy assessment of the term project.

Chapter 4

Data Acquisition

The data used for the simulations in this paper is collected through five animal experiments performed in the animal faculty of NTNU. These experiments were conducted on five anesthetized pigs whose endogenous insulin and glucagon secretions were suppressed using Octreotide (Sandostatin) with a rate of 5 µg/kg/h. In addition, intravenous glucose infusion was used to simulate different meals. In order to control the BG level, intraperitoneal insulin and glucagon administrations were used.

The CGM sensors used in these experiments were the Medtronic Enlite sensor (Northridge, Canada), which is assumed related to the ISO 15197:2015 standard. These sensors were paired with Inreda Diabetic transmitters (Goor, the Netherlands), providing measurements with a sampling rate of 1.2 s. In order to measure the BG level directly, blood samples were taken sporadically, varying between every 5 min-1 hour, and analyzed by ABL800 FLEX analyzer (Copenhagen, Denmark), which is a BGA system.

Chapter 5

Implementation

This chapter will present the literature search and the code implementation of this thesis' work. A list of all code files, as well as a short description of their main function, and input and output variables can be found in Appendix A, and the code itself is available in the attachments.

5.1 Literature Search

Searching for appropriate models was done trough a literature search using Google Scholar, and reviewing the results of the term project [1]. Much of the work in the term project is based on the modeling of glucose dynamics in [14], hence this paper was once again a first inspiration of choosing model, which resulted in the rate-only model, explained in Section 2.4.3. Other models found during the literature search was the Setil-Rebrin model, [52], see Equation (2.152), and the rearranged Steil-Rebrin model, [12], see Equation (2.156).

Having established models, their model parameters were needed identified for this thesis' provided data sets. The theory for this is mostly gained through the help of this thesis' co-supervisors, as well as [56].

Once models were chosen, and parameters were identified, the next step was to decide what estimation algorithms to use. A standard Kalman filter had already been tested in the term project, however seen as only one model was used in that project, the filter was once again considered in this thesis. The Kalman filter used in this thesis is based on the description given in [31], explained in Section 2.2.6. By reviewing literature the unknown input filter from [46], explained in Section 2.2.7 was found, as well as the robust filter in [50], explained in Section 2.2.8.

Accuracy assessment of estimates is greatly based on the work from the term project [1]. However some additional considerations and theory is retrieved from [30] and [31], namely considerations of bias and variance, and assessment of estimate standard deviation, respectively.

5.2 Code Implementation

All code developed for this thesis is done so in Matlab, using a NTNU student Matlab license, and the code is run on a computer with a Intel(R) Core(TM) i5-8250U CPU @ 1.60GHz 1.80 GHz processor. Matlab provides a wast library of inbuilt functions, which is greatly utilized in the thesis' code. All specific inbuilt functions will not be listed or mentioned here, with the exception of functions which serve a main purpose in the described methods. Below, all function- and script files will be explained in detail, both how they are built and how to run them. Figures, not referenced in the caption, are made using Microsoft PowerPoint.

5.2.1 Model Parameters Identification

Model parameters are identified in `modelParamEst.m`, which is a separate Matlab script file, hence this file is not connected to the main file of the code. The identification process is developed in line with the explanation given in Section 2.5. Experiments obtaining data had been performed prior to the thesis, hence the experimental design step of Figure 2.11 was skipped. Difference in sampling time between CGM and BGA measurements are dealt with by the developed function, `getEqualLenVec.m`, which finds the closest measurements in time between the two vectors, and generates a new vector containing only interpolated measurements.

The time constant from the Steil-Rebrin model, see Equation (2.152), is identified first, by estimating the ISF glucose level, given BG level as inputs. Then by comparing the estimated ISF glucose level to actual CGM measurements, the RSS is calculated. Minimizing the RSS then becomes an optimization problem, with T as the changing variable:

$$J(T) = min_T(y - \hat{y}(T))^2. \tag{5.1}$$

The minimum is found using `fminsearch(...)` with T as the changing variable. `fminsearch` uses the Nelder-Mead simplex algorithm to find the minimum [57], and it solves the optimization problem in an unconstrained manner. When discretizing the differential equation in Equation (2.152) Δt is set to 5 min.

The identification of the rate of the decay of the BG level, a from Equation (2.161) is done in a similar manner. Again the cost function Equation (5.1) is used, however now $\hat{y}$ is computed using Equation (2.161). Using the BGA measurements, the first and second derivative of the blood glucose is computed. The first derivative is then used as an input in order to generate an estimated second derivative using Equation (2.161). Then using the actual calculated second derivative from the BGA measurements as y, the corresponding RSS value is calculated. The code implementation of the optimization problem using a as the variable was implemented the same way as the identification of T.

5.2.2 Model Construction

The construction of models is dealt with by a function called `setModel.m`. The function checks for which model is requested, and provides a structured array, where the model specifics are set as data

fields. The models are implemented in accordance with the descriptions given in Section 2.4.1 and Section 2.4.3.

5.2.3 Estimation Algorithms

The estimation algorithms are implemented in separate Matlab function files, and are requested and called from the main Matlab file. All estimation algorithms are fed the same function parameters: CGM time and measurement vector, specified model parameters, CGM sampling time Δt, BGA time and measurement vector for plotting and variable arguments for either plotting or enchantments of the estimate. The structure of the variable arguments, and the handling of them, is greatly inspired by [58].

Further, the functions are built using approximately the same structure. First, the requested arguments are handled by a helper function, then the CGM time vector is verified as or changed to relative time, using `convertToRelativeTime.m` which is a borrowed function from [58]. Then a model is built, storage for important vectors are declared and vectors are initialized, corresponding to the model requirements. A for loop is next, where the relevant estimation algorithm is performed for a number of iterations, corresponding to the length of the CGM time vector. Once done, an output structured array is built, containing all estimates and estimate standard deviations, before plotting, if requested, is performed. Helper methods, where necessary, are located below the main function of the individual estimation function files. The individual estimation function files are `FD-approx.m`, `standardKF.m`, *robustTwoStageKFui.m* and `MrobustKF.m`, and the estimating structure of the for-loops are implemented as described in Section 2.2.5, Section 2.2.6, Section 2.2.7 and Section 2.2.8, respectively.

Available models and enhancement methods for each estimation algorithm can be found in Table 5.1, while tuning variables, and their locations, are listed in Table 5.2.

5.2.4 Enhancement Methods

Enhancement methods are implemented such that they are optional, and have to be requested by a user, for each estimation algorithm. The choice is given as a variable argument, for which if non is specified, will be set to zero, which equals not to run the method.

Low Pass Filter

In order to perform low pass filtering of measurements the relevant model has to be augmented by an additional state, in order to compensate for introduced time lag by the filter. This is done in the `augmentWithLPF.m` function.

The filtering itself is implemented according to the description given in Section 2.2.2, and is performed at the start of the estimation algorithms for-loop. The smoothing factor, see Equation (2.14), is set in `main.m`.

Moving Average Smoother

MA smoothing is implemented using the inbuilt Matlab function `smooth(...)`, which uses moving average estimation according to Section 2.2.3. Smoothing is performed after a given number of iterations has passed, `Ns`, which is specified in the individual estimation algorithm function files, and is always performed after the computation of the current estimate. The span of the MA smoother is the same as the number of iterations between every smoothing execution. If MA smoothing is requested the filter output structured-array is expanded to include a new field containing the smoothed BG level estimate.

Regression

Linear regression is implemented according to the description given in Section 2.2.4, and WLS LR is implemented according the description given in Section 2.2.4, in a separate Matlab function file, called `linearRegression.m`. Regression is performed after a specified number of iterations, `Nreg`, which is set in the individual estimation algorithms function files.

The function is implemented with two bool parameters, referring to using intercept or not, and for using WLS or not. In the estimation algorithm the first execution of linear regression always uses intercept, while the subsequent executions are by default set to not use intercept, in order to get piece-wise connected regression of estimates. The last element of the previous regressed estimate, is then used as the starting point of the current regression. By default, regression is also performed using WLS LR in all estimation algorithms. The filter output structured array is expanded to include a new field containing the regressed BG level estimate, if the method is requested.

5.2.5 Accuracy Assessment

Accuracy assessment is done in the function file `computeError.m`, and uses the definitions of MSE, see Equation (2.142), and MAPE, see Equation (2.144), to measure accuracy of estimates. Due to the different lengths of BGA and CGM measurement, `getEqualLenVec.m` is used to interpolate the two vectors, before the accuracy is calculated. Accuracy assessment is performed in the individual estimation algorithm function files, after calculation of the estimates.

The calibration time window is not used in the accuracy calculations, in order to achieve a fair comparison. Therefor the end-of calibration window were needed identified. This is done by locating the end-of calibration window on the x-axis, and then finding the corresponding iteration number in the CGM and BGA time vectors.

5.2.6 CGM and BGA data

Functions for collecting data from CGM and BGA data sheets are called `getCGMdata.m` and `getBGAdata.m`, respectively. The structure of these functions were provided by the co-supervisors of this thesis.

5.2.7 Main file

At the start of `main.m`, all data sets are listed. Choosing one data set for running estimation simulation is done by uncommenting the requested data set. Data is retrieved by use of `getBGAdata.m` and `getCGMdata.m`. Once data is retrieved the time vectors are handled by `convertToRelativeTime.m`.

Model parameters are then set, and if required, adjusted. The model parameters in question are the diffusion time constant `T`, the BG level rate of decay, `a`, the LPF smoothing factor, `b` and the sampling time of CGM measurements, `dt`.

Next is the section of choosing which estimation algorithm to use. This is implemented as `do_X`, `X` referring to the estimation algorithms, where if, set to `1`, the algorithm is run, and if set to `0` it is not run. In addition to estimation algorithms, optional measurement comparison is also included here.

The reminder of the main file then consists of if-sentences checking if the `do_X` variable is set true, or not. Inside the if-sentences the estimation algorithm is performed, generating an output consisting of the filter output and the accuracy assessment output. The measurement comparison is the exception to this structure, where only accuracy assessment is computed and the plotting of the measurements are performed. Requested enhancement methods are specified in the calling of the estimation algorithms.

5.2.8 Simulated System

In addition to the M-robust KF function file itself, it was decided to make a script for M-robust estimation, using a simulated data. This is done in `SimSys.m`, and the file includes a true system response, a M-robust KF estimate and a standard KF estimate, for comparison. The simulated system is simulated using the rate-only model in combination with the Steil-Rebrin model, and noise processes are modeled as $\sigma_w = 1$ [mmol/L] and $\sigma_v = 0.5$ [mmol/L]. Seen as the noise processes are known, no tuning of the corresponding noise covariance matrices are needed. Simulation time duration is set to 250 iterations, with sampling time $\Delta t = 0.02$. The implementation of random noise affecting the state and measurement vector during the for-loop, as well as triggering outliers in the measurement vector, are inspired by an example system from [59].

5.3 Tuning and Noise Modeling

The measurement noise covariance matrix, R, is set according to ISO 15197:2015 standard in all variation of filters, see Section 2.1.2 for exact values. Process noise covariance, Q, is tuned individually between every model, through a trial and error approach. This approach entails observing the filter response in figures, comparing it to BGA samples, as well as trying to minimize the MSE and MAPE of the estimate. A similar strategy was used to tune the LPF smoothing factor b, with the added consideration of bias-variance trade off, as well as introduced time lag. Smoothing and regression intervals respectively, are tuned according to the bias-variance trade-off, as well as keeping an eye on iteration run time.

Table 5.1: Matrix showing which model is available to use for which estimation algorithm, as well as what estimation algorithm is implemented with what type of enhancements method.

		FD approximation	KF	RTSKF-UI	M-Robust KF
Model	Steil-Rebrin, G_p as input	0	0	1	0
	Rearranged Steil-Rebrin	1	0	0	0
	Rate-only	0	1	0	1
Enhancements	Low-pass filter	0	1	0	1
	MA smoother	1	1	0	1
	WLS LR	1	1	0	1

Table 5.2: Tuning variables, and their respective locations in the Matlab project file.

Tuning variable	Location
`Q`	`setModel.m`
`R`	`setModel.m`
`b`	`main.m`
`Nreg`	`FDapprox.m`, `standardKF`, `robustTwoStageKFui.m`, `MrobustKF.m`
`Ns`	`FDapprox.m`, `standardKF`, `robustTwoStageKFui.m`, `MrobustKF.m`

Chapter 6

Results

This section will present results based on the data sets, the model parameter identification, the simulation of the estimation algorithms and the accuracy assessments. Only results from the Mar 5th, 2021 data set, see Figure 6.2, is displayed in this section. Please see Appendix B for results regarding the remaining data sets. Results relating to the central-remote rate model can be found in the term project report, see [1], or in a pending approval conference paper, see Appendix D.

6.1 Data Sets

Based on visual interpretations of the data sets, the Nov 18th, 2020 data set is omitted from the estimation part of this thesis, due to flawed sensor readings. This results in four data sets, from now on referred to as the data sets.

The weight of the animals in the animal experiments are reported in Table 6.1. Notice that two of the cells are not filled, the ones for Nov 20th, 2020 and Nov 18th, 2020. These weights are unknown in this work.

The identified end-of calibration window, which marks the time in which the sensor is finished calibrating, was identified and the results are displayed in Table 6.1, as are the identified start- and end of meal time, given in iteration number of the BGA measurement vector.

In Figure 6.1b there are depicted a set of characteristics from the CGM sensor readings, identified as significant for this thesis's work, and the observed characteristics are evident in all data sets. (1) describes the sensor calibration window, (2) describes typical sensor anomalies, while (3) is a close up of the measurement slope characteristics.

An example of the diffusion process time constant effect can be viewed in Figure 6.1a, where the difference in time is the colored column between the two marked points.

6.2 System Identification

Results from model parameter identification can be found in Table 6.2, where T, see Equation (2.152) and a, see Equation (2.160), are identified for all data sets. The starting point was set to 10 min and -0.05 for T_0 and a_0, respectively, in all identification processes.

Three different time constants will be used throughout the estimation procedures, on order to asses the overall best general time constant. The chosen time constants are of the lower end, the middle end, and the higher end of the spectrum of time constants identified, see Table 6.2. For simplicity the time constant values are rounded up, or down, to whole numbers, meaning the three time constants are $T = 4, 6, 8$ min, which gives three simulations, while a will be set as the averaged of all identified a's, due to minimal estimate reaction when adjusting the value within the interval of identified a's. This results in $a = -0.0018$.

6.3 Estimation Results

In all displayed figures, estimated BG level is referred to as $\hat{G}_p$, MA smoothed estimates are referred to as $\hat{G}_{p,s}$, regressed estimates are referred to as $\hat{G}_{p,reg}$, while low-pass filtered measurements are referred to as CGM_{lpf}. ISF glucose level estimate is referred to as $\hat{G}_{isf}$, while BG level rate of change is referred to as $d\hat{G}_p$. BGA and CGM measurements are referred to as BGA and CGM, respectively. In figures displaying estimate standard deviation, σ_x will describe the standard deviation of estimate $\hat{x}$.

Only simulations with $T = 6$ min are displayed in this section, as well as in Appendix B and Appendix C, while MSE and MAPE are reported for all different T's. The estimates are shown for the entire experiment time window, as well as a close up for one meal.

The maximum running time per for-loop iteration can be found for all estimation algorithms, with all available enhancement methods, in Table 6.4.

6.3.1 FD Approximation

Resulting FD approximation of BG level, in addition to the available enhancement methods for FD approximation, can be found in Figure 6.3, while the corresponding MSE and MAPE scores can be found in Table 6.5-Table 6.8. Observe highly oscillating noisy characteristics of the estimates, appearing as blocks of color in the figures. Also take note of whenever CGM measurements are seen having a slightly more dramatic increase or decrease, the estimate responds by spiking even more dramatically. Accuracy scores appear decent, for both the filter and the enchantment methods, as well as consistent among different time constants.

6.3.2 Kalman Filter

Results for KF estimation of BG level, in addition to the available enhancements methods for the KF approach, can be found in Figure 6.4, while the corresponding MSE and MAPE scores can be found in Table 6.5-Table 6.8. Observe that whenever the CGM changes with a higher than normal rate, the KF estimate mimic the changes more aggressively. This characteristic are smoothed with the MA smoother, and slightly worsened by the WLS LR. With LPF measurements such effects appear softer, however, are not eliminated. Notice the increase in standard deviation of estimates, when using LPF for the measurements, which is visible in Figure 6.5. Accuracy scores between Mar 1st, 2021 and Mar 5th, 2021 are similar in value, while their scores differ for what is reported for Mar 10th, 2021 and Nov 20th, 2020. Note that accuracy scores are pretty consistent among different diffusion time constants.

6.3.3 Robust Two Stage Kalman Filter with Unknown Inputs

RTSKF-UI estimation results of BG level can be found in Figure 6.6, while the corresponding MSE and MAPE scores can be found in Table 6.5-Table 6.8. Notice that the estimate show much of the same characteristics as the FD approximated BG level does. The noisy appearance is reflected in the SD figure, see Figure 6.6b, where the BG level is seen having much higher SD, compared to the estimated ISF glucose level. Accuracy scores are quite low, but still among the highest reported in this thesis.

6.3.4 M-Robust Kalman Filter

M-robust KF estimation results of BG level, in addition to the enhancement methods available for this approach, can be found in Figure 6.7, while the corresponding MSE and MAPE scores can be found in Table 6.5-Table 6.8. Notice how similar the robust estimate is to the normal KF estimate, which is also reflected in the accuracy scores, where the scores between the two methods are remarkably similar. The same standard deviation response to LPF of measurements is seen in Figure 6.8, as was observed for the KF.

Robustness of the M-robust KF estimate is more visible in Figure 6.9, where a rate-only model is used with simulated ISF glucose measurements. Take note of the similarities between the true response of the real system and the M-robust estimate of the ISF glucose level, and how the KF estimate differ.

6.4 Tuning Results

Final tuning values for process- and measurement noise covariance matrices, LPF smoothing factor, and smoothing and regression intervals are given in Table 6.3. Additional tuning results, based on extremes of the reported final tuning values, are located in Appendix C.

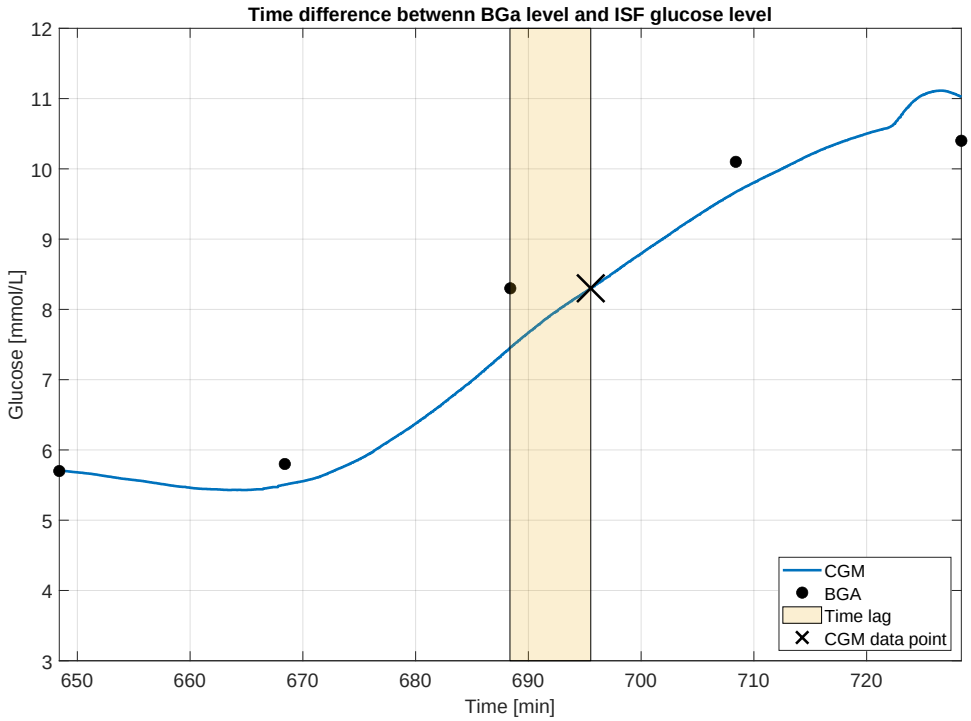

(a) Figure for illustrating the difference in time between BG level, measured by a BGA, and ISF glucose level, measured by a CGM sensor.

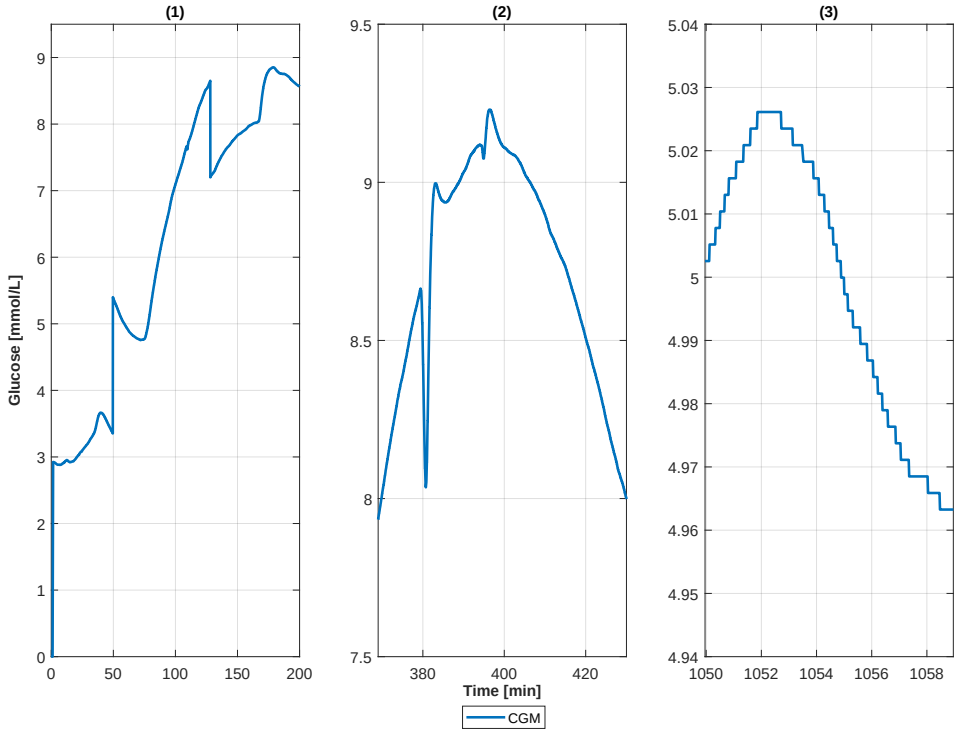

(b) Observations about the CGM sensor readings characteristics. (1) shows the sensor calibration interval, (2) shows the sensor anomalies and (3) shows a close up of the measurement slope.

Figure 6.1: Observations of CGM measurements, based on Mar 5th, 2021 data set

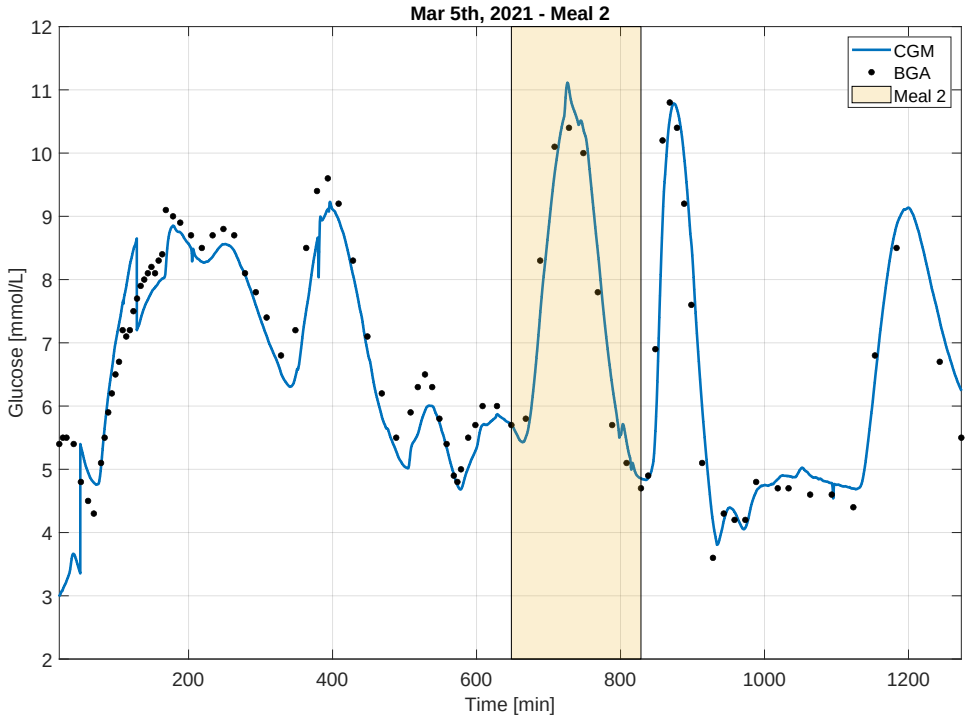

Figure 6.2: Mar 5th, 2021 data set, with highlighted interval for meal number two.

Table 6.1: Weight of experiment animal in [kg], experiment duration in minutes and number of samples of CGM and BGA, CGM_{tot} and BGA_{tot}, respectively, identified end-of calibration window for BGA measurements, $BGA_{eoc,i}$, identified start of and end of one meal for BGA measurements, $BGA_{i,Mstart}$ and $BGA_{i,Mend}$, respectively, and MSE and MAPE values between CGM and BGA measurements, given in [$mmol^2/L^2$] and [%], respectively, all of which is reported for each data set.

	Data set			
	Mar 10th, 2021	Mar 5th, 2021	Mar 1st, 2021	Nov 20th, 2020
Weight [kg]	40	36	36	-
CGM_{tot}[min]/CGM_{tot}	1352.8/80742	1291.5/75870	1279.2/73419	717.2/42834
BGA_{tot}[min]/BGA_{tot}	688.8/64	1273.4/94	1259.6/87	695.4/96
$BGA_{eoc,i}$	6	19	19	9
$BGA_{i,Mstart}$	7	60	54	9
$BGA_{i,Mend}$	45	70	65	51

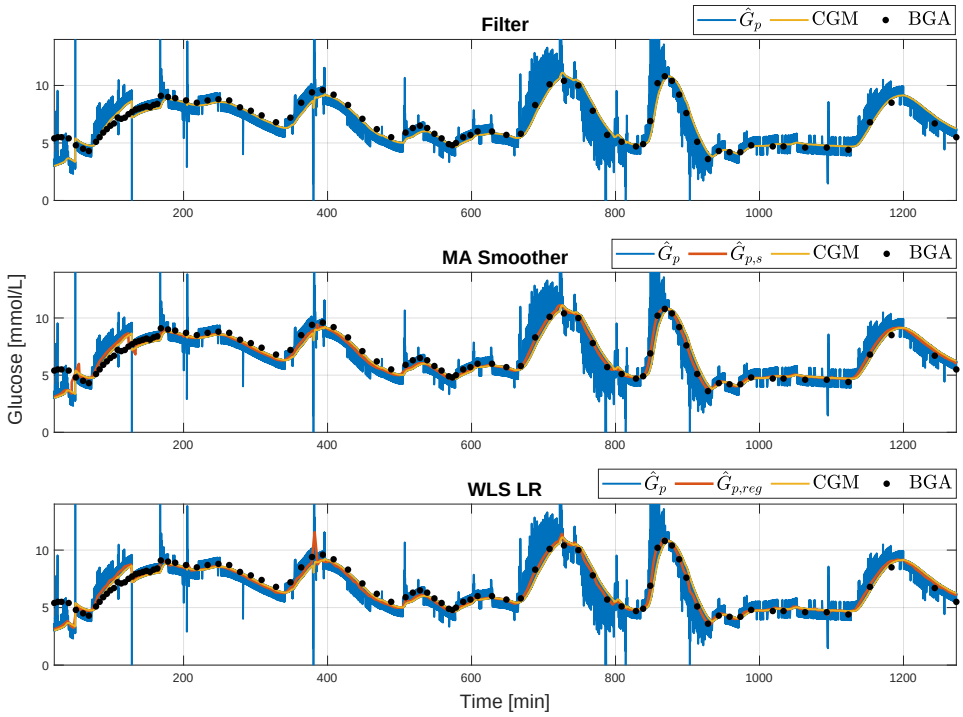

(a) FD approximation of BG level, with enhancements MA smoothing and WLS LR.

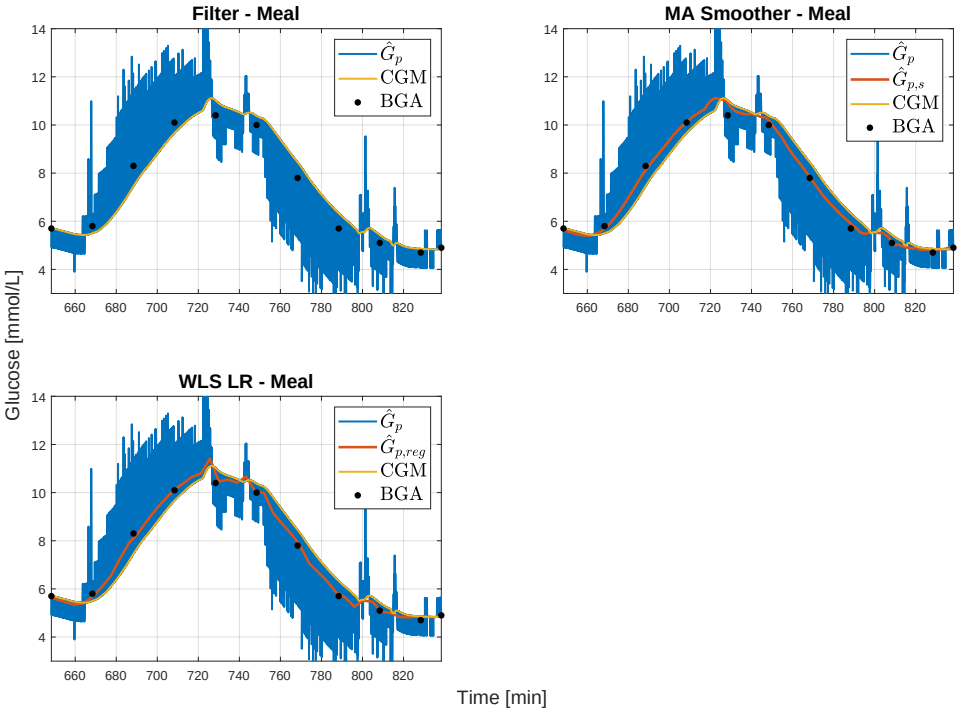

(b) FD approximation of BG level, with enhancements MA smoothing and WLS LR, zoomed in on meal number two.

Figure 6.3: FD approximation results for the Mar 5th, 2021 data set.

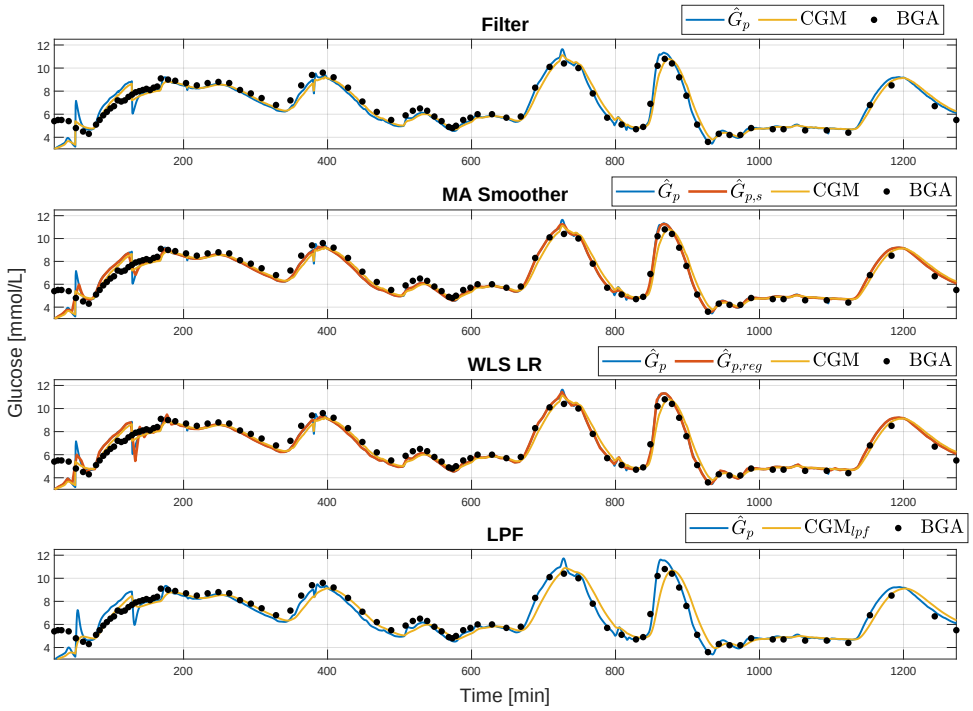

(a) KF estimate of BG level, with enhancements.

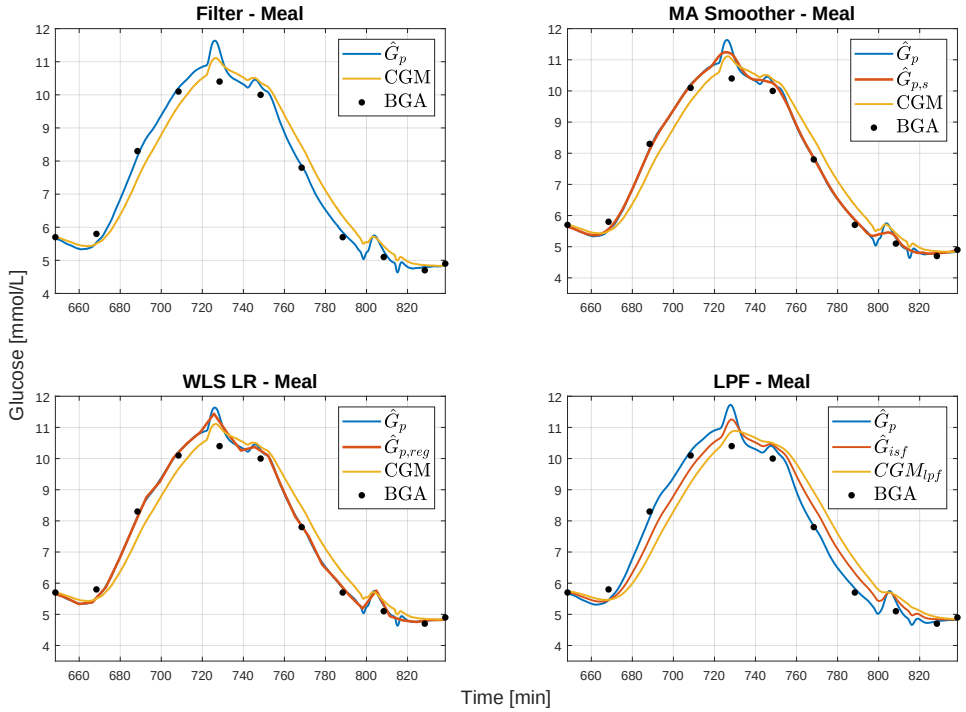

(b) KF estimate of BG level, with enhancements, zoomed in on meal number two.

Figure 6.4: KF results for the Mar 5th, 2021 data set.

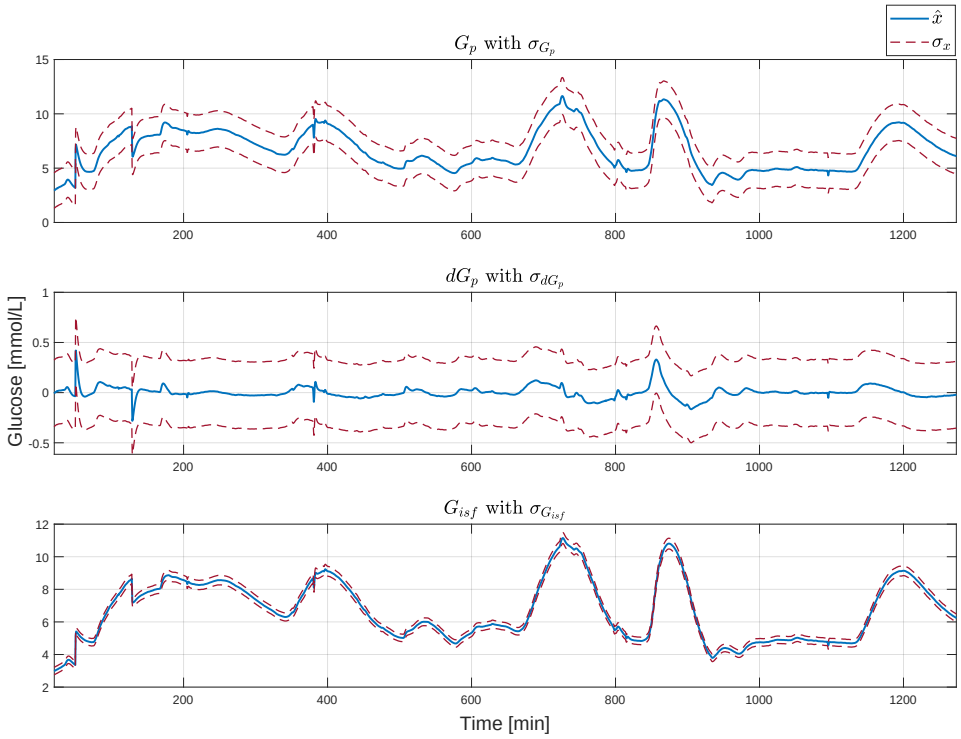

(a) KF estimate of BG level, with SD.

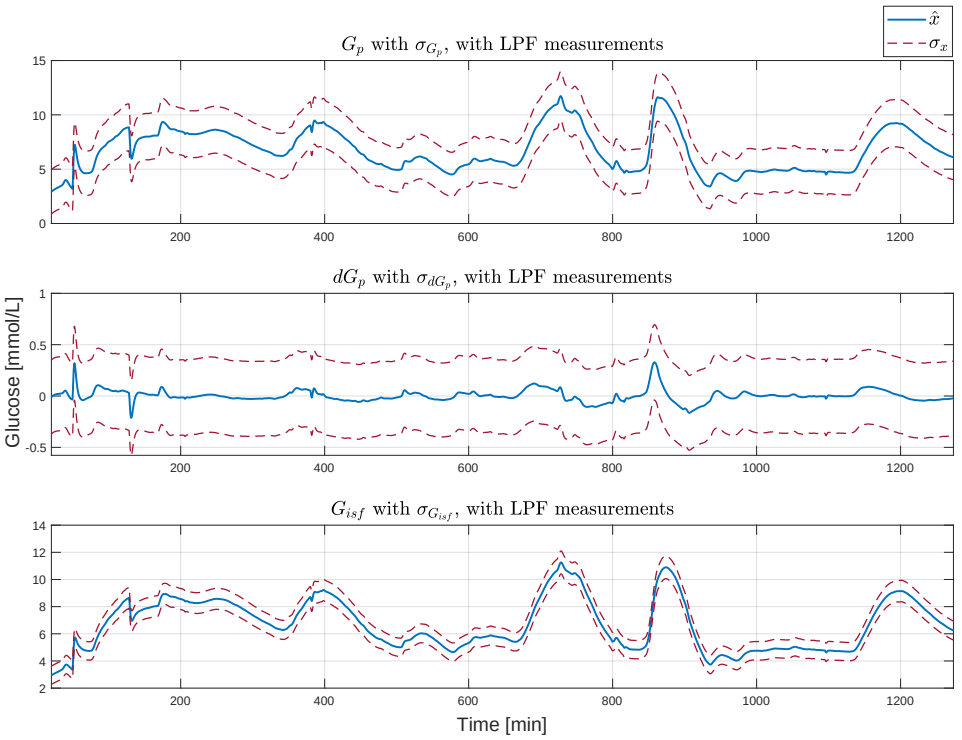

(b) KF estimate of BG level, with LPF measurements, with SD.

Figure 6.5: KF results for the Mar 5th, 2021 data set, displayed with SDs. $\hat{x}$ describes estimate x, while σ_x referrers to the standard deviation of estimate x.

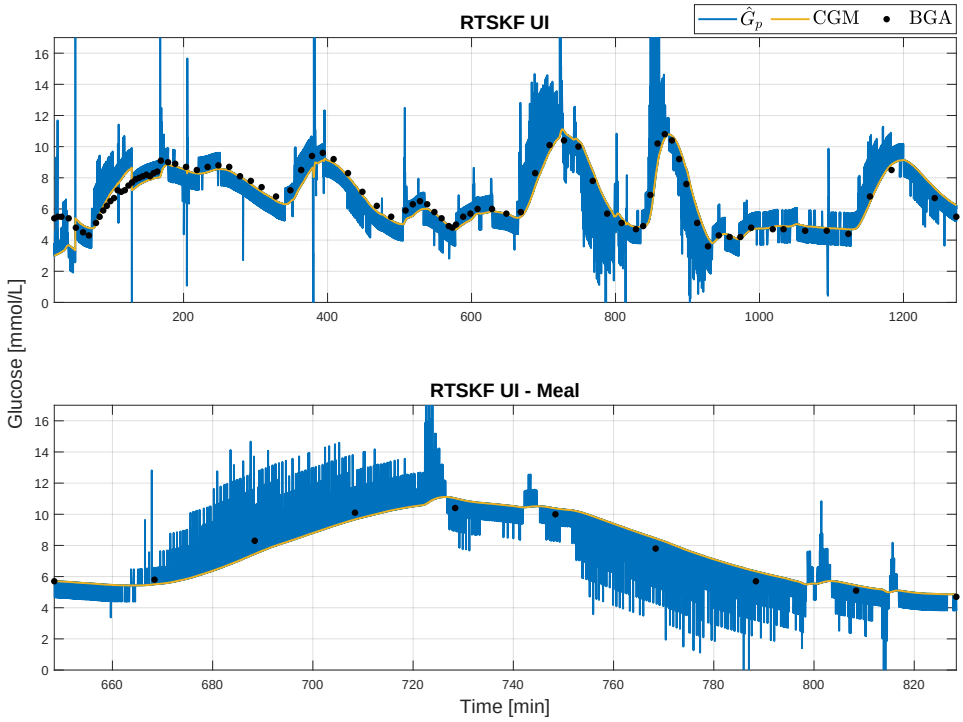

(a) RTSKF-UI estimate of BG level, for the entire data set and zoomed in on a meal.

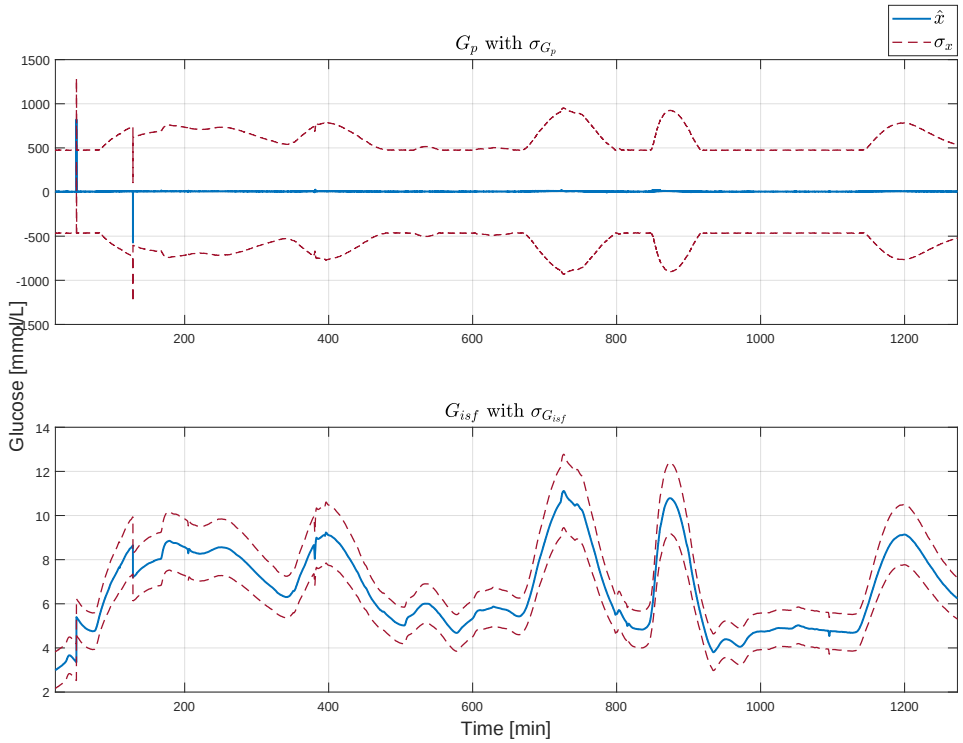

(b) RTSKF-UI estimate of BG level, with LPF measurements, with SD.

Figure 6.6: RTSKF-UI results for the Mar 5th, 2021 data set.

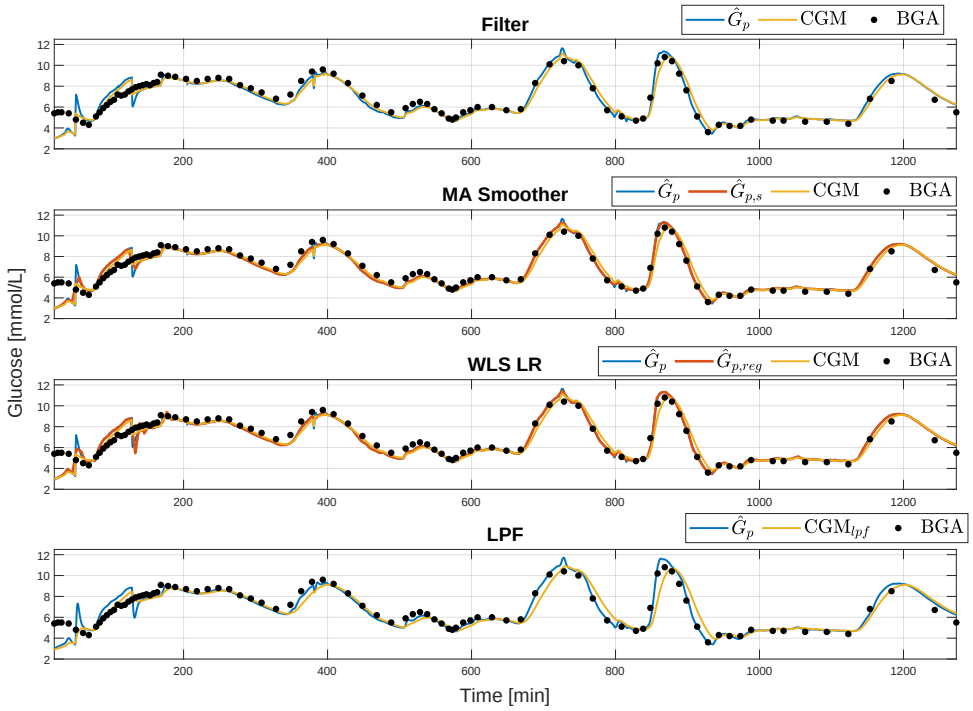

(a) M-robust KF estimate of BG level, with enhancements.

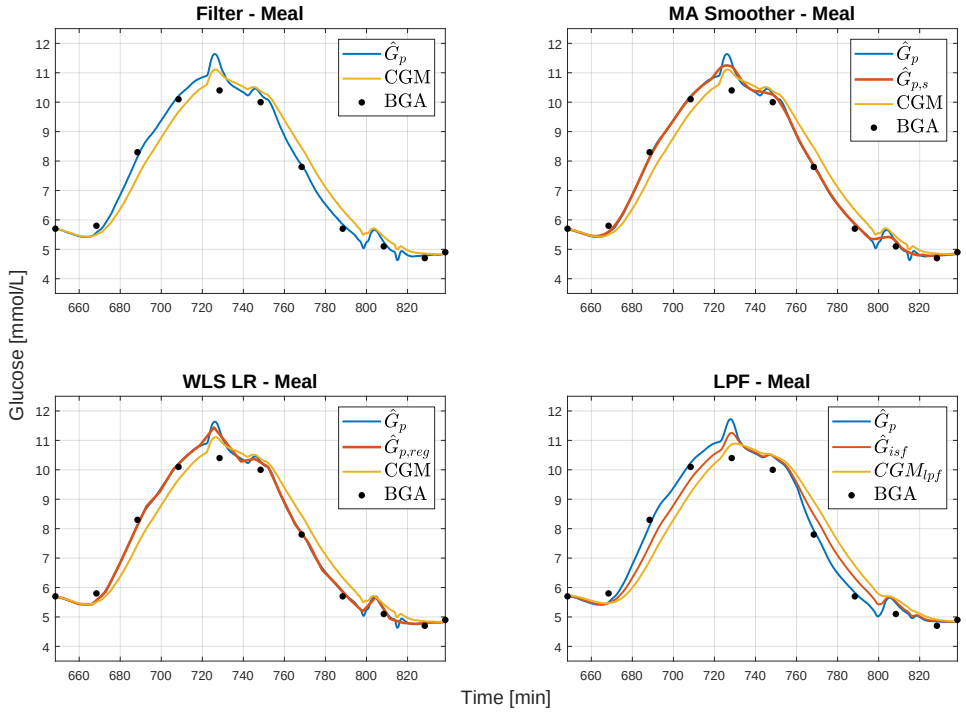

(b) M-robust KF estimate of BG level, with enhancements, zoomed in on meal number two.

Figure 6.7: M-robust KF results for the Mar 5th, 2021 data set.

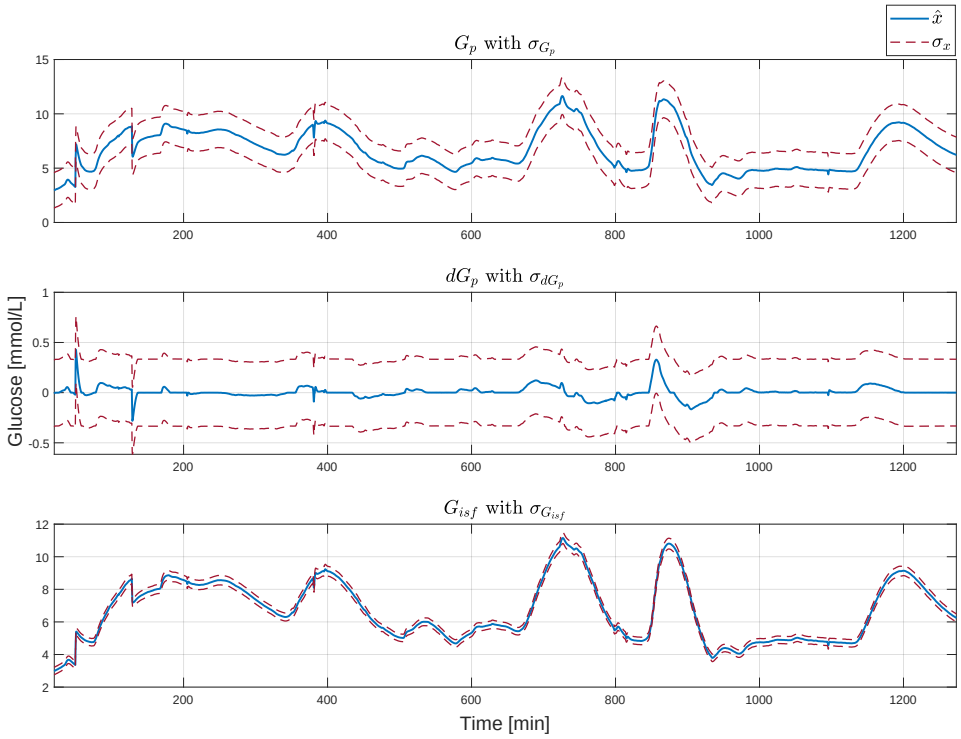

(a) M-robust KF estimate of BG level, with SD.

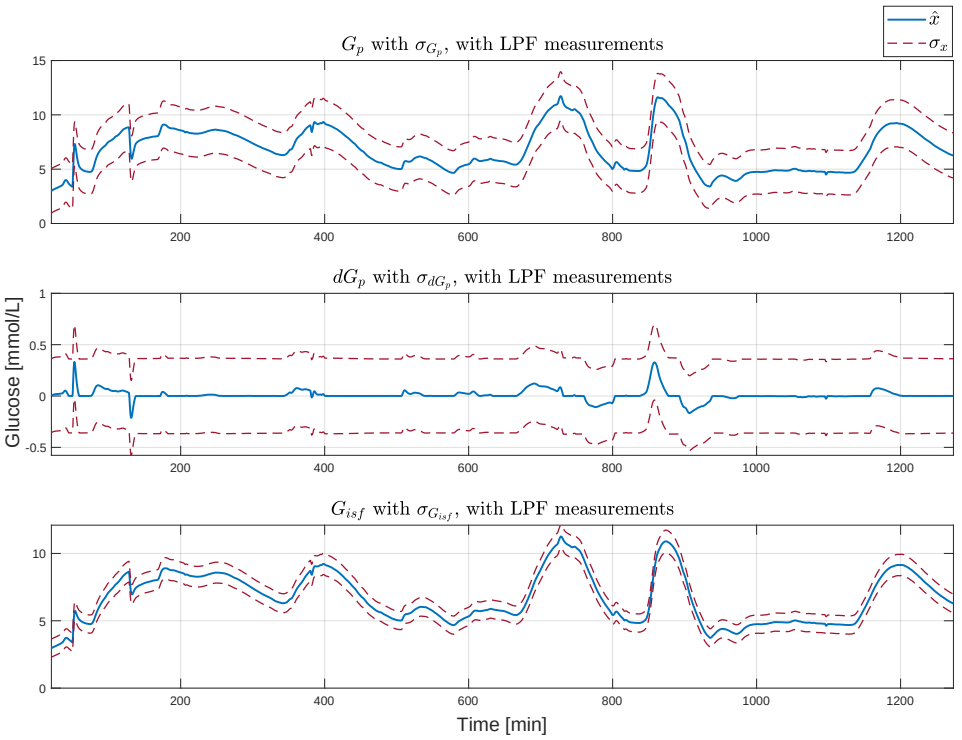

(b) M-robust KF estimate of BG level, with LPF measurements, with SD.

Figure 6.8: M-robust KF results for the Mar 5th, 2021 data set, displayed with SDs. $\hat{x}$ describes estimate x, while σ_x referrers to the standard deviation of estimate x.

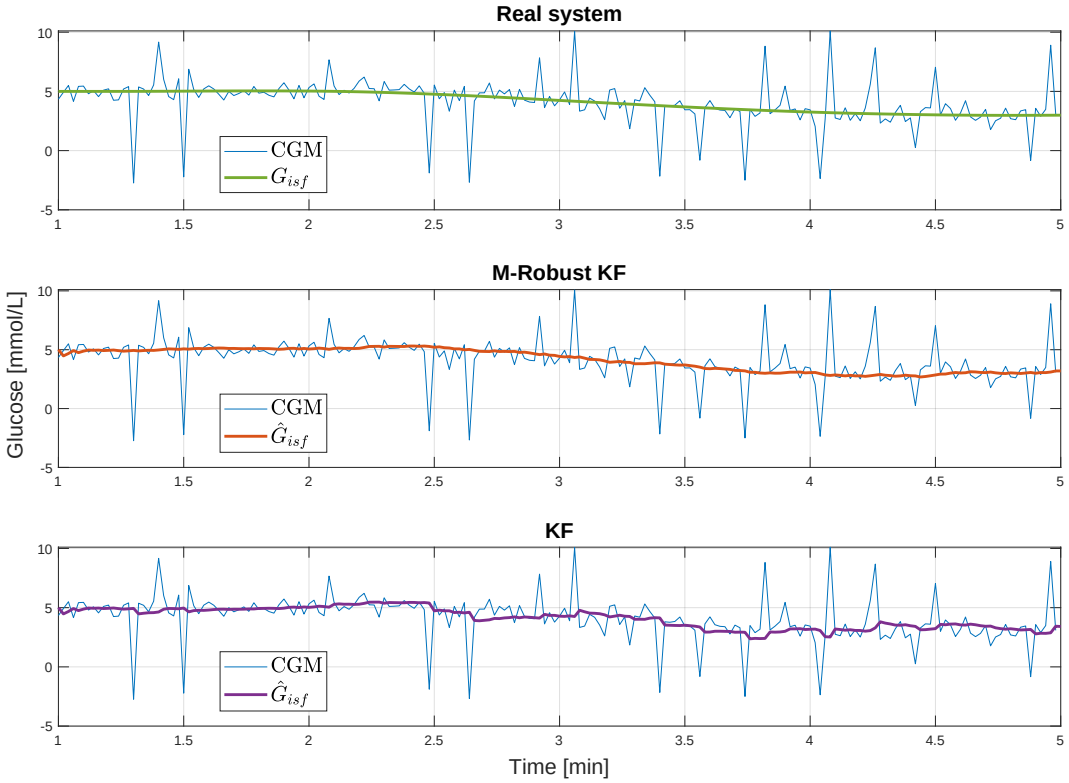

Figure 6.9: M-robust KF estimate of G_{isf}, based on a simulated system, modeled with the rate-only model with T =6 min, $a = -0.0018$ and $\Delta t = 0.02$, plotted together with the true response, and a KF estimate.

Table 6.2: Identified time constants T [min], and identified rate of decay constants a, both with corresponding RSS values.

Date	Time constant, T [min]	RSS_T	Rate of decay, a	RSS_a
Mar 10th, 2021	4.9	39.60	-0.0012	0.039
Mar 5th, 2021	4.1	66.90	-0.0035	0.10
Mar 1st, 2021	4.3	82.24	-0.0023	0.073
Nov 20th, 2020	7.9	49.75	-0.0024	0.026
Nov 18th, 2020	7.4	994.26	-0.00029	0.059

Table 6.3: Final tuning values of Q, R, b, N_{reg} and N_s, for all relevant models, where N_{reg} and N_s are given in number of iterations.

Models	Q [mmol^2/L^2]	R [mmol^2/L^2]	b	N_{reg}	N_s
Steil-Rebrin with UI	0.01	ISO 15197:2015	-	-	-
Rate-only	$\begin{bmatrix} 10^{-3} & 0 & 0 \\ 0 & 7 \cdot 10^{-5} & 0 \\ 0 & 0 & 10^{-3} \end{bmatrix}$	ISO 15197:2015	0.004	375	600
Rearranged Steil-Rebrin	-	-	0.004	250	600

Real-time threshold = 1.2 sec	
Estimation Algorithm	Maximum iteration running time [sec]
FD approximation	0.0008
FD approximation, MA smoothing	0.0112
FD approximation, WLS LR	0.0046
KF	0.0024
KF, MA smoothing	0.0121
KF, WLS LR	0.0033
KF, LPF	0.0270
M-Roust KF	0.0306
M-Robust KF, MA smoothing	0.0303
M-Robust KF, WLS LR	0.0403
M-Robust KF, LPF	0.0310
RTSKF with UI	0.0018

Table 6.4: Mean iteration running time for all tested estimation algorithms, with and without enhancements.

Table 6.5: MSE [$mmol^2/L^2$] and MAPE [%] scores based on Mar 10th, 2021 estimation results, both with and without enhancements, as well as raw CGM measurements, all with BGA as the true value.

Mar 10th, 2021		MSE [$mmol^2/L^2/$]			MAPE [%]		
CGM		0.41			8.60		
	T [min]	4	6	8	4	6	8
Filter	FD	0.28	0.30	0.38	7.49	7.63	8.55
	KF	0.23	0.18	0.15	7.12	6.42	5.74
	RTSKF-UI	0.25	0.24	0.29	6.92	6.67	7.23
	M-Robust KF	0.22	0.20	0.18	6.85	6.78	6.13
MA smoothing	FD	0.21	0.15	0.11	6.83	6.02	5.22
	KF	0.21	0.15	0.12	6.89	6.11	5.36
	RTSKF-UI	-	-	-	-	-	-
	M-Robust KF	0.21	0.18	0.14	6.62	6.48	5.79
WLS LR	FD	0.31	0.36	0.49	7.63	7.20	6.78
	KF	0.24	0.19	0.17	7.38	6.60	5.83
	RTSKF-UI	-	-	-	-	-	-
	M-Robust KF	0.23	0.22	0.19	7.10	6.96	6.22
LPF	FD	-	-	-	-	-	-
	KF	0.22	0.17	0.14	6.92	6.18	5.12
	RTSKF-UI	-	-	-	-	-	-
	M-Robust KF	0.25	0.18	0.16	7.13	6.00	5.80

Table 6.6: MSE [$mmol^2/L^2$] and MAPE [%] scores based on Mar 5th, 2021 estimation results, both with and without enhancements, as well as raw CGM measurements, all with BGA as the true value.

Mar 5th, 2021		MSE [$mmol^2/L^2/$]			MAPE [%]		
CGM		0.25			5.84		
	T [min]	4	6	8	4	6	8
Filter	FD	0.35	0.44	0.56	5.17	6.58	8.44
	KF	0.15	0.15	0.17	4.65	4.46	4.69
	RTSKF-UI	0.21	0.26	0.34	5.17	5.71	6.49
	M-Robust KF	0.17	0.16	0.18	4.74	4.49	4.82
MA smoothing	FD	0.11	0.09	0.10	4.31	3.80	3.84
	KF	0.14	0.13	0.15	4.61	4.30	4.46
	RTSKF-UI	-	-	-	-	-	-
	M-Robust KF	0.15	0.15	0.16	4.68	4.35	4.54
WLS LR	FD	0.31	0.28	0.30	4.55	4.18	4.39
	KF	0.18	0.19	0.23	4.73	4.59	4.79
	RTSKF-UI	-	-	-	-	-	-
	M-Robust KF	0.19	0.21	0.24	4.78	4.59	4.90
LPF	FD	-	-	-	-	-	-
	KF	0.20	0.21	0.25	4.99	4.91	5.31
	RTSKF-UI	-	-	-	-	-	-
	M-Robust KF	0.21	0.21	0.20	4.93	4.75	4.61

Table 6.7: MSE [$mmol^2/L^2$] and MAPE [%] scores based on Mar 1st, 2021 estimation results, both with and without enhancements, as well as raw CGM measurements, all with BGA as the true value.

Mar 1st, 2021		MSE [$mmol^2/L^2/$]			MAPE [%]		
CGM		0.17			4.86		
	T [min]	4	6	8	4	6	8
Filter	FD	0.17	0.23	0.34	4.61	5.31	6.22
	KF	0.12	0.12	0.13	3.99	3.88	4.04
	RTSKF-UI	0.20	0.26	0.36	5.00	5.48	6.06
	M-Robust KF	0.14	0.13	0.14	4.18	3.93	3.98
MA smoothing	FD	0.10	0.09	0.09	3.56	3.33	3.38
	KF	0.11	0.11	0.12	3.73	3.64	3.80
	RTSKF-UI	-	-	-	-	-	-
	M-Robust KF	0.12	0.11	0.13	3.96	3.74	3.87
WLS LR	FD	0.10	0.10	0.10	3.66	3.52	3.61
	KF	0.15	0.17	0.20	4.03	4.05	4.38
	RTSKF-UI	-	-	-	-	-	-
	M-Robust KF	0.16	0.18	0.21	4.25	4.16	4.38
LPF	FD	-	-	-	-	-	-
	KF	0.13	0.13	0.15	3.97	3.94	4.17
	RTSKF-UI	-	-	-	-	-	-
	M-Robust KF	0.18	0.18	0.15	4.71	4.69	4.34

Table 6.8: MSE [$mmol^2/L^2$] and MAPE [%] scores based on Nov 20th, 2020 estimation results, both with and without enhancements, as well as raw CGM measurements, all with BGA as the true value.

Nov 20th, 2020		MSE [$mmol^2/L^2/$]			MAPE [%]		
CGM		0.36			7.78		
	T [min]	4	6	8	4	6	8
Filter	FD	0.26	0.29	0.38	6.90	7.18	7.83
	KF	0.24	0.20	0.18	6.69	6.39	6.27
	RTSKF-UI	0.31	0.34	0.40	7.23	7.75	8.66
	M-Robust KF	0.26	0.23	0.20	7.06	6.74	6.67
MA smoothing	FD	0.35	0.35	0.37	6.62	6.17	5.85
	KF	0.27	0.23	0.20	6.72	6.39	6.24
	RTSKF-UI	-	-	-	-	-	-
	M-Robust KF	0.30	0.26	0.22	7.08	6.77	6.67
WLS LR	FD	0.23	0.19	0.16	6.46	5.99	5.78
	KF	0.25	0.21	0.19	6.82	6.58	6.47
	RTSKF-UI	-	-	-	-	-	-
	M-Robust KF	0.27	0.24	0.22	7.18	6.94	6.89
LPF	FD	-	-	-	-	-	-
	KF	0.26	0.23	0.21	6.93	6.71	6.67
	RTSKF-UI	-	-	-	-	-	-
	M-Robust KF	0.31	0.37	0.24	7.73	7.84	7.05

Chapter 7

Discussion

In this chapter discussion based on the aim, the theory, the method and the results is given. The discussion is segmented into sections which, during the work of this thesis, was experienced as significant, and worth discussing.

7.1 The Aim

As explained in Section 2.1.1, the glucose regulatory loop in individuals with diabetes, cannot autonomously regulate glucose level without exogenous insulin injections, either in the form of an insulin pump or manual injections of insulin. In critical situations, the pump or the individual may have to act immediately in order to properly respond, with ISF glucose level measurement as reference. Absorption and effect of hormones are not instantaneous in the body, hence using CGM measurements in such situations may cause overdue responses to BG level fluctuations. It is therefore believed that eliminating the lag, introduced by the impulse response between the BG level and ISF glucose level, and compensating for dynamical differences between the two compartments, will contributed to tighter glycemic control, which will help avoid hyper- and hypoglycemic events. Emphasize on robustness will also help avoid incorrect sensor readings, due to outliers, which can contribute in avoiding single erroneous sensor readings, and may provide cleaner glucose trend analysis.

The main goal of this thesis is then to eliminate the inconveniences of measuring ISF glucose levels, instead of BG levels directly, through estimation of BG level based on ISF glucose level measurements, with emphasize on estimate robustness. The goal is well established, however some remarks has to be made regarding the available data, and the impact the data have on achieveing this goal. The data sets provided for this project are retrieved from animal experiments lasting from about $12-48\,\mathrm{h}$. Despite successfully accomplishing estimating the BG levels from these data sets, it will still be unknown how the potentially successful algorithms will perform using data covering longer time spans.

Biofouling, inflammation and corrosion are known problems of implantable sensors, such as CGM sensors, see Section 2.1.2. Such phenomenons are all due to bodily reactions which takes time before they truly start affecting measurement quality. The provided data sets may then not exhibit great

examples of such responses, due to short experiment time span, and how the resulting estimates will be affected by it, will remain unknown. Movement is another factor to mention, which is known to affect sensor readings. The animals used in the experiment were anesthetized, hence no movement occurred while collecting the data, which also provides uncertainties about the estimation algorithms performance outside of clinical settings.

Despite the clinical setting of the provided data, the results from this project can be counted as a first attempt at this particular problem, a possibility assessment of sorts. This work will serve as a spring board for further research on the topic, and may provide insight into the problem of estimating BG level based on ISF glucose level measurements, while also provide results from methods which can be further developed.

Another goal of this thesis was to implement estimation algorithms that is applicable in real time. Perfect real time algorithms are of-course not achievable, due to computational time, hence a threshold of time consumption per for-loop iteration was established, seen as the estimation process is preformed in for loops for this project. This threshold was set to 1.2 sec, due to the fact that this is the sampling time of the relevant CGM system transmitter. The argument then being that the estimate based on one measurement should be finished calculated, before a new measurement arrives.

7.2 The data

7.2.1 BGA

For the purpose of this thesis it is chosen to compare the resulting estimates to BGA measurements, in order to assess the estimates performance. The reasoning behind this decision is that the BGA system uses an invasive measuring technique which is known to be quite accurate, as well as the availability of BGA measurements in the provided data sets. However there are problems regarding the BGA measurements which should be addressed.

The first issue being, the BGA measurement is sampled at a different rate compared to the CGM. New CGM measurements arrive every 1.2 sec, while a varying amount of time passes between every new BGA measurement, averaging at about 5 min, although as much as 1 h is registered to have passed between two BGA readings. Looking at Figure 6.2, the effect of different sampling times can be seen. CGM measurements are resembling a continuous slope, while BGA measurements are sparse.

When BGA readings are far apart from each other in time, the BGA measurements might not be catching all of the BG dynamics. Therefore at certain times in the data set time windows, there will be uncertainty of the actual BG level, due to missing information. This raises some implications when comparing estimates to BGA measurements, especially when estimates behave somewhat different compared to the next available BGA reading. It might even be said that at certain times the estimates may actually describe the BG level more accurate than the BGA measurements, simply due to different sampling rate. This should be kept at the back of the mind, during the comparing part of the estimate evaluations.

BGA measurements are also used as the true value in the statistical analysis, for all estimation algorithms. Again the sampling time prove somewhat problematic. Where the estimates are vectors consisting of tens of thousands of samples, the BGA are vectors averaging at just under 100 samples.

The more data available for comparison, the more accurate an analysis will be, hence it can be considered that with more BG level samples to compare with, the statistical scores would more accurately reflect the true performance of the estimates. This is also the case in the model parameter identifications process. However, it is deemed good enough for the purpose of this thesis.

7.2.2 CGM

CGM measurements serve as the base of all attempted BG level estimation procedures. As mentioned above the sampling time is about 1.2 sec, which over a 24 −48 h window, provides a good amount of data to work with. Per data set two CGM sensors are given, however the quality between these two sensors was quite varying. Where one sensor was seen to produce a very sensible slope of the ISF glucose level, the other sensor was excessively flawed in most data sets. Ways to overcome this does exists, however, was not emphasized in this thesis, hence time was not spent on the flawed sensor readings. Instead one sensor was chosen from four out of five data sets, based on first impression of the quality: Mar 10th, 2021, Mar 5th, 2021, Mar 1st, 2021 and Nov 20th, 2020.

Comparing CGM and BGA sensor readings, as is done in Figure 6.1a, one clearly see the diffusion process between blood and ISF effect on the corresponding glucose level between the two compartments. CGM sensor readings are consistently lagging behind the BGA samples, most noticeably at meal times, when there is a drastic increase in the rate of change of the glucose level. In the flatter areas the lagging effect is less evident, which is in line with the theory, see Section 2.4.1.

In the first part of the time window, the CGM is calibrating. This causes the CGM readings to spike, and act very ill-logical if seen through the eyes of how the glucose level should change, see (1) in Figure 6.1b. Due to this, the calibrating section of the sensor readings is taken out of the accuracy assessment of the estimation algorithms simulation time window, in order to assess a fair set of measurements to work from.

The method used for locating the end-of calibration window, as well as start and end of meal times, does introduce some uncertainty, seen as it is not a formal way of identification. Only identifying by visual impression may cause variability in accuracy between the different identification processes between data sets. However, it was observed that this small variability between data sets did not impact the estimate accuracy greatly, or even significantly. It was experienced that the impacting part was the calibration window itself, and once removed, independent of how exact the window of removal was, the estimate accuracy improved. The meal times are only used for improving the visual quality of the figures, hence variability in start and end of meal times does not affect the estimates.

The data sets containing the CGM sensor readings provided for this thesis are characterized by a special phenomenon, which does effect all estimation procedures. At certain occasions the CGM measurements can be seen suddenly either dropping or increasing, with a rate unnatural to what one would expect from ISF glucose dynamics, see (2) in Figure 6.1b. This is especially evident in the March 5th, 2021 and March 1st, 2021 data sets. However incidences do occur, only at a smaller scale, in the other data sets as well. At first glance these anomalies could be characterized as outliers, due to the assumed sudden changes, and the fact that the BGA measurements does not show similar responses. However at closer inspection the sections of measurements portray completely different dynamics, compared to the rest of the data.

Initially the anomalies were indeed incorrectly classified as outliers, which again fueled the motiv-

ation of utilizing robust filters. Hence the M-robust KF was investigated, implemented and tested. However, robust KF's are robust against outliers, which does not include big sections consisting of several data points. The M-robust KF is discussed in further detail in Section 7.5.6. Once the M-robust KF did not improve the slope of the BG level estimate, the anomalies were further explored. It was discovered that the anomalies lasted several minutes each, which, considering the sampling time of 1.2 sec, includes a lot of data. Having a long flawed window of data may then have falsely tricked the robust filter into interpret the flawed data as a part of the system dynamics, hence it is not registered as outliers.

Due to the structure, the anomalies can better be classified as minimal incidents of drifts. The word minimal refers to the sensors ability to recover from the drift without outside interference. The exact cause behind these minimal drifts is not established in this thesis' work. However some theories will be presented, and discussed. Pressure induced sensor attenuation (PISA) is a phenomenon known to affect CGM sensor readings [60], hence it seems possible this is the cause of the drifts. PISA occurs once pressure is induced on the skin close to sensor mounting site, and is characterized by a sudden decrease in glucose level, that violates physiological rate-of-change limits [60]. The sensor then takes some time to recover, and has a negative rate-of-change during the recovering phase. Although the description of PISA fits with the visual interpretation of the sensor anomalies, it can only be considered as speculation. The animals were anesthetized during the experiment, hence it should be expected that they did not move, which ultimately brings the question: What induced the pressure?

It may be noticed that some of the PISA looking sensor anomalies occurs very close, or at exact the same time as a BGA measurement sample. Due to the invasive nature of the BGA measuring device, this may have caused some pressure in the animals body. It may even be possible that drawing blood for the analysis affects the blood flow around the sensor mounting sites, ultimately disturbing the sensors. However, seen as the majority of BGA samples do not induce the same responses in the CGM sensor, it cannot be known for certain that this is the cause.

Given more time, further investigation into these peculiar sensor drifts would be done. However, seen as it is slightly outside this thesis scope, ways to tackle the drifts was prioritized instead, such as smoothing and regression. These enhancement methods are discussed under Section 7.5.2.

7.3 The models

A very important part of estimation, is the choice of model. For the purpose of this thesis, some demands for models were made. Relationship between blood and ISF had to be part of the model, seen as only ISF glucose level was to be known, hence the model also needed to be fully observable, with only ISF glucose measurements as outputs. In addition, it was seen beneficial to use a simple model, in order to reduce complexity. In the term project a four state model was used, and although the results were promising, the model was considered overly complex, given the purpose of usage.

Considering model simplicity a bit further, it may be noticed that the models are quite sparse when considering inputs, BG level being the exception. This is more of a choice than a demand. A great deal of inspiration for this thesis' work is based on [14], where they argue in favor of inputless models. The arguments being that complex models require information about insulin and meals going into the system, and such data sets are often erroneous or incomplete, unless recorded in a

strictly controlled research setting, and even then complex glucose metabolism models are often not observable with glucose measurements alone [14]. In the data sets used in this thesis, data considering insulin, glucagon and meals are present, however including that information would greatly increase the model complexity, which goes against the simpler model suggestion. This thesis' aim, and the intent in [14], are comparable, and so is the method of achieving so, hence inputless models were considered favorably also in this thesis.

Based on the above argumentation, three models were chosen, namely the Steil-Rebrin model, where BG level was set as an unknown input, rearranging the Steil-Rebrin model such that ISF glucose level is the input, and a rate-only model for BG dynamics, combined with the Steil-Rebrin model.

7.3.1 Steil-Rebrin Model

This model is the most established way of modeling the pharmacodynamics of glucose between blood plasma and subcutaneous tissue, based on the authors perception of the literature. The model established in [52], is mentioned in [61], [14], [11] and [54], among some. Despite being well established, critique of this model does exist.

One of those critiques being the lag between ISF glucose and BG is not constant, but in fact varying within the same individual. The time lag is reported to depend on factors such as insulin action, and other type of drugs acting in the body [62]. The correlation between ISF glucose and BG are most correct when the glucose level is somewhat stable, and during rapid changes, which may be induced by for example meals and exercises, the time lag between these two compartments is significantly reduced [62]. It has also been hypothesized that insulin stimulated glucose uptake near the sensor implantation site may cause the time lag between blood and ISF glucose levels to vary, however such effects was stated as negligible in [52], where they found no sensitivity change of the sensor during episodes of differing insulin levels.

Estimating the time constant simultaneously with the other states is a possibility, however such an addition require BG level measurements for calibration, at the minimum. The BGA samples could have been used for such a purpose in this work, however it would take away from the sole purpose of this thesis, which is to estimate the BG level with CGM measurements only. The experiment animals were anesthetized throughout the experiment, hence no events such as exercises were relevant considerations to handle. In future work however, a variable time lag should be considered, as it may significantly improve the estimate, during rapid glucose changing events.

The model also builds upon the assumption that, when the blood and ISF glucose levels are equal, the expected value of g, see Equation (2.149), is 1. In [53] they issue that re-calibration of CGM sensors are needed to get a calculated g close to 1. This limits the use of the model for longer periods of time, and indicates that the estimates will worsen over time, without BG level measurements for re-calibration. Just as for the time constant, the limiting time window, as well as the controlled setting, limits the investigation on how well the resulting estimates would have performed over a longer period of time, without re-calibration.

Furthermore, there are aspects of the ISF glucose level not covered by the Steil-Rebrin model. Such aspects include the exchange of glucose between blood and ISF across the capillary membrane, the glucose utilization by cells and the accessory route of the lymphatic system by which glucose returns to the blood after a delay [53]. Such arguments count in favor of the claim that the Steil-Rebrin model

is over simplifying the ISF glucose dynamics. However, seen as it is the most established model for explaining such dynamics, having been tested on large data sets for years [53], the model is seen as sufficient in this thesis. Newer models lack such verification, hence any claim of outperforming the Steil-Rebrin model, will be thin.

7.3.2 Rearranging the Steil-Rebrin Model

The rearranged Steil-Rebrin model is the most simplistic method of presenting the BG level used in this thesis, first presented in [52]. Despite the model being able to compensate for time lag, it is said to be very sensitive to noise, and in [52] they found it necessary to reduce the noise by using a three point moving average filter. Based on this, it was already known that the model would perform poorly, and result in a noisy estimate. However, seen as simplicity is given a lot of attention in this thesis, it was considered beneficial to observe that some models may in fact be *too* simple, and insufficient in describing the relevant dynamics.

7.3.3 Rate-Only Model

The rate-only model is an inputless model and is in [14] called the simplest dynamic system that can be said to represent blood glucose dynamics. This claim made the model a natural choice to investigate in this thesis, seen as model simplicity is highlighted. In addition the only model parameter needing to be identified in order to use the model is the rate of BG decay, a.

Looking a bit more closely at a, and how it impacts the model, it becomes clear that a is in fact the secret ingredient, making this model work as successfully as it does. Looking at Equation (2.160), it can be seen that the rate of change state is gained by a, and inspecting Table 6.2 where a is reported below zero for all data sets, the impact of this model parameter becomes clearer. a can be said to limit the rate of change to sudden changes of process noise, preventing the rate of BG level change to grow indefinitely, ultimately acting like a time constant.

The model describes only the BG dynamics, hence in order to be observable with CGM measurements, the model is combined with the Steil-Rebrin model. This makes the final model a three state model, which is one state shorter than the central-remote rate model, see Section 2.4.4. According to the model preferences, this immediately make the rate-only model the more attractable model of the two, from a theoretical stand point. If the model stands, in a practical sense, will be addressed in the subsequent estimation algorithm discussions.

7.4 System Identification

Once a selection of models were established, their model parameters were needed identified. Due to the similarities between all models chosen for this project, there were only two model parameters needing to be identified. That is the diffusion process time constant, T, and the observed BG rate of decay, a.

First the identification of T is addressed. The choice of the initial starting point of the identification

of the diffusion process time constant was based on [6], which reports $4-10$ min, hence T_0 was set to the upper scale of this interval, 10 min. However, changing the initial start point did not change the resulting value, which indicates global minimums were found in all data sets. All identified T's are also within the reported interval from [6], see Table 6.2. Such results give credibility to both the identification method, as well as the sensors.

Secondly, there is a substantial increase in T between the Mar 1st, 2021 data set, and the Nov 20th, 2020 data set. The data sets from 2021 are inclining towards the lower end of the reported interval, while the data sets from 2020 are inclining towards the upper end of the interval. It was investigated whether different sensors where used between the 2021 and 2020 experiments, however the sensor type was reported to be equal between the two.

The weight of the animals were also theorized to be the cause of the difference in T. The weights identified for the 2021 experiments are displayed in Table 6.1, while the weights for the 2020 experiments were, unfortunately, not identified. The reason behind this theory is that recent studies have reported that body mass index (BMI) may be associated with subcutaneous sensor's, like the CGM sensor's, accuracy [63]. In [64] it was identified that CGM sensors significantly underestimated glucose levels in children with high BMIs, while slightly overestimating the glucose level in children with normal leveled BMI, when comparing to BG level measurements. The study was conducted with the FreeStyle Libre Pro CGM sensor, and all volunteering children were considered medically healthy.

With a higher BMI, the total fat mass and fat percentage is usually increased, which again suggests an increase in subcutaneous fat. An increase in subcutaneous fat may potentially alter the diffusion rate of glucose between the blood and ISF compartments, which could explain changes of accuracy in CGM sensors between different BMIs [64]. However, fairly little is known about the varied CGM sensor performance between different levels of fat percentage and weights [63], hence more research is need in order to state these observations as facts. Nonetheless, a substantial increase in time lag between the BG level measurements and ISF glucose level measurements does effect the CGM sensor accuracy, which based on the above, may suggest that the 2020 experiment animals were of different weights, compared to the 2021 experiment animals.

Based on the reported values of T in Table 6.2, three values of T were chosen for the estimation part of this thesis. Now, the argument for these values are simply a matter of avoiding problems relating to over- and under-fitting. BGA level measurements were considered unavailable in the estimation process of this project, hence no adjustment of T based on BG level measurements can be performed once the estimation process has started. This means that arbitrary of the data set, only one T can be assumed. This implies that there is now a problem relating to finding the T which among all data sets provides the most accurate estimate. If then T was set equal to one of the reported T's, it can be assumed that the estimate would be over-fitted for that particular data set, while under-fitted for the remaining data sets. In addition, it was considered informative to observe how the estimation algorithms would perform, if a too high, or too low, T was used.

Now, identification of BG rate of decay will be addressed, which is a relevant model parameter for the rate-only model, see Section 2.4.3. Identify that the RSS values for identified a's are significantly lower than the reported RSS of the identified T's, see Table 6.2. This could simply be a matter of the measurements. When identifying T two different measurement vectors are used, while only one measurement vector is needed for the identification of a. This naturally eliminates uncertainty, thereby lowering the baseline of the related RSS values.

The starting point of a, a_0, was set to be -0.05, seen as this is the reported value from [14]. Looking at Table 6.2, it can be noted that the values are significantly lower than what was used in [14]. One reason for this could be that in [14] an SMBG sensor is used, while in this project BG samples are measured using a BGA device. SMBG samples tend to be more sparse, than what is observed for the BGA measurements in this thesis' data sets, which might contribute to altering the identification of the parameter. Different sensing systems may also possess different degree of accuracy, which may give rise to different rate of decay values, however, such aspects were not investigated during this thesis, hence the above will remain as pure speculation, but will stand as an interesting observation.

The reported RSS per identified a are close in value, which can indicate similar BGA measurement quality between data sets, which is confirmed by visual inspection of the CGM and BGA figures, see Figure 6.2 and Figure B.1.

It was noticed that during the estimation process, the choice of a had little impact on the estimate accuracy, hence an average of all identified a's was used as the BG rate of decay in the rate-only model. This is perhaps an oversimplification of the model parameter, however it was considered sufficient in this thesis, due to lacking estimate accuracy improvements when adjusting a.

7.5 Estimation Algorithms

7.5.1 Noise modeling

An essential part of Kalman filters, regardless of the type of filter, is the noise modeling, which includes the process noise, w, and the measurement noise, v. The covariance matrices, Q for the process noise covariance and R for measurement noise covariance, are used by the Kalman filters, in order to achieve an optimal estimate, hence some space is dedicated to discussing the modeling of these noise processes.

In order to keep the models as simple as possible, meals, insulin- and glucagon injections are not considered inputs to the system, but rather unknown disturbances. This decision was inspired by [14], which emphasized the generality of inputless models. However, this decision does call for some consideration, specifically that Q has to be set large enough to accommodate glucose excursions originating from meals or insulin injections. Choosing Q then becomes an issue of finding the value which ensures that the error band of the estimate will grow quickly enough to envelop the worst case glucose excursion, such as post meal-times or insulin injections [14].

Initial value of Q, in the rate only-model was set to $\sigma^2_{dG_p} = 0.05 \cdot \Delta t$ [mmol^2/L^2], where Δt is the sampling time, and the other variances set equal to zero. This is equal to the reported Q for the rate only model in [14]. From this the matrix was tuned, by a trial and error approach, by observing the statistical scores, as well as the estimate appearance in the figures. It was observed that while tuning there was a mismatch between the statistical scores and the estimate appearance. Achieving the lowest possible MSE and MAPE, at $\sigma^2_{dG_p} = 0.007$ [mmol^2/L^2], results in a more responsive estimate, making the slope react dramatic to minimal changes in CGM measurements, while a smoother G_p estimate was achieved when $\sigma^2_{dG_p} = 7 \cdot 10^{-5}$ [mmol^2/L^2]. However, reducing the variance gave a slight increase in the scores, for some of the data sets. After some consideration, the slight increase in scores was accepted, due to smoother estimate slope, when the variance of dG_p was set quite low.

$\sigma^2_{G_p}$ and $\sigma^2_{G_{isf}}$ were early on set to 0.001 [mmol^2/L^2], which, after finding a good value for $\sigma^2_{dG_p}$, seemed to produced a good estimate, both considering the scores and the estimate slope in the figures. Slightly adjusting these values were not experienced to result in big changes in the estimates, which, when considering the model, is not surprising.

Steil-Rebrin model with BG set as the UI is the next model to consider. Here the process noise covariance matrix consist only of one variance, $\sigma^2_{G_{isf}}$, due to the structure of the model. Tuning this value did not seem to impact the BG level estimate, which is not surprising considering the filter structure. The ISF glucose level variance were after trial and error approached tuning, set to 0.01 [mmol^2/L^2].

Extremes for the values of Q matrices were also tested, simply to observe the response. Such result can be found in Appendix C. The results are, for all relevant filter, as one would expect. Increasing Q drastically gives high standard deviation for the corresponding states, and, considering $\sigma^2_{dG_p}$ and $\sigma^2_{G_p}$ specifically, makes the estimate slopes more oscillating, appearing noisier. While reducing the variances results in lower SD for the relevant states, but also makes the BG level estimate more similar to G_{isf}, hence the filter is less effective in compensating for the time lag.

In regards to the measurement noise, the CGM sensor is assumed related to the ISO 15197:2015 standard, as stated in Chapter 4, and explained in Section 2.1.2. Given that this is an established international standard, no adjustments where made to the measurement covariance matrix, R, in the filters where it relevant.

7.5.2 Enhancement Methods

Due to the nature of the measurements, robust filters did not improve on estimate robustness, which is discussed in detail in Section 7.2.2. Eliminating the drifts were still considered an important part of this thesis, hence other methods were investigated, which resulted in the enhancement methods MA smoothing, WLS LR and LPF of measurements. MA smoothing and WLS LR are performed directly on the filter estimate in a post-processing manner, while LPF is affecting the estimate more indirectly by pre-processing the measurements. Their inclusion in this project is based on the idea that these methods may result in estimates that are more robust against drifts or anomalies, not resembling typical outlier noise characterization.

The inclusion of such methods is not problem free, and some of the relating issues will be addressed here, the first issue being increase in algorithm run-time. Despite slight increases in run time, all attempted methods stay below the real-time threshold, see Table 6.4, which allows for the enhancement methods to be used in real time, with the relevant transmitter. Not surprisingly the MA smoothing seems to be the method which demands the most time. This is in line with how the MA is calculated, and the result is exactly as expected. The WLS LR for the M-robust KF is however, a bit more surprising. Calculation of the weights naturally increases the time, compared to just simple LR, however, the fact that WLS LR results in higher maximum time consumption than even MA smoothing for the M-robust KF, is odd. The result may just have been an odd outlier, seen as the time consumption calculations are done in a very simplistic manner, which does give room for a lot of variations. Regardless, the value is below the threshold, hence it gives no reason for worry. Further, the LPF time consumption, which includes processing of the measurements, in addition to a larger state vector, is evaluated to be logical.

The next issue is regarding adjustment of the estimate, by operations like smoothing and regression. Such operations performed directly on the estimate, may be referred to as an estimate of an estimate, which is controversial. For this reason it was decided that, in the case of MA smoothing and WLS LR, the output structured array is given an additional field for the smoothed or regressed estimates. Such a structure also allows for rapid switching between the filter estimate and the estimates of the filter estimate, which could be beneficial. This is not done for the LPF, since it was considered less crucial for this method, seen as the whole model is altered, and much of the added uncertainty is handled by the filter itself. Whenever drifts appear in CGM measurements, regressed or smoothed estimates may be preferred and chosen by a control algorithm, in order to eliminate the drift effects on the estimate, and ultimately a controller's potential decision. Once such a drifting window has passed, the control algorithm can switch back to the filter estimate. Such an algorithm will require drift detection, which is not implemented in this thesis.

Finally, there is the problem regarding bias and variance. Whenever an estimate is calculated, based on measurements or data, regardless of the approach, it gives rise to an issue relating to the variance of that data. The question being: How much variance should be allowed in the estimate, and can it be reduced by introducing bias? In the relevant case, some bias is introduced when using the filters, because if not the filter would be allowed to follow the measurements, without constrictions. When using smoothing and regression, substantially more bias is introduced. This is the whole idea, because bias has to be included, in order to get rid of the CGM drift effect on the filter estimates. The issue, specifically here, is then related to how much bias can be allowed, without loosing the true BG dynamics?

For this reason, N_{reg} and N_s, the interval of regression and smoothing, respectively, are considered tuning variables. In Appendix C results are given, showing the effect of having too big intervals, Figure C.1b and Figure C.2b and too small intervals, Figure C.1a and Figure C.2a, for regression and MA smoothing, respectively. Naturally having a too big interval, too high bias, result in loss of BG dynamics. In the regression case this is realized by the estimate being too rigid, which ultimately makes the estimate miss some of the filter estimates slope, and at certain times all together wrongfully predict the filter estimate, while in the smoothing case the smoothed estimate misses the highest peaks, and the slope's minimums, due to being overly smoothed. Having too small intervals, not enough bias, the figures show that close to nothing is achieved by the regressed or smoothed estimates. The drifts still affects the estimates, and for the regressed estimate the effects are worsened.

Considering the LPF method, bias and variance were experienced to be less problematic, the effect of tuning the smoothing factor showed other concerns. Decreasing the smoothing factor, b, caused the standard deviation of the estimate to grow, while when being increased the standard deviation was still bigger than in the no-LPF case, while not achieving any significant improvements to the estimate. Figures showing these effects may be found in Figure C.3. Increase in standard deviation is generally unwanted, seen as this means the filter is uncertain about the estimate. Regardless, the LPF method is not able to eliminate the CGM sensor drifts as effectively as MA smoothing and regression, for any filter, making it less favorably in handling the CGM sensor drifts.

Considering MSE and MAPE the general trend, among all filters where these methods are used, is that the values are slightly reduced using MA smoothing, and slightly increased when using WLS LR and LPF. Inspecting Figure 6.4, MA smoothing does seem to be the most effective in eliminating the effects of CGM drifts, or anomalies. This claim is also backed by the subsequent data sets in Appendix B, in the figures B.5, B.7 and B.9. Taking into consideration that MA smoothing, despite having the averaged highest maximum time consumption per for-loop iteration, manages to stay

below the real-time threshold, it seems to be the best option for enhancing the estimate, making it more robust against CGM drifts, and sensor anomalies.

7.5.3 FD Approximation of Blood Glucose Level

Rearranging Equation (2.152), and using FD approximation in order to achieve an estimate from the blood glucose is the simplest estimation algorithm tested throughout this project. The model requires only the diffusion time constant and the sensor sampling time in order to be complete, and due to the simplistic FD approximation approach only one line of code per iteration is necessary to reconstruct the BG level. The latter makes this a fast estimation algorithm, having the lowest maximum time in seconds per iteration among all estimation algorithms tested. The corresponding statistical analysis also speaks in favour of the FD approximation, which can be found in Table 6.5-Table 6.8, having low scores for both the MSE and MAPE, both with and without enhancements.

However, looking at Figure 6.3a the methods downfall become very visible. The estimate can be seen as extremely noisy, oscillating at such high frequency that the slope of the estimate bear more resemblance to blocks of color, rather than a smoothed slope. Because of this it can be argued that the surprisingly good statistical scores are achieved by nothing more than good luck. Due to the rapidness of the noise, and the sparsity of comparing BGA samples, the estimate slope may just hit the best point for the comparison by luck.

Observe the CGM sensor readings in Figure 6.2. They appear to be very smoothed and continuous. This is an optic illusion, due to the long time window, and zooming in reveals that the CGM measurements are in fact not smooth at all, see (3) Figure 6.1b. Numerical differentiation will amplify already present noise, often to the point of results appearing unstable. This is due to the derivative operator frequency response, where the gain will increase linearly with frequency, hence areas of a signal with high frequency are greatly amplified. Noisy areas are great examples of high frequency areas, and although Figure 6.1b is not necessarily noisy in the general sense, the discrete time steps does introduce high frequencies, regardless. In addition, moving from Equation (2.152) to Equation (2.156) essentially means moving from derivation to integration, which is known to introduce high frequent noise to the output signals.

The scores for FD approximation in Table 6.5-Table 6.8, show improvements made by the enhancement methods smoothing and regression. However, seen as the FD approximation showed surprisingly good scores to begin with, the now improved estimates scores might not accurately describe the actual improved response. This is more evident in the figures, see Figure 6.3b.

The noisy estimate slope benefits greatly from both regression and smoothing, without it going at the cost of real-time application. However, there are drawbacks making the FD approximation a less favourably estimation algorithm. There is no form of evaluation of process or measurement noise, meaning that the filter is at all times, fully trusting both the model and the measurements. In addition nothing is ever known of the estimate uncertainty, which again is problematic because the estimate is considered perfect at all times by the algorithm. Such drawbacks outweighs the fast computation time of this algorithm, given the purpose of this thesis.

7.5.4 Kalman Filter

Kalman filtering was tested during the term project, with the central and remote rate model, see Section 2.4.4. The method was further improved with a MA smoother for a pending approval conference paper, see Appendix D. Based on the results and discussions from both the project and the paper, the Kalman filter algorithm was still considered a suitable method for estimating BG level based on CGM measurements, hence it remained a method to be tested for in this thesis. Based on the estimate slope, see Figure 6.4 and the accuracy scores, see Table 6.5-Table 6.8, the KF produces a decent BG level estimate, using the rate-only model, but some remarks have to be made.

The biggest critique of KF from the term project was the lack of robustness, against what was at the time considered outliers in the CGM measurements. This is still an issue, even with the new rate-only model and improved tuning, however, due to the already explained nature of these anomalies in the CGM measurements, lack of robustness is not consider a reason for disregarding the filter. The KF simply interprets these anomalies as the dynamics, due to the amount of data points these anomalies consists of.

A more concerning issue is the fact that the filter seems to consistently overreact to changes in the CGM measurements. This characteristics is best explained by Figure 6.4b, where the KF BG level estimate is overestimating the peak, and acts overly dramatic to the jumps in CGM measurements towards the end of the meal. These reactions were discovered to be very dependant on the tuning of the process noise covariance matrix, see Section 7.5.1. When $\sigma^2_{dG_p}$ was set high, these reactions got worse. This is not surprising, seen as when the elements of Q are increased, the filter is essentially told to trust the model less, hence putting more trust in the measurements. Setting $\sigma^2_{dG_p}$ lower helped minimize these reactions, but as it may be seen from Figure 6.4 they are not all together eliminated.

It is believed that these flaws are more linked with the model rather than the tuning of the filter. $\hat{G}_p$ is not directly linked with the measurements, hence some added uncertainty will always be present in this state. In some way it might be related to an irreducible error such as is described in Section 2.3.3. This will inevitably cause the filter to over-estimate BG level peaks. However, interestingly enough it may be observed in Figure 6.4a that this characteristics works in the estimates favor when estimating the lower BG levels at around 950-1000 min, see Figure 6.4. Such observations could indicate that a simple three state model may not be sufficient in estimating the BG level, based on CGM measurements only, and inputs such as meals and insulin are needed in order to estimate more precisely.

Regardless, the KF does a good job, with the model it is given, estimating the BG level. This is evident in Figure 6.4, where the estimate manages to hit most of the BGA points, especially in the later peaks, and in Figure 6.5a, where the SD is very consistent throughout the simulation and does not display concerning values. KF, even with enchantments, is also considered a very fast algorithm, see Table 6.4, which indicates it to be well equipped for the real time demand of this thesis' aim.

7.5.5 RTSKF-UI

Already during the term project it was suggested that an unknown input Kalman filter might provide a useful method in achieving BG level estimates. Such a filter was developed during that project.

However it was not successfully implemented, which resulted in the filter producing incorrect estimates. If interested please refer to [1]. The exact reason for this response was never fully discovered. However, erroneous implementation of code is considered a likely cause.

At the start of this thesis it was therefor early on decided that an unknown input Kalman filter should be attempted implemented again and tested, and the choice of filter fell upon the presented filter in [46]. The change of filter from term project is rooted in that the precise cause of the errors were never fully disclosed, in addition to trust in the presented method being compromised.

The model used in this filter is the Steil-Rebrin model, see Equation (2.152), where BG level is simply set as the unknown input, which require neither tuning nor initial values for the input, or the input error covariance. Due to the two stage structure, the ISF glucose level is also the only state, part of the state vector, making the corresponding variance the only element of the process noise covariance matrix. This greatly simplifies the tuning process for this filter, which in any kind of application is beneficial. The superiority over augmenting the state vector to include an unknown input state is mentioned in [46], where it is claimed that a two stage structure reduces the computational burden, compared to an augmented state-vector filter. Their choice of making the states unaffected by the inputs also eliminates compromised filter performance by poor choice of process noise regarding the inputs [46].

Despite the promising structure of the filter, it is not suited for estimating the unknown input itself. This is not explicitly stated in the paper, however [46] does refer to the presented problem as "*estimating the state of a linear time varying discrete system in the presence of unknown inputs*", which does indicate that the main goal is estimating the states themselves, and not the inputs. Regardless of the filter's intent, it was still considered interesting to see how the filter would predict the unknown BG level input of the Steil-Rebrin model. Hence this filter is primarily tested, and reviewed based on curiosity, and to investigate how well the filter is able to handle unknown inputs.

Looking at Figure 6.6a, as well as Figure 6.6b it is very evident that the robust part of the filter is aimed at the state stage, and not the unknown input stage. The filter manages to provide a good G_{isf} estimate, while the G_p estimate bears more resemblance to the G_p estimate of the FD approximation approach, which is also the case for the other data sets, see Appendix B.

High noise ratio in the estimate is further proved by the corresponding standard deviation of the estimate. Here, the RTSKF-UI provides more information compared to the FD approximation, where nothing is known of the estimate uncertainty. $\sigma_{G_{isf}}$ seems to behave similarly to the KF standard deviation of the ISF glucose level estimate, indicating that this filter is doing a fair job at estimating the states of the system. The value of the unknown input standard deviation however is much less promising, being in an interval of approximately [-750 750] [mmol/L]. Obviously this is not acceptable in the field of diabetes technology and engineering, hence the standard deviation is one reason for immediately disregarding this filter.

Seen as it was discovered very early on that this filter was unsuited for the task at hand, no enhancement methods were implemented for this estimation algorithm. The similarities between the FD approximation results and the RTSKF-UI results, makes the resulting enhancement methods quite similar, hence if interests in how MA smoothing and regression perform on such a noisy signal is present, the reader is referred to FD approximation results, Figure 6.3a, and the corresponding discussion,Section 7.5.3.

When investigating as to why $\hat{G}_p$ behaves as it does in Figure 6.6a, some observations can be made.

The Kalman gain regarding the unknown input, K_d, is very consistent throughout the simulation, being about 300.5 in value. This is quite high, but seen as K_d is dependent on the error covariance of the unknown input P_d, it is not surprising. However, looking at how P_d is defined, see Equation (2.117), nothing stands out as the source of the increased variance.

Keeping an eye on the equations, a source of the noise may become apparent. In Equation (2.115), where the unknown input is defined for iteration k, one may notice that d_k is explicitly dependent on the current innovation, and no prior value of itself, and given K_d, the innovation is consistently gained with a high value. Looking at (3) in Figure 6.1b, it becomes clear that considering the innovation only is problematic, due to the rapid changes between the CGM measurements. Solely considering the innovation, also rips the unknown input of any dynamical individuality, seen as it is minimized to only explain the value of the innovation.

Limitations of the filter in regards to the current problem are, by the above analysis, very clear, however future use in areas outside blood glucose estimation should not be disregarded, just yet. As stated in [46], the filter is able to robustly estimate the states, even with presence of unknown inputs. Including G_p in the state vector is then more beneficial, and having other bodily phenomenons act as the unknown inputs. This was not done in this thesis, seen as the purpose of using an unknown input filter was to observe the performance when G_p was set as the unknown input.

In a potential different project it could make sense to consider for example biofouling and erosion, as bodily phenomenons acting as unknown inputs, seen as they affect CGM sensors and are notoriously hard, if even possible, to measure. Letting RTSKF-UI then estimate G_{isf} could be very interesting, seeing if the robust characteristic remains throughout the measurement window, and if the filter is able to identify such unknown inputs, and eliminate their effect.

7.5.6 M-Robust KF

Due to added emphasis on estimate robustness in this thesis, and due to promising results using KF, it was natural to investigate robust Kalman filters for BG estimation. Robust KFs have been given quite a great deal of attention from research in recent years, hence there is a wast ocean of filters to choose from. [50] caught the authors attention, mainly due to the formulation of the KF by use of regression, which was considered very interesting.

In Section 2.2.8 an exact way of finding the M-robust estimate is explained, however this method is not used in the thesis code. In the code the estimate is found through minimizing Equation (2.134), using the Huber score function Equation (2.136). This was a design choice made based on the fact that even through using the Matlab function `fminsearch`, time consumption did not over-exceed the time threshold of 1.2 sec per for-loop iteration, which is documented in Table 6.4. Solving the optimization problem in this manner is by that considered good enough in the current context. The exact solution is still included in the theory, in order to show that the M-robust KF can perform even faster, should the need arise.

The M-robust filter uses the same model as the KF, the rate-only model. Due to this, the resulting tuning of the KF, is used as the initial starting point of tuning for this filter. No better performance was obtained through tuning the process noise covariance matrix of the M-robust filter, and the same responses triggered by adjusting the tuning variables were observed. The same can be said about the LPF smoothing factor, as well as the regression and smoothing intervals, hence all tuning variables

are set equal between the two filters, see Table 6.3.

Despite promising theory backing the filters robust claims, it did not perform significantly better than the normal KF. It was anticipated that the filter would make the estimate robust against sensor anomalies, such as is depicted in (2) in Figure 6.1b, but by inspecting Figure 6.7, it becomes clear that this anticipation is unfortunately let down. The M-robust estimate suffers from the same flaws as the KF estimate, and is not able to stay robust during the sensor anomalies. After further inspection of the anomalies, the reason behind this was discovered, which is discussed in Section 7.2.2. There are simply too many data points drifting, for a prolonged window of time, for the M-robust filter to act in a robust manner.

Seen from the filter's perspective, the drift is viewed as simply the dynamics, and not as outliers. An outlier is by definition high intensity noise realizations, which deviates from the Gaussian model. When errors or flaws consists of multiple data points, no such deviation from the Gaussian model occurs, hence no outliers are detected. This theory is further backed by the statistical scores in Table 6.5-Table 6.8, where the M-robust KF scores are very similar to what is reported for the KF estimates.

Due to the lack of robust behaviour in the M-robust KF estimates, simulated data containing outlier typical noise characteristics was constructed, in order to properly see the robust filter actively act robust against outliers. The system was implemented to resemble the actual data sets, having a sampling time of 1.2 sec, and using the rate-only model, with $T = 6\,\text{min}$ and $a = -0.0018$. Then by randomly generating outliers as part of the measurement noise, the difference between the robust and the non-robust filters became apparent, see Figure 6.9. Take note of that the state depicted is G_{isf}, and not the estimate BG level. This is simply because, seen as the outliers is part of the measurement noise, which is only related to the ISF glucose level state, it is considered more visually clean to show the M-robust filter performance this way. The M-robust estimate is consistently and smoothly following the real system G_{isf}, without being corrupted by the outliers, while the KF estimate is affected by the outliers. Between the two filters, there is no denying that the M-robust filter show exceptional results in eliminating outlier effect, and is the preferred filter under the given circumstances.

The M-robust filter may not have worked as anticipated by making the estimate robust against the relevant sensor anomalies in the real data. However, absence of actual outliers may not persist in future data sets. Because of this the M-robust filter should not be disregarded, seen as Figure 6.9 clearly show the power of the filter in the presence of outliers. It is therefore the authors recommendation that the filter should be further explored, and tested, because of its potential superiority over the standard KF, in presence of noise which deviates from the Gaussian model.

7.6 Accuracy Assessment

The accuracy assessment of the estimates in this project involves evaluating MSE and MAPE values, with BGA measurement as the comparing value, and inspecting the estimates standard deviation, where it available. This is an improvement from the term project, where only statistical scores were considered, and such measures were seen as sub optimal when estimates portrayed high degree of noise, see [1]. The measures root mean square error and MAE was also part of the accuracy assessment from that project. However due to similarities with MSE and MAPE, respectively, their

inclusion is experienced redundant, hence they are excluded here.

The sub-optimality of only considering statistical scores can be seen in practice in Table 6.5-Table 6.8, where the RTSKF-UI and FD approximation filter is seen having MAPE scores below 10%, for which an estimate is considered very accurate, and MSE scores are somewhat similar to the KF and M-robust KF scores. The estimates themselves, see Figure 6.6a and Figure 6.3a, tell another story, where they appear very noisy, and for any practical usage would be considered completely useless. This claim is backed by inspecting Figure 6.6b, where it can be seen that the filter itself is highly uncertain about the estimate, due to excessively high estimate standard deviation.

Another important point about including the standard deviation in accuracy assessment, is the availability of BG level measurements, or rather the lack there off. In a real life use of the algorithms, BG level measurements may not be available for comparison, in order to asses the estimate performance. Under such circumstances the standard deviation is the best way to investigate estimate performance, if standard deviation is available in the filter algorithm, naturally. In KFs, error covariance is calculated at every filter iteration, providing a solid amount of data to investigate, compared to sparse BGA measurements in the project's data sets, or considering a more real-life example, potentially even more sparse SMBG samples.

A bit more discussion is needed for explaining as to why the MAPE and MSE scores portray a good estimate in the case of RTSKF-UI and FD approximation, despite the opposite being true. Looking at Figure 6.6a and Figure 6.3a, the BGA samples can be seen "inside" what is perceived visually as colored blocks, hence it is highly likely that the estimates hits these comparing samples at the exact right time by chance, creating a false impression of the performance. This may also explain why in some cases the enhanced FD estimates are shown having worse scores than the filter itself, indicating these estimates as less accurate, which, by looking at the figures can be claimed as incorrect.

Due to these observations, the accuracy scores of the RTSKF-UI and FD approximation are classified as non-informative, and their performance will be based solely on the standard deviation in the RTSKF-UI case, as well as visual impressions of the figures. This decision is based on the above discussion, and is made in order to avoid confusion when discussing the scores, seen as the relevant scores are, according to theory, considered decent. Still, it is interesting having observed how simple accuracy measures may fail, in the presence of high frequent noise, which is an observational enrichment worth remembering. Either way, it stands to prove, that the assumption of needing more information about estimate accuracy in the term project, in order to properly asses accuracy, was indeed correct.

Regarding the KF and M-robust KF accuracy, it can immediately be experienced that the scores better represents the estimates behaviour in the figures. See Table 6.5-Table 6.8 for the scores, and please compare them to Figure 6.4 and Figure 6.7, respectively. The scores between the KF and the M-robust KF are experienced very similar. This is not surprising, seen as they operate alike in the absence of outliers, and as it has already been established, few outliers are present in the data sets. The comparison between a KF and a M-robust KF in Figure 2.10, on the other hand indicates that had outliers been present, the M-robust filter would have produced lower scores than the KF.

Notice that the scores for Mar 5th, and Mar 1st, 2021 are consistently lower than the Mar 10th, 20210 and the Nov 20th, 2020 data sets, for all three variants of time constants. Looking at Table 6.1, it can also be noticed that the experiment time duration are considerably shorter for Mar 10th, 2021 and Nov 20, 2020 compared to the other data sets. It might be that over time the sensor becomes more reliable, adjusting to the bodily environment it is injected into, which might affect accuracy of measurements. Measurement accuracy affects scores for estimate accuracy, hence this might be a

cause of the difference in scores.

Meals might be another factor to account for, seen as mostly one large meal is present in Mar 10th, 2021 data set and Nov 20th, 2020 data set, while several meals are recorded in the other data sets. The estimate will perform best when time lag is more evident, which is during rapid chaining glucose events, such as meals. This claim is backed by observing the figures, where BG level estimate is closer to BGA samples at rising and falling BG level, compared to flatter areas.

Regardless, MSE and MAPE for all time constants and data sets are lower than the scores of the comparison between CGM and BGA measurements, see Table 6.5-Table 6.8. MAPE is also below the 10% barrier in all cases, which indicates that KF and M-robust KF are accurate methods for estimating BG level. This is also reflected in the standard deviation plots of both methods, see Figure 6.5 and Figure 6.8. M-robust KF standard deviation is slightly higher than KF standard deviation, for all three state estimates. However, the difference is not dramatic. This could also simply be the robustness of the M-robust filter, and it might even be to the filter's advantage in the presence of outliers.

7.7 Comparison between Central-Remote Rate model and Rate-Only Model

Based on the above discussion, it is pretty clear that the rate-only model using either KF or M-robust KF is the model to be preferred, among the tested models, for BG level estimation. However, one important questions still remains: Does the simpler rate-only model out-compete the four state central-remote rate model? In addressing this, some remarks have to be made. First, the comparing result for the central-remote rate model will be the results from the pending approval conference paper, see Appendix D, due to it being the most recent use of the model by the author. Secondly, the diffusion process time constant in the paper is set to 7 min, while the time constants in this thesis vary from $4-8$ min. Thirdly, neither MSE, nor evaluation of estimate standard deviation, was part of the accuracy assessment in the paper, hence only MAPE values and figures can be compared between the two. Lastly, only Mar 5th and Mar 1st, 2021 data sets were used in the paper, so only results from these data sets will be compared.

MAPE values between these two models does not portray clear evidence of which model can be considered the superior. For Mar 5th, 2021 the central-remote rate model performs best, but the opposite is true for the Mar 1st, 2021 data set. The filter estimate slope appears smoother for the rate-only model, but this is most likely due to different tuning of the process noise covariance matrix, and similar result might be achieved with the central- and remote rate model by adjusting Q, while differences in smoothed estimates may be the result of different smoothing intervals.

One model can by that not be said to be significantly better than the other. However, seen as the rate-only model achieves results at the same level as the more complex central-remote rate model, it might be the preferred model, when model complexity is an issue. This statement is made, based only on the current tuning of Q, for both models. Regardless, the goal of achieving a BG level estimate, using a simple model, is, based on this discussion, considered achieved.

Chapter 8

Concluding remarks

8.1 Conclusion

FD approximation filter with rearranged Steil-Rebrin model, RTSKF-UI with Steil-Rebrin model where BG level is set as unknown input, standard KF with rate-only model in combination with Steil-Rebrin model and M-robust KF with the same model as KF, all show great real time properties. However, only KF and M-robust KF are experienced sufficient for real-time estimation of BG level, using only ISF glucose level measurements. Further, out of the two, the M-robust KF is considered superior, simply due to the potential implications outliers may induce upon future data, despite not showing robust qualities in this work.

Robustness of filter estimates themselves is not achieved in this thesis, due to wrongful initial interpretation of CGM measurement anomalies, which is eventually classified as minimal drifts. It is observed that robust filters are not capable of handling multiple data samples, which are drifting for a prolonged window of time. Small drifting incidences of CGM measurements are therefor handled by enhancement methods such as MA smoothing, WLS LR and LPF of measurements. MA smoothing show the best performance in dealing with such circumstances, while also staying below the real-time threshold. Implication of regressing and smoothing filter estimates is addressed, and such implementations are viewed as a decent short term solution, but it is acknowledged that more research is needed into the topic.

In evaluating filter performance, accuracy assessment is improved from the term project assessment, with the added addition of observing estimate standard deviation during the simulations. This allows for real time estimate uncertainty evaluation, and in terms of this thesis, either backs or disproves claims about estimate accuracy based on MSE and MAPE, with BGA samples as the comparing value.

8.2 Future work

This section will list suggestions for future work, which is by the author believed to be beneficial if further research based on results from this thesis, is to be conducted. The suggestions are based upon the authors experience and interpretations made during the thesis work, as well as tasks which were needed down-prioritized, due to time shortage.

Topic 1 Fault detection, specifically targeted towards sensor drifts, should be implemented in order to allow for Kalman filters to handle such circumstances, without need of outside methods, such as smoothing or regression.

Topic 2 Implementation of PISA detection, based on [60], may increase knowledge about CGM sensor anomalies, and their origin, if PISA related.

Topic 3 Further testing of KF and M-robust KF is needed to verify M-robust KF superiority over KF in the presences of outliers, using real data.

Topic 4 Verification of filter performances for long-time use is needed. Longer time span experiments are needed in order to confirm, or disprove the filter capabilities against sensor issues like bio-fouling, erosion etc.

Topic 5 RTSK-UI, or other unknown input filters, should be tested in the presence of other unknown inputs, such as bio-fouling, erosion etc. in order to observe filter ISF glucose level estimate response.

Topic 6 More complex models should be tested, in order to investigate if the overestimation characteristic of KF and M-robust KF may be eliminated, or simply see if the estimate may improve it's stability. Inclusion of insulin, glucagon and meal modeled as inputs in a new model, and compare with the simple rate-only model could lead to interesting results.

Topic 7 New model proposals for describing ISF glucose dynamics should be tested, such as the presented model in [53], in order to either verify the Steil-Rebrin superiority, or become aware of the model's flaws.

Bibliography

[1] M. Halvorsen, 'Estimating blood glucose level based on subcutaneous sensors and analysis of blood samples,' *in attachements*, 2021.

[2] S. A. Evensen, *Blodplasma*, https://sml.snl.no/blodplasma (accessed: 25.05.2022).

[3] FreeStyle, *Hva er interstitialvæske eller vevsvæske?* https://www.freestyle.abbott/no-no/my-guide/oppdag-freestyle-libre_2/hva-er-interstitialvaeske-eller-vevsvaeske.html (accessed: 25.05.2022).

[4] D. Yetman, *What is subcutaneous tissue, also known as superficial fascia?* https://www.healthline.com/health/subcutaneous-tissue (accessed: 25.05.2022).

[5] A. Cinar and K. Turksoy, *Advances in Artificial Pancreas Systems, Adaptive and Multivariable Predictive Control*. Gewerbestrasse 11, 6330 Cham, Switzerland: Springer International Publishing AG, 2018.

[6] F. Chee and T. Fernando, *Closed-Loop Control of Blood Glucose*. Springer-Verlag Berlin Heidelberg, 2007.

[7] Wikipedia, the free encyclopedia, https://en.wikipedia.org/wiki/Glucose_meter (accessed: 25.01.2022).

[8] S. R. Patton, M. A. Clements and Children's Mercy Hospital, Kansas City, 'Continuous glucose monitoring versus self-monitoring of blood glucose in children with type 1 diabetes- are there pros and cons for both?' *US Endocrinology*, vol. 8, no. 1, pp. 27–29, 2012.

[9] G. Cappon, M. Vettoretti, G. Sparacino and A. Facchinetti, 'Continuous glucose monitoring sensors for diabetes management: A review of technologies and applications,' *Diabetes and Metabolism Journal*, vol. 43, no. 4, pp. 383–397, 2019. DOI: 10.4093/dmj.2019.0121.

[10] G. Schmelzeisen-Redeker, M. Schoemaker, H. Kirchsteiger, G. Freckmann, L. Heinemann and L. del Re, 'Time delay of cgm sensors: Relevance, causes, and countermeasures,' *Journal of Diabetes Science and Technology*, vol. 9, no. 5, pp. 1006–1015, 2015. DOI: 10.1177/1932296815590154.

[11] A. Facchinetti, G. Sparacino and C. Cobelli, 'Reconstruction of glucose in plasma from interstitial fluid continuous glucose monitoring data: Role of sensor calibration,' *IEEE Transactions on Biomedical Engineering*, vol. 1, no. 3, pp. 671–623, 2007. DOI: 10.1177/193229680700100504.

[12] B. Bequette, 'Optimal estimation applications to continuous glucose monitoring,' in *Proceedings of the 2004 American Control Conference*, vol. 1, 2004, 958–962 vol.1. DOI: 10.23919/ACC.2004.1383731.

[13] M. Kuure-Kinsey, C. C. Palerm and B. W. Bequette, 'A dual-rate kalman filter for continuous glucose monitoring,' in *2006 International Conference of the IEEE Engineering in Medicine and Biology Society*, 2006, pp. 63–66. DOI: 10.1109/IEMBS.2006.260057.

[14] O. M. Staal, S. Sælid, A. Fougner and Ø. Stavdahl, 'Kalman smoothing for objective and automatic preprocessing of glucose data,' *IEEE Journal of Biomedical and Health Informatics*, vol. 23, no. 1, pp. 218–226, 2019. DOI: 10.1109/JBHI.2018.2811706.

[15] E. J. Knobbe and B. Buckingham, 'The extended kalman filter for continuous glucose monitoring,' *Diabetes Technology & Therapeutics*, vol. 7, no. 1, pp. 15–27, 2005. DOI: 10.1089/dia.2005.7.15.

[16] Artifical Pancreas Trondheim, https://www.apt-norway.com/ (accessed: 19.01.2022).

[17] P. Kierulf and B. Svihus, *Glukose*, https://sml.snl.no/glukose (accessed: 22.03.2022), 2022.

[18] J. Hall, *Guyton and Hall Textbook of Medical Physiology*, 12th ed. 1600 John F. Kennedy Blvd., Ste 1800, Philadelphia, PA 19103-2899: Saunders, 2011.

[19] B. O. Åsvold, *Blodsukker*, https://sml.snl.no/blodsukker (accessed: 22.03.2022), 2021.

[20] Institute for Quality and Efficiency in Health Care, *Hyperglycemia and hypoglycemia in type 1 diabetes*, https://www.ncbi.nlm.nih.gov/books/NBK279340/ (accessed: 22.03.2022), 2017.

[21] Centers for Diseases Control and Preventing, *What is type 1 diabetes?* https://www.cdc.gov/diabetes/basics/what-is-type-1-diabetes.html (accessed: 22.03.2022), 2022.

[22] International Diabetes Fedartion, *Type 1 diabetes*, https://idf.org/aboutdiabetes/type-1-diabetes.html (accessed: 22.03.2022), 2020.

[23] A. L. Fougner, *TTK26 lysark diabetes glukoseregulering måling*, https://ntnu.blackboard.com (accessed: 4.12.2021), 2021.

[24] J. R. Castle and W. K. Ward, 'Amperometric glucose sensors: Sources of error and potential benefit of redundancy,' *Journal of Diabetes Sicence and Techonolgy*, vol. 4, no. 1, pp. 221–225, 2010. DOI: 10.1177/193229681000400127.

[25] ISO, *Iso-standards*, https://www.iso.org/standards.html (accessed: 07.04.2022).

[26] Standard Norge, *Ns-en iso 15197:2015*, https://www.standard.no/no/Nettbutikk/produktkatalogen/Produktpresentasjon/?ProductID=765929 (accessed: 07.04.2022).

[27] World Health Organization, *Blood gas/ph/chemistry point of care analyzer*, https://www.who.int/medical_devices/innovation/blood_gas_analyzer.pdf (accessed: 11.12.2021), 2011.

[28] Wikipedia the free encyclopedia, *Arterial blood gas test*, https://en.wikipedia.org/wiki/Arterial_blood_gas_test (accessed: 11.12.2021), 2021, (accessed: 03.04.2022).

[29] J. Bjørnstad, *Estimat*, https://snl.no/estimat (accessed: 21.04.2022).

[30] G. James, D. Witten, T. Hastie and R. Tbshirani, *An Introduction to Statistical Learning*, 1st ed. Springer, 2013. DOI: 10.1007/978-1-4614-7138-7.

[31] D. Simon, *Optimal Estimation*. John Wiley & Sons, Inc., Hoboken, 2006.

[32] MathWorks, Inc, *Low-pass filter*, https://se.mathworks.com/discovery/low-pass-filter.html?s_tid=srchtitle_low%20pass%20filter_1 (accessed: 25.05.2022).

[33] J. G. Balchen, T. Andresen and B. A. Foss, *Reguleringsteknikk*, 6th ed. Odd Bargstads plass 2D, 7491 Trondheim: Institutt for teknisk kybernetikk, 2016.

[34] F. Haugen, *Derivation of a discrete-time lowpass filter*, http://techteach.no/simview/lowpass_filter/doc/filter_algorithm.pdf (accessed: 25.05.2022).

[35] E. Ostertagovà and O. Ostertag, 'Forcasting using simple exponential smoothing method,' *Acta Electrotechnica et Informatica*, vol. 12, no. 3, pp. 62–66, 2012. DOI: 10.2478/v10198-012-0034-2.

[36] S. Glen, *Moving average: What it is and how to calculate it*, https://www.statisticshowto.com/probability-and-statistics/statistics-definitions/moving-average/ (accessed: 07.04.2022).

[37] Wikipedia the free encyclopedia, *Moving average*, https://en.wikipedia.org/wiki/Moving_average (accessed: 30.04.2022).

[38] Wikipedia the free encyclopedia, *Weighted least squares*, https://en.wikipedia.org/wiki/Weighted_least_squares (accessed: 30.04.2022).

[39] Carnegie Mellon University, *Lecture 24–25: Weighted and generalized least squares*, https://www.stat.cmu.edu/~cshalizi/mreg/15/lectures/24/lecture-24--25.pdf (accessed: 21.04.2022).

[40] W. S. Cleveland, 'Robust locally weighted regression and smoothing scatterplots,' *Journal of the American Statistical Association*, vol. 74, no. 368, pp. 829–836, 1979. DOI: 10.1080/01621459.1979.10481038.

[41] R. J. LeVeque, *Finite Difference Methods for Ordinary and Partial Differential Equations: Steady-State and Time-Dependent Problems*, 1st ed. 600 Market Street, 6th Floor, Philadelphia, PA 19104-2688 USA: Society for Industrial and Applied Mathematics, 2018.

[42] J. T. Xing, 'Chapter 11 - mixed finite element–computational fluid dynamics method for nonlinear fluid–solid interactions,' in *Fluid-Solid Interaction Dynamics*, Academic Press, 2019, pp. 409–485, ISBN: 978-0-12-819352-5. DOI: https://doi.org/10.1016/B978-0-12-819352-5.00011-2.

[43] kakitc, *Finite difference*, https://en.wikipedia.org/wiki/Finite_difference#/media/File:Finite_difference_method.svg (accessed: 25.05.2022).

[44] W. J. Richard E.Thomson, *Data Analysis Methods in Physical Oceanography*, 3rd ed. Elsevier Science Publishing Co. Inc., 2014.

[45] R. G. Brown and P. Y. C. Hwang, *Introduction to Random Signals and Applied Kalman Filtering*, 4th ed. John Wiley & Sons Inc., 2012.

[46] C.-S. Hsieh, 'Robust two-stage kalman filters for systems with unknown inputs,' *IEEE Transactions on Automatic Control*, vol. 45, no. 12, pp. 2374–2378, 2000. DOI: 10.1109/9.895577.

[47] P. K. Kitanidis, 'Unbiased minimum-variance linear state estimation,' *Automatica*, vol. 23, no. 6, pp. 775–778, 1987, ISSN: 0005-1098. DOI: https://doi.org/10.1016/0005-1098(87)90037-9. [Online]. Available: https://www.sciencedirect.com/science/article/pii/0005109887900379.

[48] C.-S. Hsieh and F.-C. Chen, 'Optimal solution of the two-stage kalman estimator,' *IEEE Transactions on Automatic Control*, vol. 44, no. 1, pp. 194–199, 1999. DOI: 10.1109/9.739135.

[49] E. Ronchetti, 'The main contributions of robust statistics to statistical science and a new challenge,' *Metron*, no. 79, pp. 127–135, 2021. DOI: 10.1007/s40300-020-00185-3.

[50] Z. Durovic and B. Kovacevic, 'Robust estimation with unknown noise statistics,' *IEEE Transactions on Automatic Control*, vol. 44, no. 6, pp. 1292–1296, 1999. DOI: 10.1109/9.769393.

[51] P. J. Huber, 'Robust regression: Asymptotics, conjectures and monte carlo,' *The Annals of Statistics*, vol. 1, no. 5, pp. 799–821, 1973, ISSN: 00905364. [Online]. Available: http://www.jstor.org/stable/2958283 (visited on 06/04/2022).

[52] K. Rebrin, G. M. Steil, W. P. van Antwerp and J. J. Mastrototaro, 'Subcutaneous glucose predicts plasma glucose independent of insulin: Implications for continuous monitoring,' *American Journal of Physiology-Endocrinology and Metabolism*, vol. 277, no. 3, E561–E571, 1999. DOI: 10.1152/ajpendo.1999.277.3.E561.

[53] T. Koutny, 'Blood glucose level reconstruction as a function of transcapillary glucose transport,' *Computers in Biology and Medicine*, vol. 53, pp. 171–178, 2014, ISSN: 0010-4825. DOI: https://doi.org/10.1016/j.compbiomed.2014.07.017.

[54] A. Facchinetti, S. Del Favero, G. Sparacino, J. R. Castle, W. K. Ward and C. Cobelli, 'Modeling the glucose sensor error,' *IEEE Transactions on Biomedical Engineering*, vol. 61, no. 3, pp. 620–629, 2014. DOI: 10.1109/TBME.2013.2284023.

[55] The MathWorks, Inc, https://se.mathworks.com/help/ident/gs/about-system-identification.html (accessed: 06.03.2022).

[56] K. J. Keesman, *System Identification: An Introduction*, 1st ed. Springer, London, 2011. DOI: https://doi.org/10.1007/978-0-85729-522-4.

[57] The MathWorks, Inc, https://se.mathworks.com/help/matlab/math/optimizing-nonlinear-functions.html#bsgpq6p-11 (accessed: 06.03.2022).

[58] omstaal, *Kalman-smoothing-glucose*, https://github.com/omstaal/kalman-smoothing-glucose/tree/master/smoother (accessed: 20.09.2021), 2018.

[59] S. Miloš Stojanović, *Robust kalman*, https://github.com/milsto/robust-kalman (accessed: 17.01.2022), 2018.

[60] B. Nihat, C. Fraser, B. Bruce a, W. Darrell M, C. H Peter, M. David M, B. B Wayne and IHCL, 'A novel method to detect pressure-induced sensor attenuations (pisa) in an artificial pancreas,' *Journal of diabetes science and technology*, vol. 8, no. 6, pp. 1091–1096, 2014. DOI: 10.1177/1932296814553267.

[61] C. D. Man, F. Micheletto, D. Lv, M. Breton, B. Kovatchev and C. Cobelli, 'The uva/padova type 1 diabetes simulator: New features,' *Journal of Diabetes Science and Technology*, vol. 8, no. 1, pp. 26–34, 2014. DOI: 10.1177/1932296813514502.

[62] C. Scuffi, F. Lucarelli and F. Valgimigli, 'Minimizing the impact of time lag variability on accuracy evaluation of continuous glucose monitoring systems,' *Journal of Diabetes Science and Technology*, vol. 6, no. 6, pp. 1383–1391, 2012. DOI: 10.1177/193229681200600618.

[63] X. Zhang, F. Sun, W. Wongpipit, W. Y. J. Huang and S. H. S. Wong, 'Accuracy of flash glucose monitoring during postprandial rest and different walking conditions in overweight or obese young adults,' *Frontiers in physiology*, vol. 12, no. 732751, pp. 1072–1079, 2021. DOI: 10.3389/fphys.2021.732751.

[64] N. Ghane, M. M. Broadney, E. K. Davis, R. W. Trenschel, S. M. Collins, S. M. Brady and J. A. Yanovski, 'Estimating plasma glucose with the freestyle libre pro continuous glucose monitor during oral glucose tolerance tests in youth without diabetes,' *Pediatric Diabetes*, vol. 20, no. 8, pp. 1072–1079, DOI: https://doi.org/10.1111/pedi.12910.

Appendix A

Matlab Source Code

A list of all Matlab functions, and scripts are listed below, in addition to a short description about their objective, and main purpose. For the entire code, please see attachments.

- `main.m` - Main file for running simulations. Data is retrieved, model parameters are set, and all requested functions are called. Requested functions are needed specified, so is the wanted data set for running the simulations. Model parameters may also be adjusted in this file, if need be.

- `modelParamEst.m` - Script for estimating model parameters for all data sets, the model parameters being the diffusion time constant, and the BG level rate of decay.

- `SimSys.m` - Script for running M-robust KF estimation for a simulated system, using rate-only model.

- `getBGAdata.m` - Function file for retrieving information from an xlsx file. Inputs to the function are an xlsx file, as well as a date variable. Output is a vector of BGA measurements, vectors of insulin injections, glucagon injections and meals, as well as corresponding time vectors.

- `getCGMdata.m` - Function file retrieving the CGM information from cvs files. Input is a cvs file, and output is a vector of CGM measurements, in addition to a corresponding time vector.

- `convertToRelativeTime.m` - Function file from [58]. Input is time vector consisting of date times, as well as a start time for conversion. Output is a relative time time-vector.

- `getEqualLenVec.m` - Function file for achieving equal length of CGM and BGA vectors. Inputs are a CGM measurement vector, as well as the corresponding time vector, and BGA time vector. Output are new CGM measurement and time vectors, macthed with the BGA time vector.

- `setModel.m` - Function file for model building. Inputs are a diffusion time constant, a BG level rate of decay constant, and choice of model. Output is a structured array called model, which contains the necessary fields, corresponding to the model choice.

- `augmentWithLPF.m` - Function file for augmenting arbitrary model with LPF state for measurements. Inputs are a model structured array, a smoothing factor and bool variable for inputs in the model or not. Output is a new model structured array, with the necessary fields.

- `FDapprox.m` - Function file for finite difference approximation. Inputs are CGM measurement and corresponding time vector and sampling time, diffusion process time constant, BGA measurement and time vector (for plotting), and arguments for specifying enhancement methods. Output is an output structured array containing the estimated states as fields, as well as the corresponding time vector.

- `standardKF.m` - Function file for standard Kalman filter. Inputs are CGM measurements and corresponding time vector and sampling time, diffusion process time constant, BG rate of decay, smoothing factor, BGA measurements and time vector (for plotting), and arguments for specifying enhancement methods. Output is an output structured array, containing all estimated states as fields, as well as the corresponding time vector, in addition to the corresponding standard deviation of the state error covariance matrix.

- `robustTwoStageKFui.m` - Function file for robust two-stage Kalman filter with unknown inputs. Inputs are CGM measurements and corresponding time vector and sampling time, diffusion process time constant, BG rate of decay, smoothing factor, BGA measurements and time vector (for plotting), and arguments for specifying enhancement methods. Output is an output structured array, containing all estimated states as fields, as well as the corresponding time vector, in addition to the corresponding standard deviation of the state error covariance matrix.

- `MrobustKF.m` - Function file for M-robust Kalman filter. Inputs are CGM measurements and corresponding time vector and sampling time, diffusion process time constant, BG rate of decay, smoothing factor, BGA measurements and time vector (for plotting), and arguments for specifying enhancement methods. Output is an output structured array, containing all estimated states as fields, as well as the corresponding time vector, in addition to the corresponding standard deviation of the state error covariance matrix.

- `linearRegression.m` - Function file for performing linear regression or WLS linear regression. Inputs are predictors, responses, bool variable for computation of intercept or not and bool variable for computation with WLS or not. The output a vector containing the estimated responses.

- `computeError.m` - Function file for computing MSE and MAPE. Inputs are vectors containing a true response, and an estimated response, as well as corresponding time vectors. Output is a error structured array, containing MSE and MAPE values as fields.

Appendix B

Additional Results

Data sets

Mar 10th, 2021, mar 1st, 2021 and nov 20, 2020 data sets, with identified meals can be found in Figure B.1.

FD approximation

Results of FD approximation of BG level from Mar 10th, 2021 data set can be found in Figure B.2, from Mar 1st, 2021 data set in Figure B.3 and from Nov 20th, 2020 data set in Figure B.4.

Kalman filter

Results of KF estimation of BG level from Mar 10th, 2021 data set can be found in Figure B.5 and Figure B.6 from Mar 1st, 2021 data set in Figure B.7 and Figure B.8 and from Nov 20th, 2020 data set in Figure B.9 and Figure B.10.

Robust Two-Stage Kalman Filter- With Unknown Inputs

Results of RTSKF-UI estimation of BG level from Mar 10th, 2021 data set can be found in Figure B.11, from Mar 1st, 2021 data set in Figure B.12 and from Nov 20th, 2020 data set in Figure B.13.

M-Robust Kalman Filter

Results of KF estimation of BG level from Mar 10th, 2021 data set can be found in Figure B.14 and Figure B.15 from Mar 1st, 2021 data set in Figure B.16 and Figure B.17 and from Nov 20th, 2020 data set in Figure B.18 and Figure B.19.

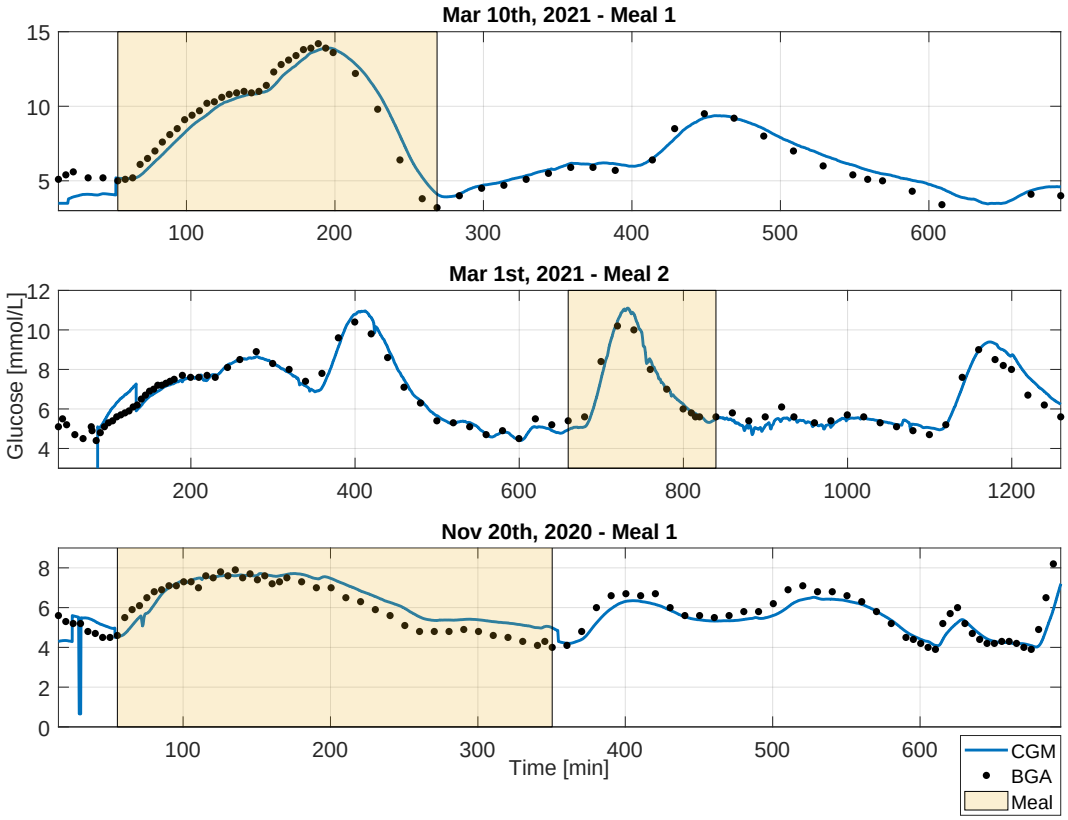

Figure B.1: CGM, BGA and one identified meal, for mar 10th, 2021, mar 1st, 2021 and nov 20, 2020 data sets.

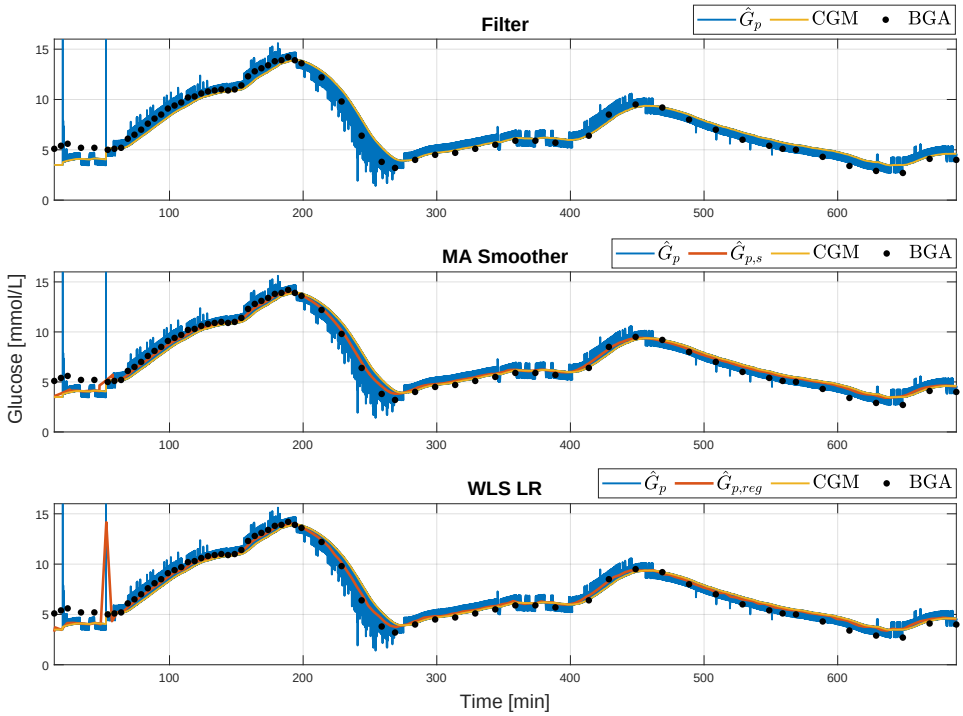

(a) FD approximation of BG level with enhancements.

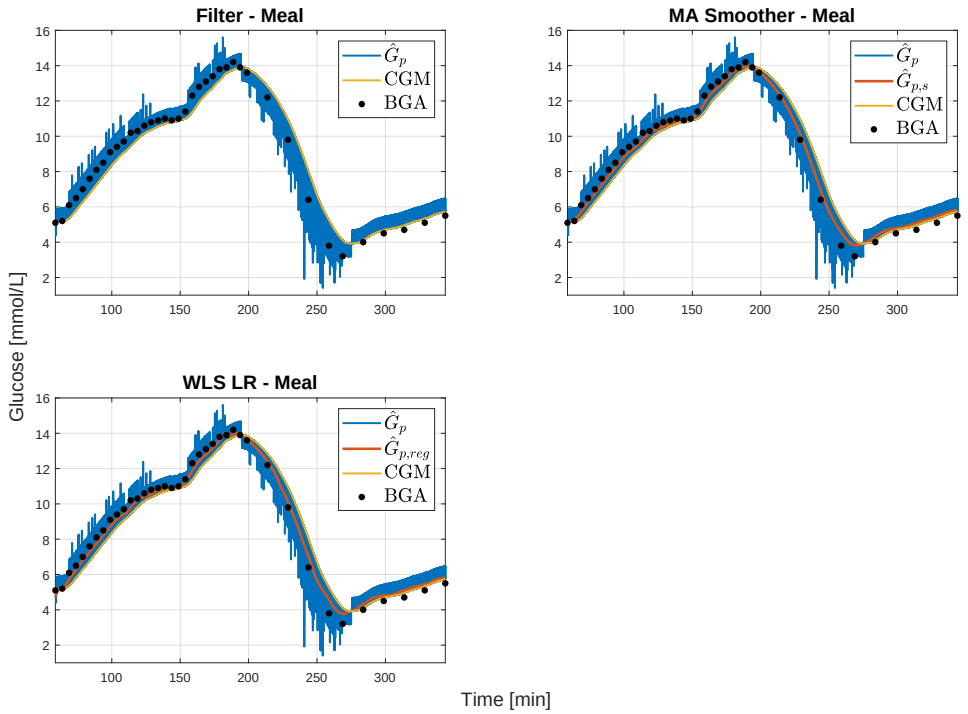

(b) FD approximation of BG level with enhancements, zoomed in on meal number two.

Figure B.2: FD approximation results for the Mar 10th, 2021 data set.

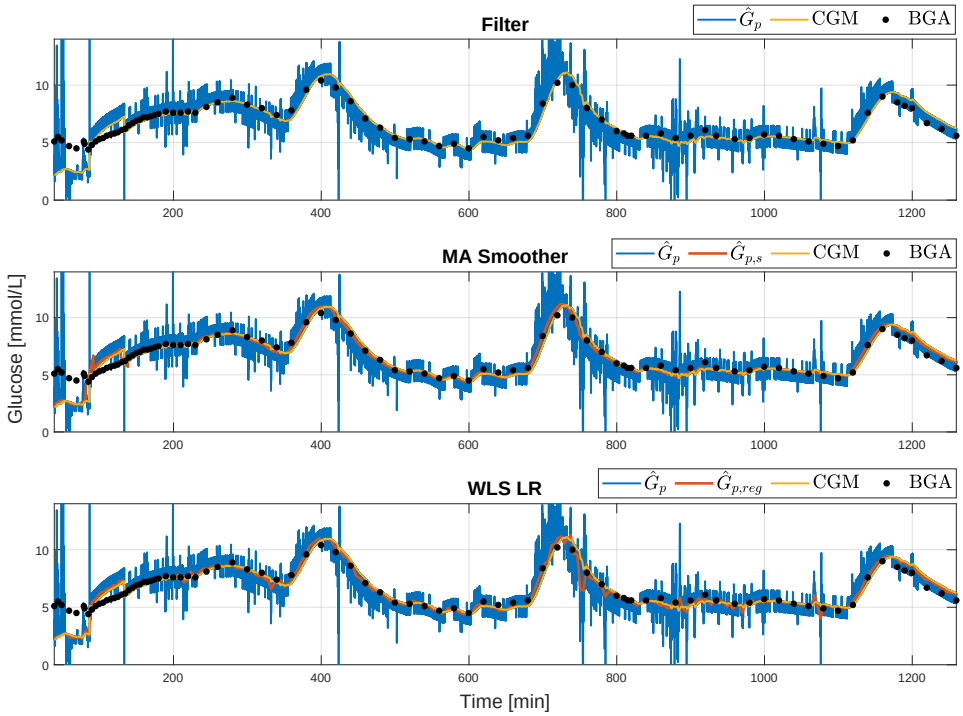

(a) FD approximation of BG level with enhancements.

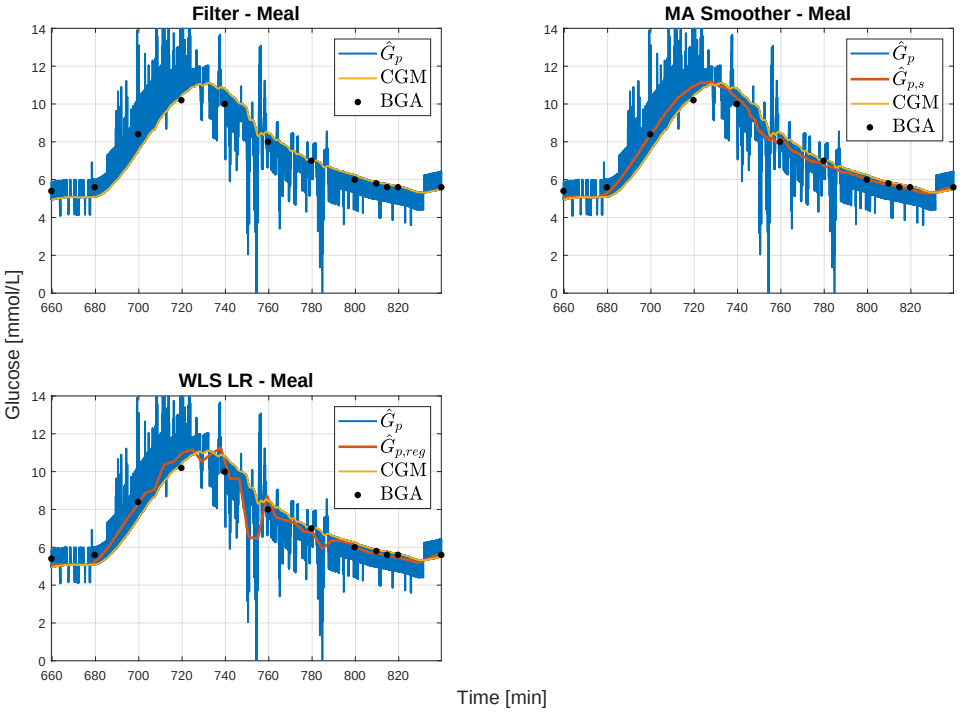

(b) FD approximation of BG level with enhancements, zoomed in on meal number two.

Figure B.3: FD approximation results for the Mar 1st, 2021 data set.

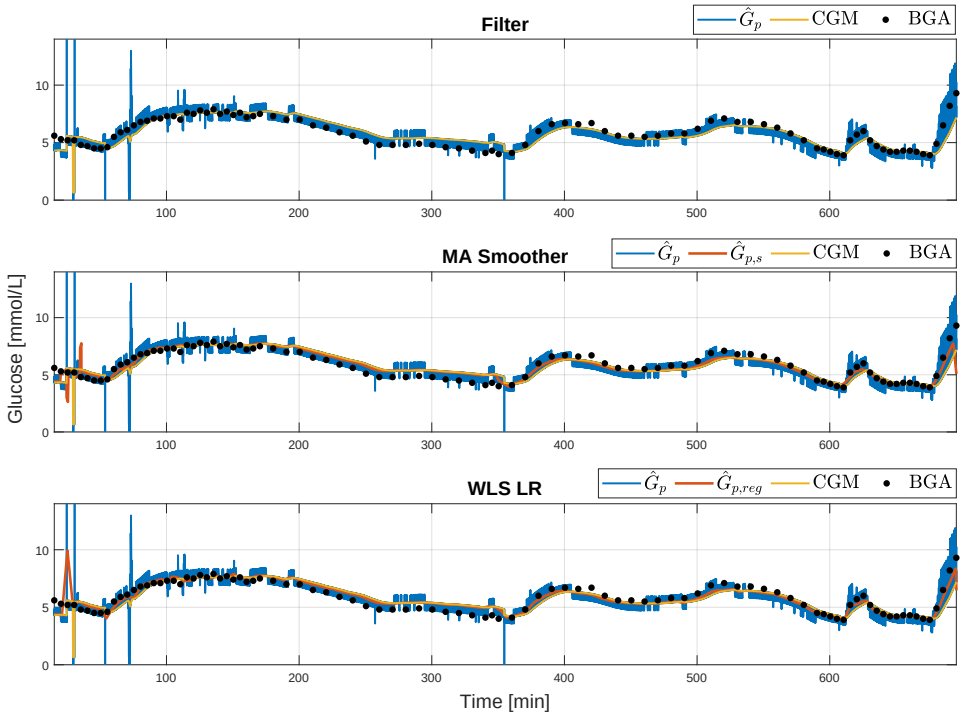

(a) FD approximation of BG level, with enhancements.

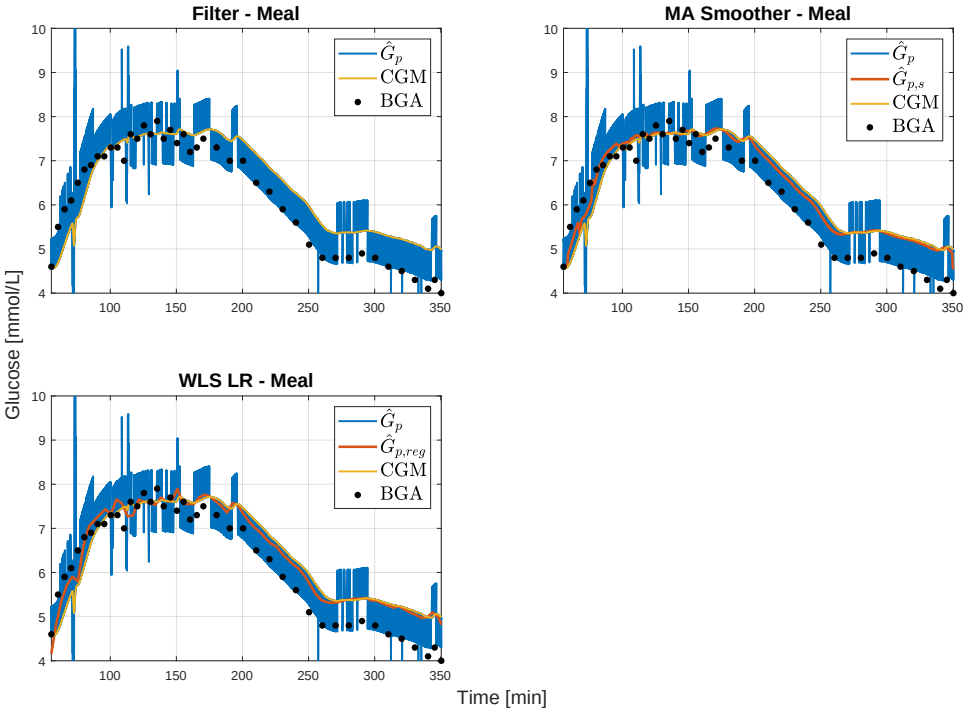

(b) FD approximation with enhancements, zoomed in on meal number one.

Figure B.4: FD approximation results for the Nov 20th, 2020 data set.

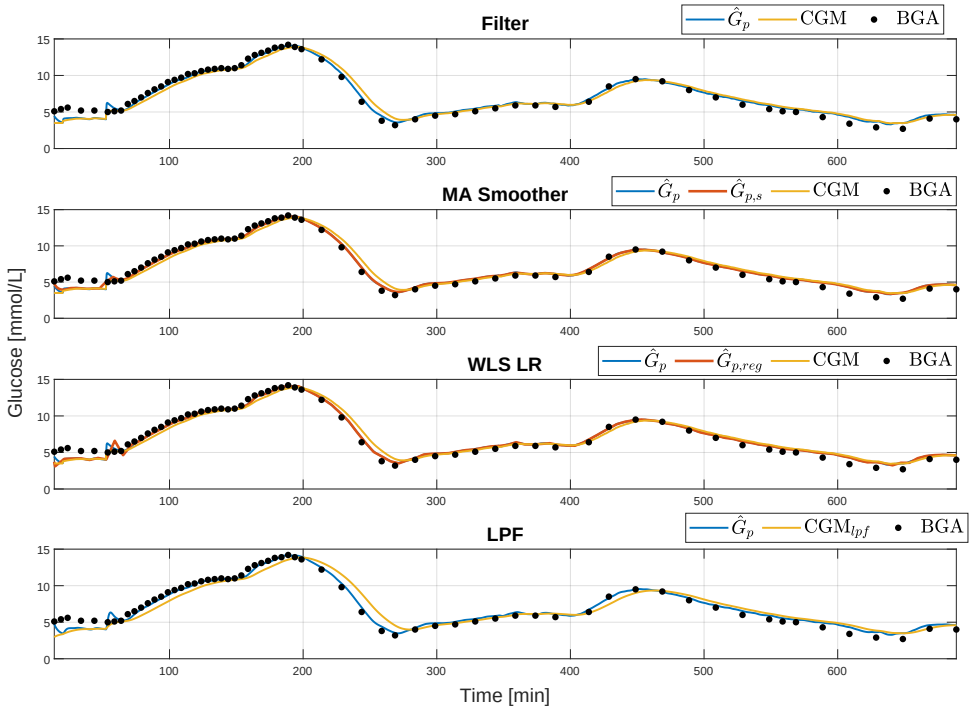

(a) KF estimate of BG level with enhancements.

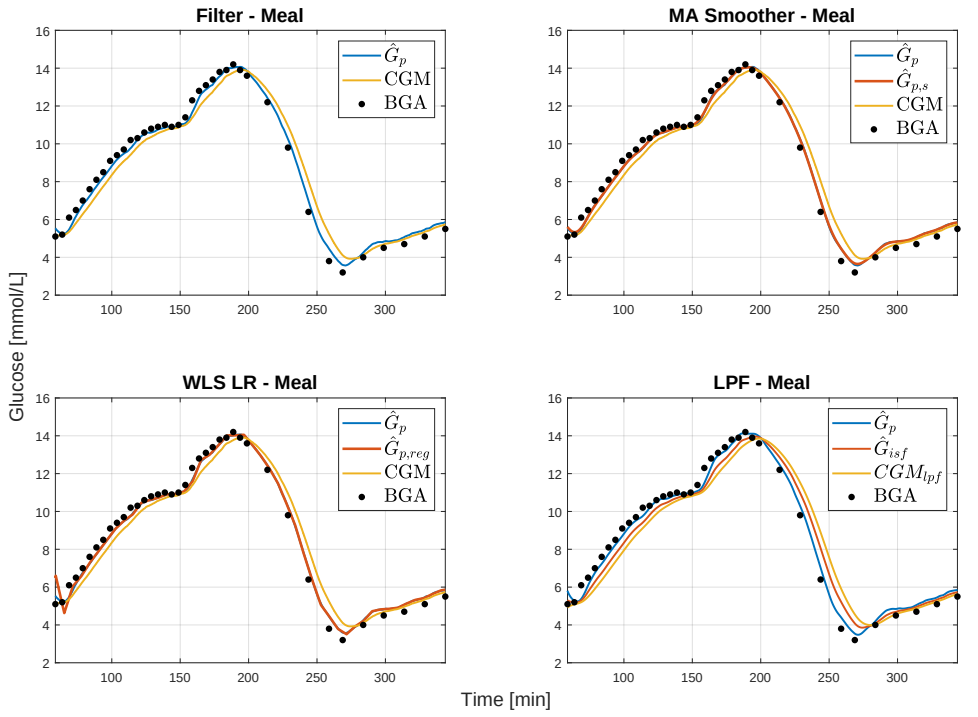

(b) KF estimate of BG level with enhancements, zoomed in on meal number one.

Figure B.5: KF results for the Mar 10th, 2021 data set.

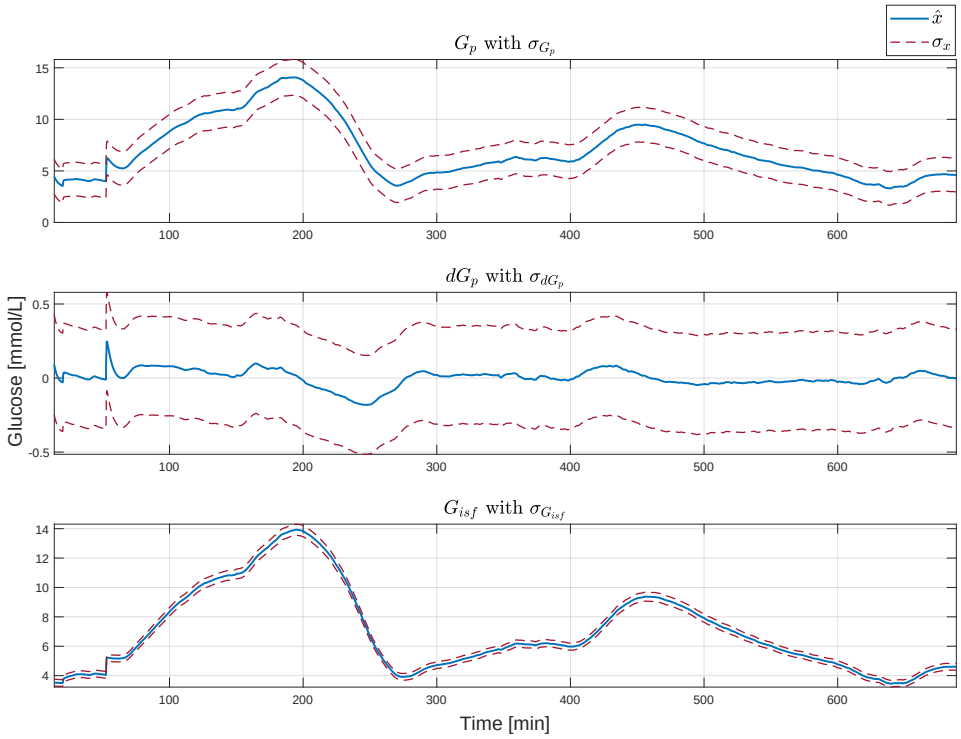

(a) KF estimate of BG level with SD.

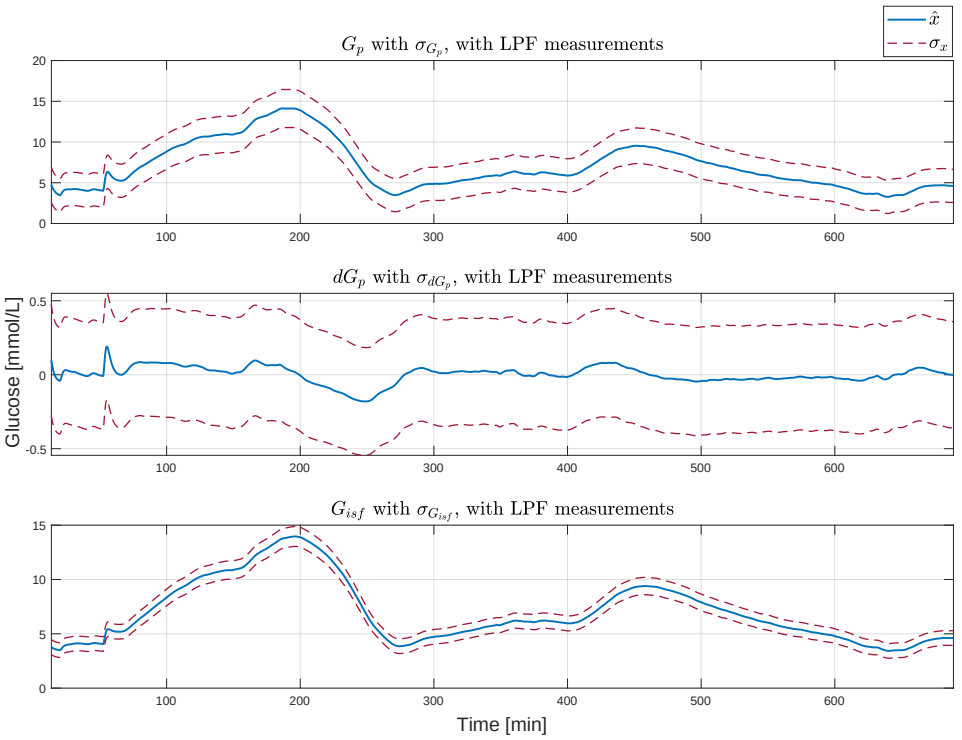

(b) KF estimate of BG level of LPF measurements, with SD.

Figure B.6: KF results for the Mar 10th, 2021 data set, displayed with SDs. $\hat{x}$ describes estimate x, while σ_x referrers to the standard deviation of estimate x.

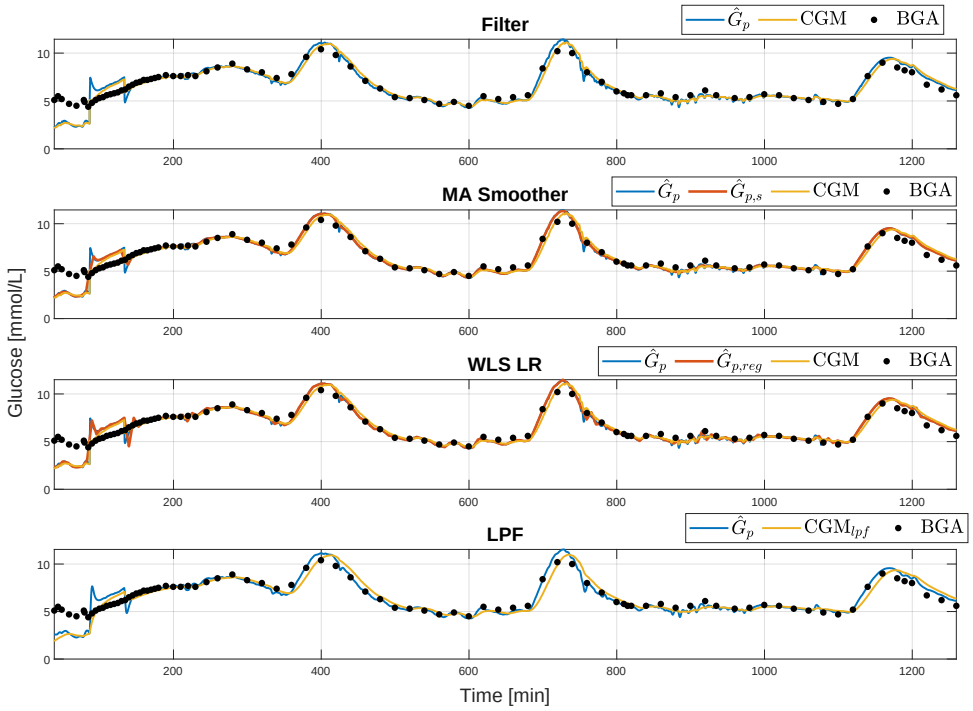

(a) KF estimate of BG level with enhancements.

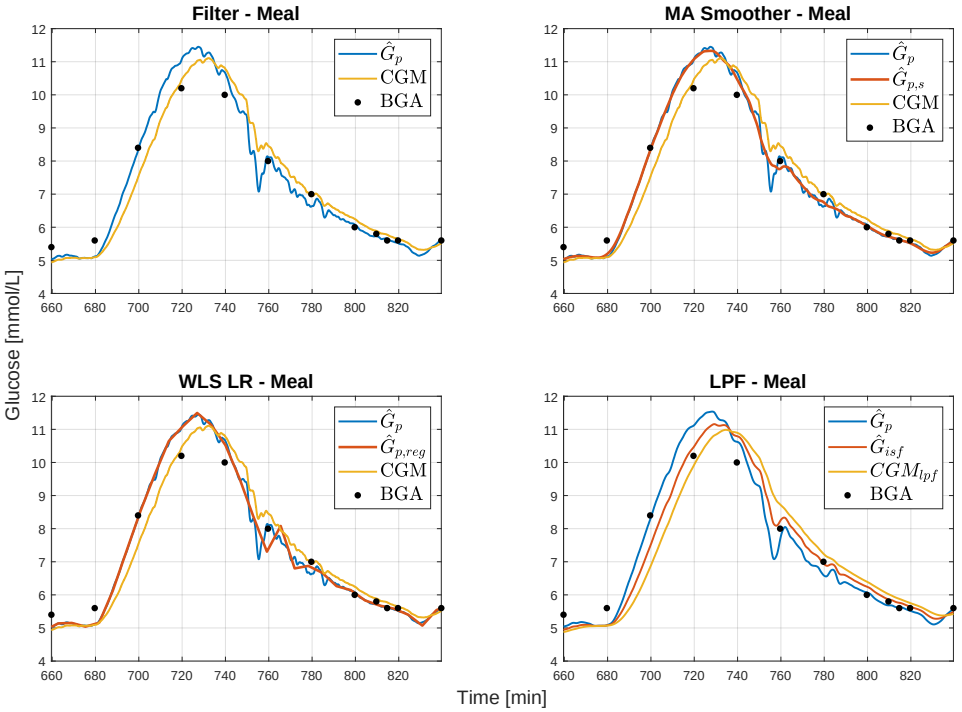

(b) KF estimate of BG level with enhancements, zoomed in on meal number two.

Figure B.7: KF results for the Mar 1st, 2021 data set.

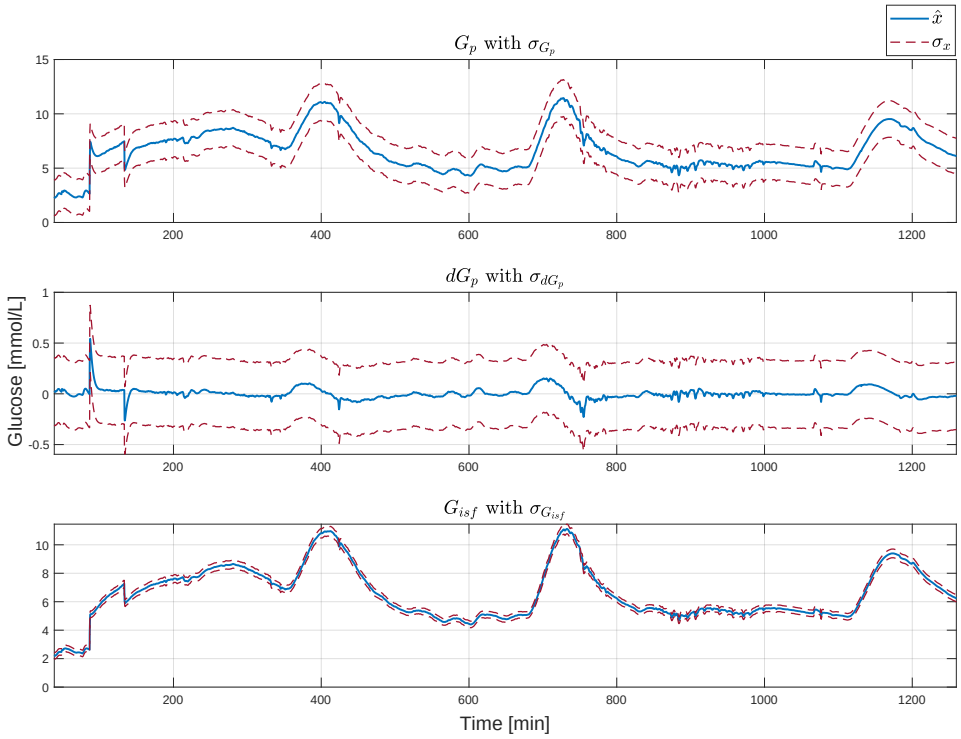

(a) KF estimate of BG level with SD.

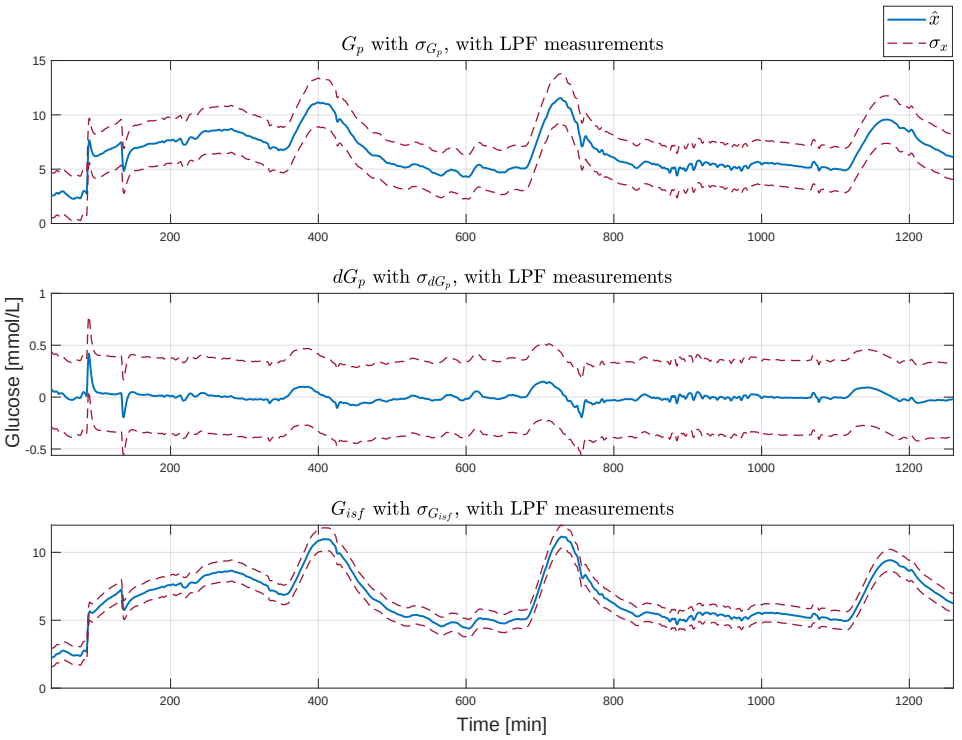

(b) KF estimate of BG level of LPF measurements, with SD.

Figure B.8: KF results for the Mar 1st, 2021 data set, displayed with SDs. $\hat{x}$ describes estimate x, while σ_x referrers to the standard deviation of estimate x.

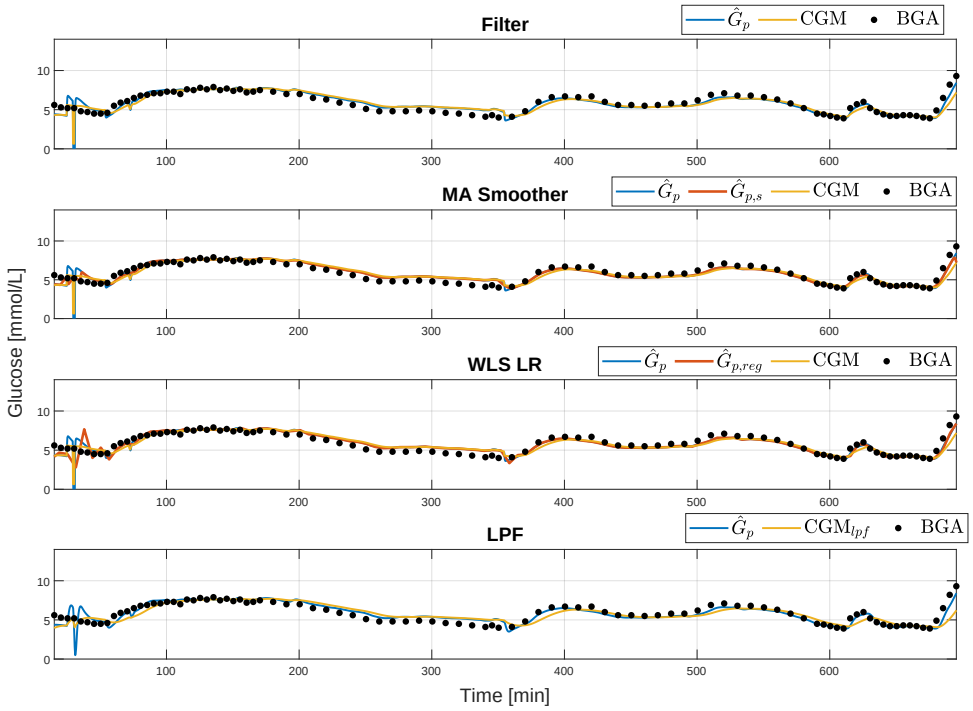

(a) KF estimate of BG level with enhancements.

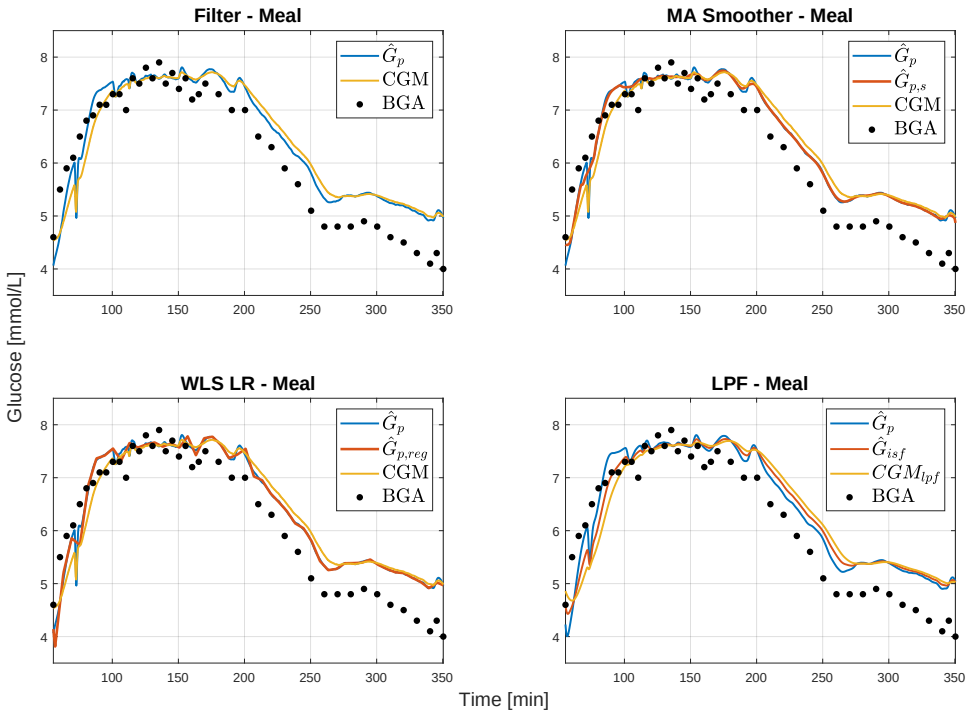

(b) KF estimate of BG level with enhancements, zoomed in on meal number two.

Figure B.9: KF results for the Mar 1st, 2021 data set.

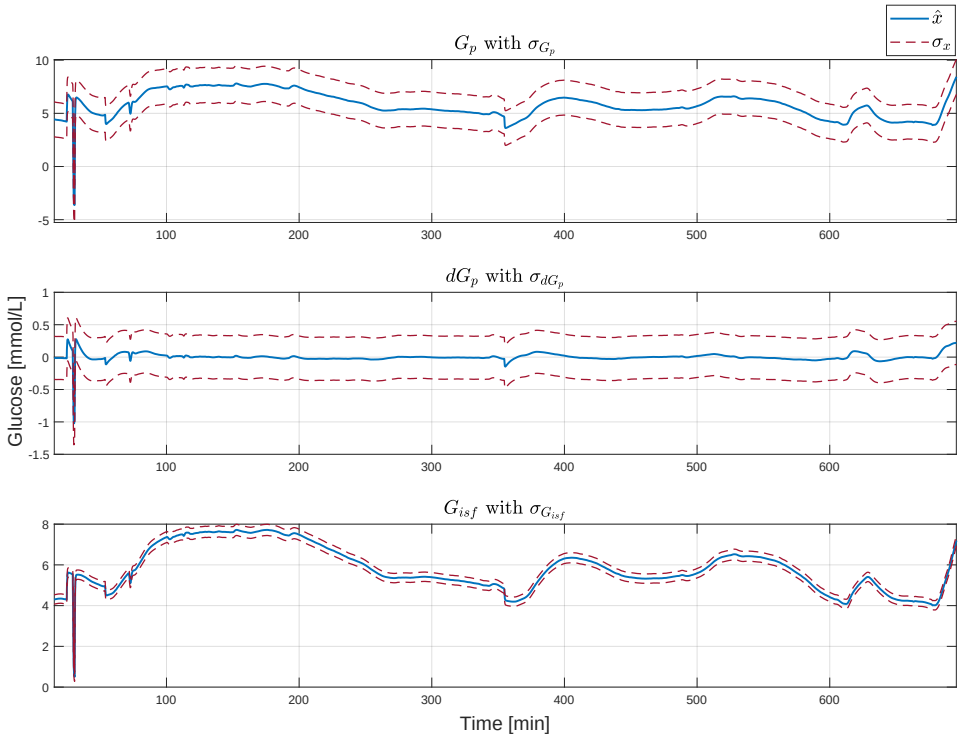

(a) KF estimate of BG level with SD.

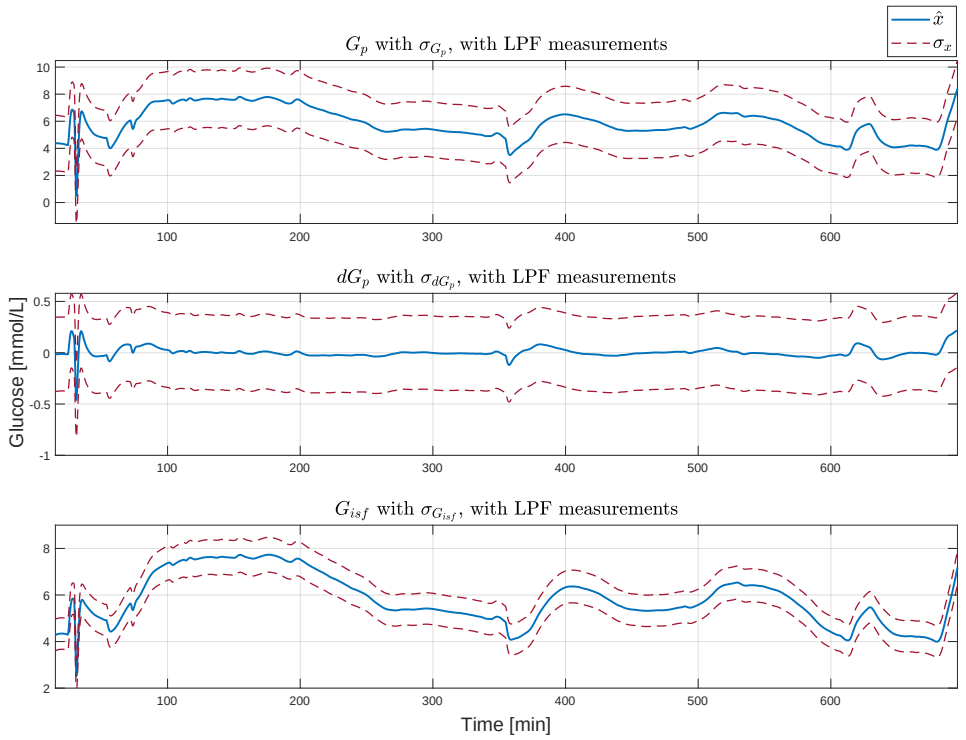

(b) KF estimate of BG level of LPF measurements, with SD.

Figure B.10: KF results for the Nov 20th, 2020 data set, displayed with SDs. $\hat{x}$ describes estimate x, while σ_x referrers to the standard deviation of estimate x.

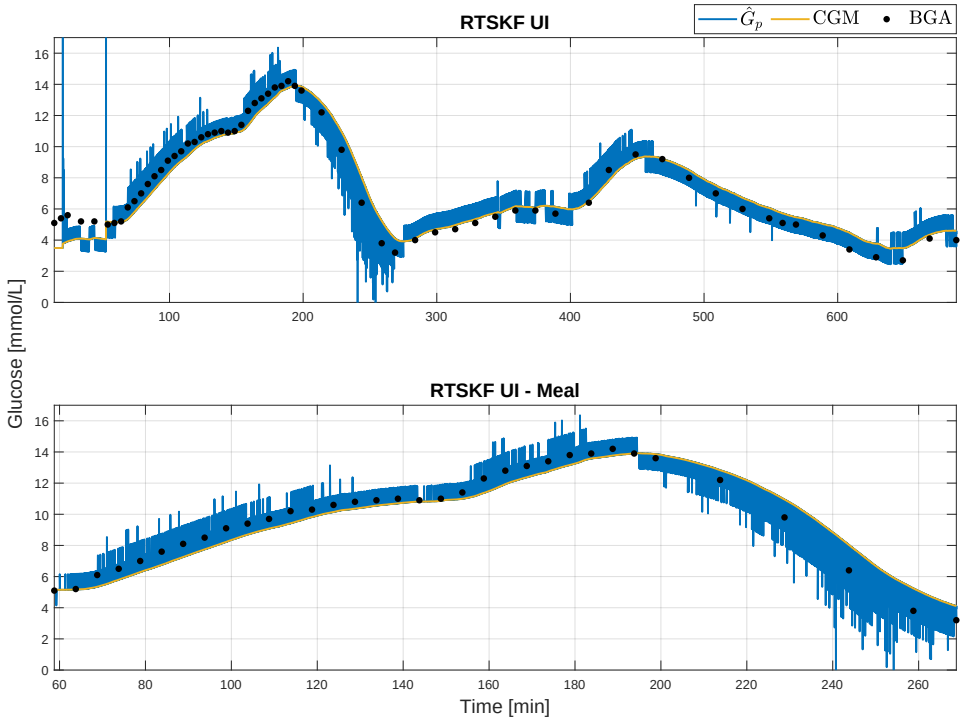

(a) RTSKF-UI estimate of BG level, for the entire data set and zoomed in on a meal.

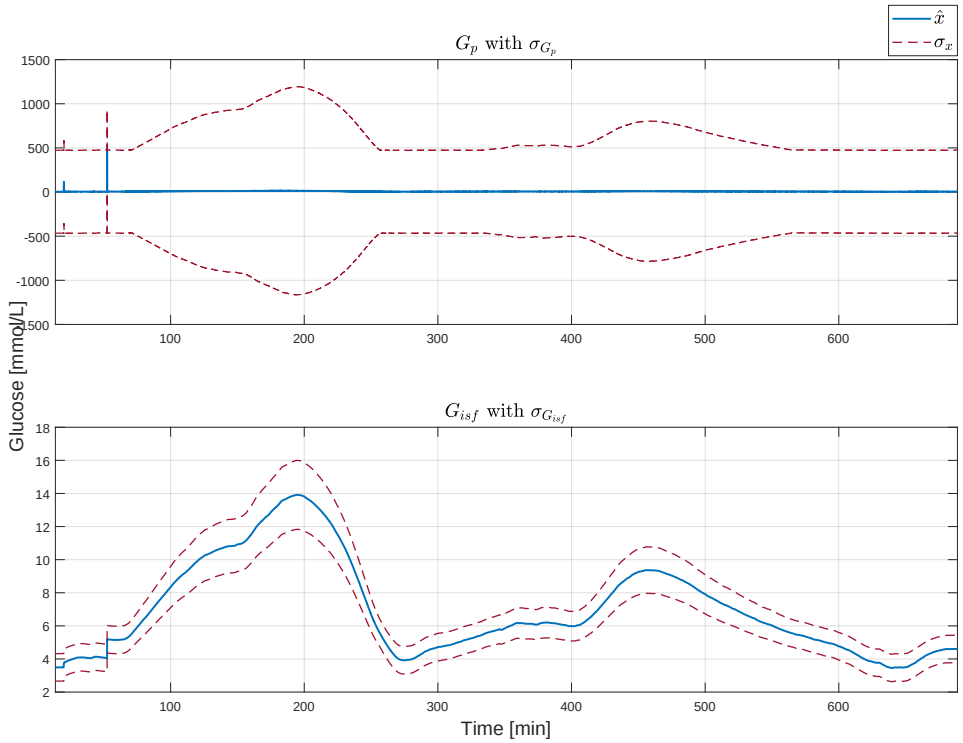

(b) RTSKF-UI estimate of BG level, with LPF measurements, with SD.

Figure B.11: RTSKF-UI results for the Mar 10th, 2021 data set.

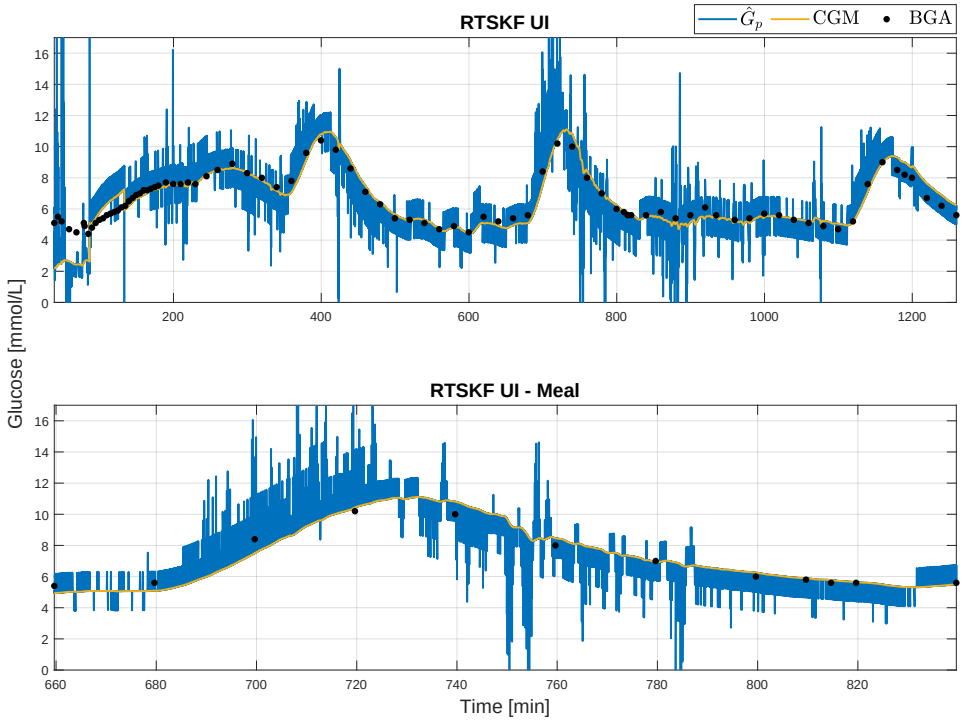

(a) RTSKF-UI estimate of BG level, for the entire data set and zoomed in on a meal.

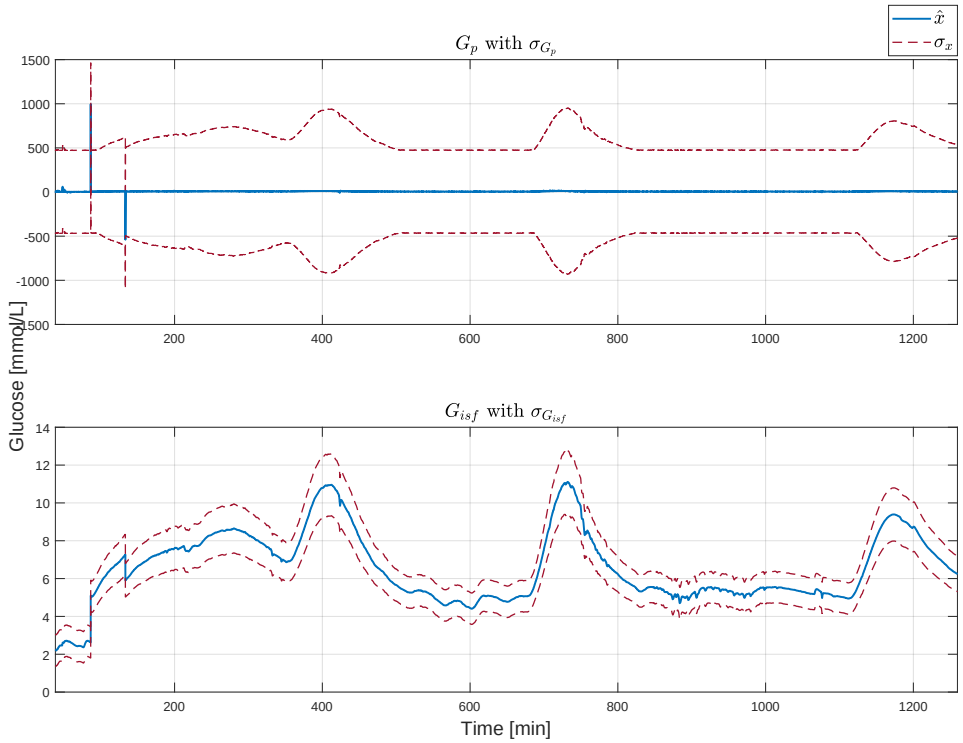

(b) RTSKF-UI estimate of BG level, with LPF measurements, with SD.

Figure B.12: RTSKF-UI results for the Mar 1st, 2021 data set.

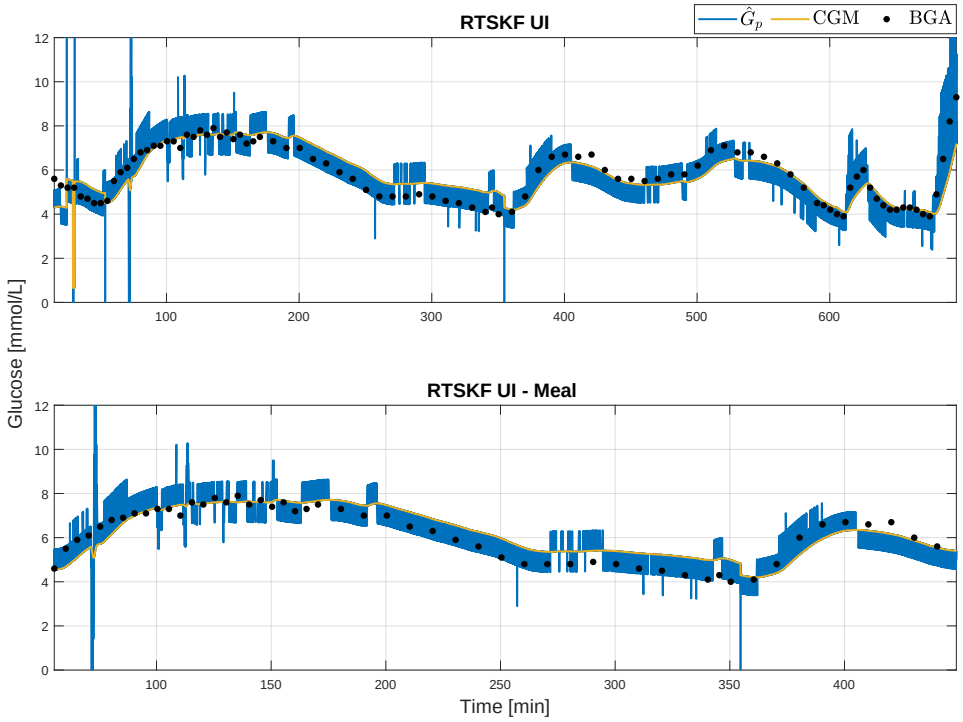

(a) RTSKF-UI estimate of BG level, for the entire data set and zoomed in on a meal.

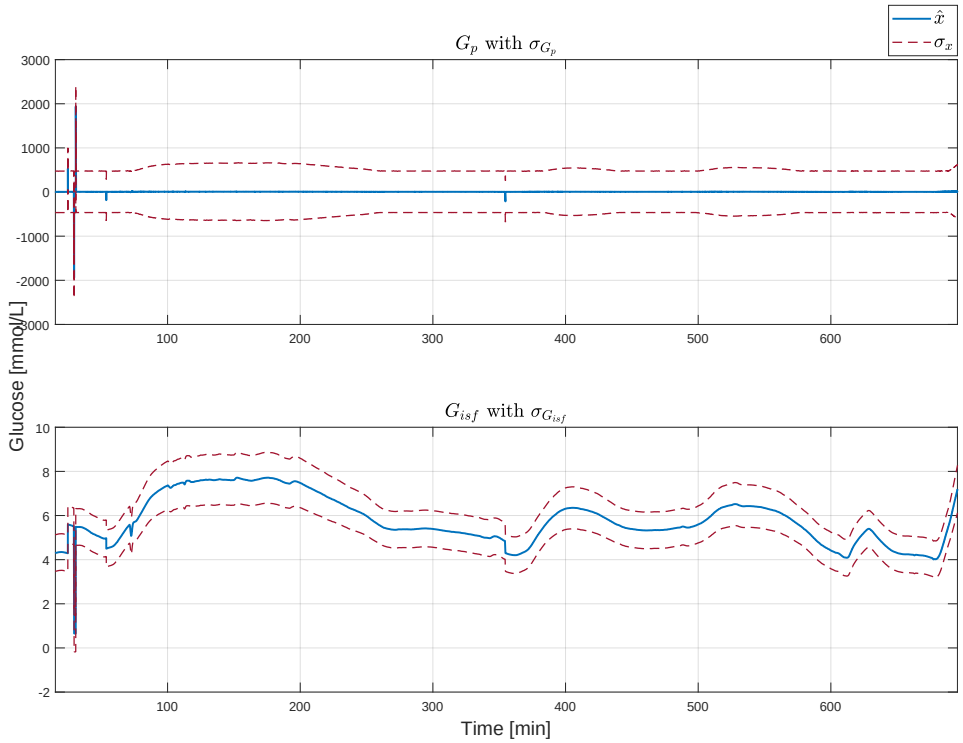

(b) RTSKF-UI estimate of BG level, with LPF measurements, with SD.

Figure B.13: RTSKF-UI results for the Nov 20th, 2020 data set.

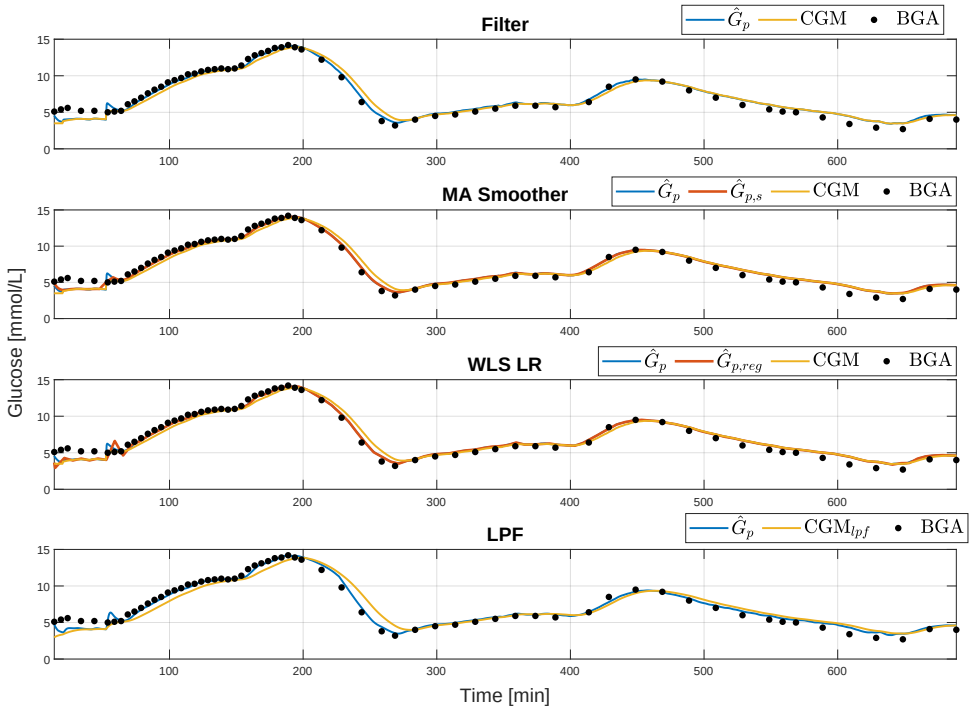

(a) M-robust KF estimate of BG level with enhancements.

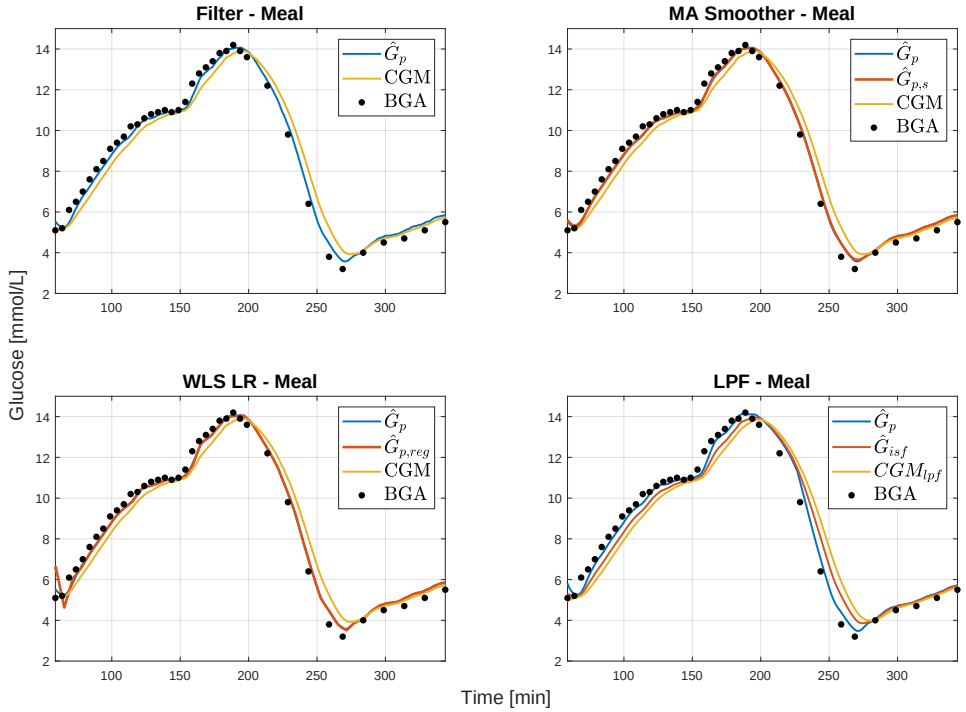

(b) M-robust KF estimate of BG level with enhancements, zoomed in on meal number one.

Figure B.14: M-robust KF results for the Mar 10th, 2021 data set.

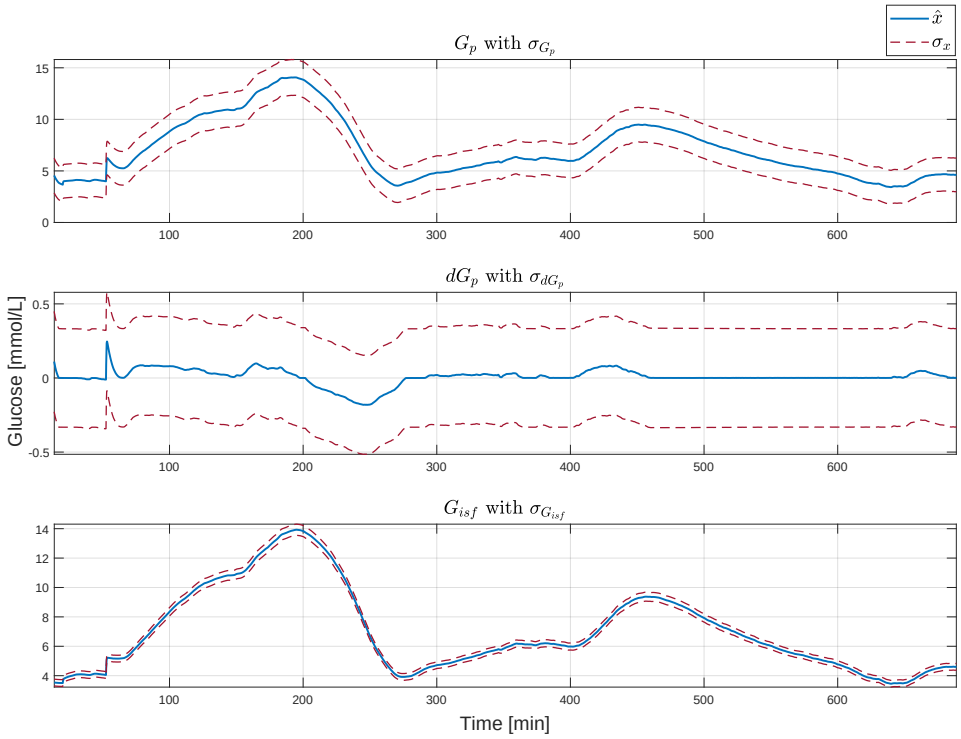

(a) M-robust KF estimate of BG level with SD.

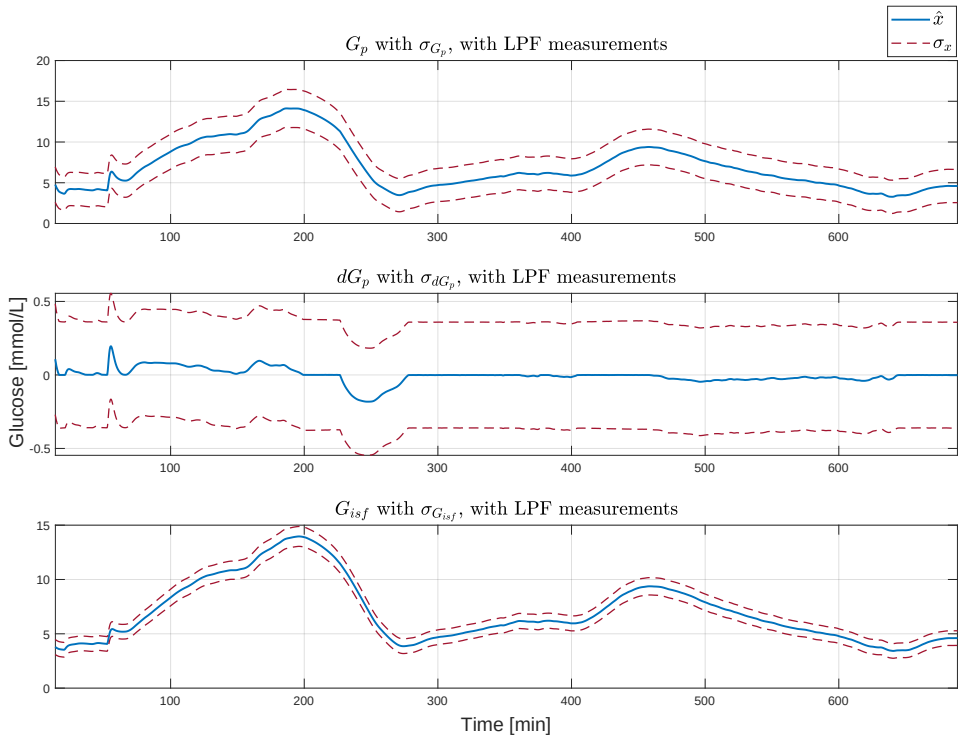

(b) M-robust KF estimate of BG level of LPF measurements, with SD.

Figure B.15: M-robust KF results for the Mar 10th, 2021 data set, displayed with SDs. $\hat{x}$ describes estimate x, while σ_x referrers to the standard deviation of estimate x.

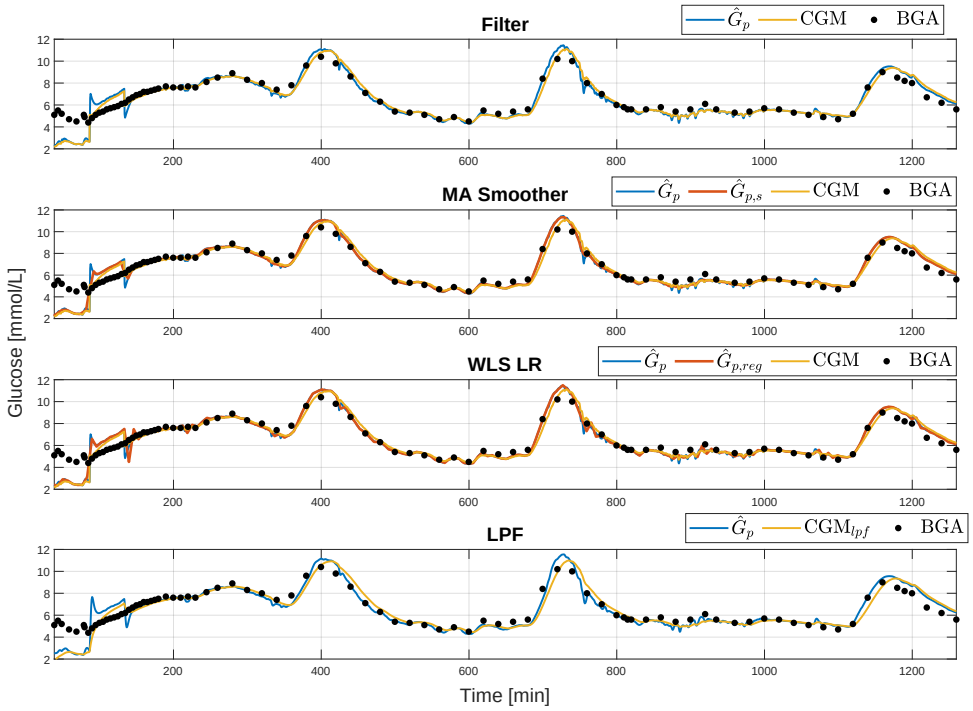

(a) M-robust KF estimate of BG level with enhancements.

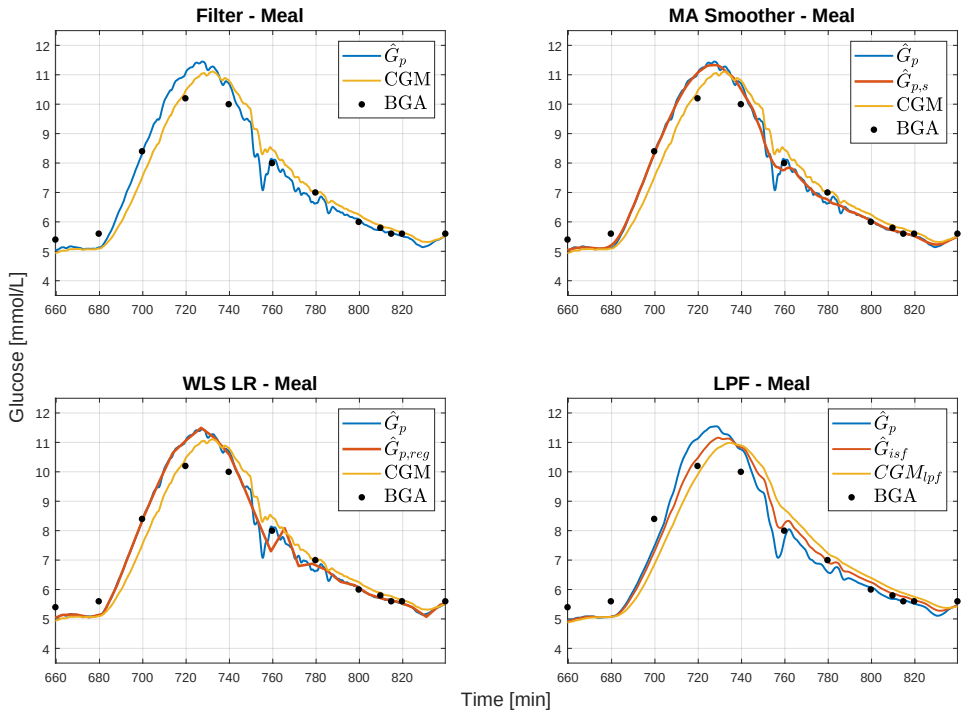

(b) M-robust KF estimate of BG level with enhancements, zoomed in on meal number two.

Figure B.16: M-robust KF results for the Mar 1st, 2021 data set.

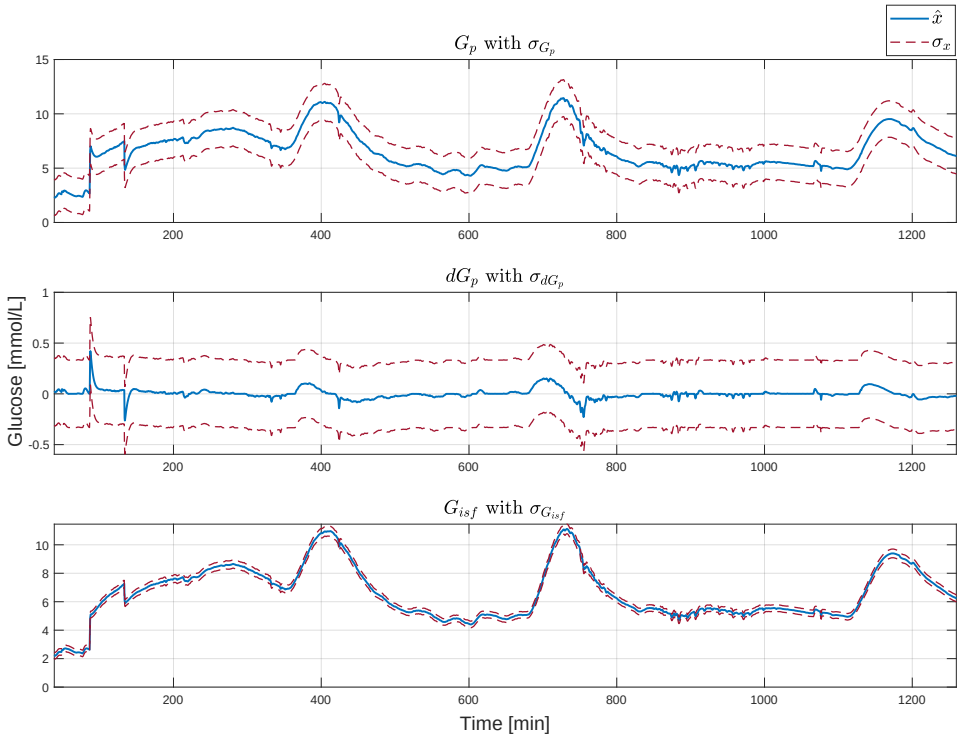

(a) M-robust KF estimate of BG level with SD.

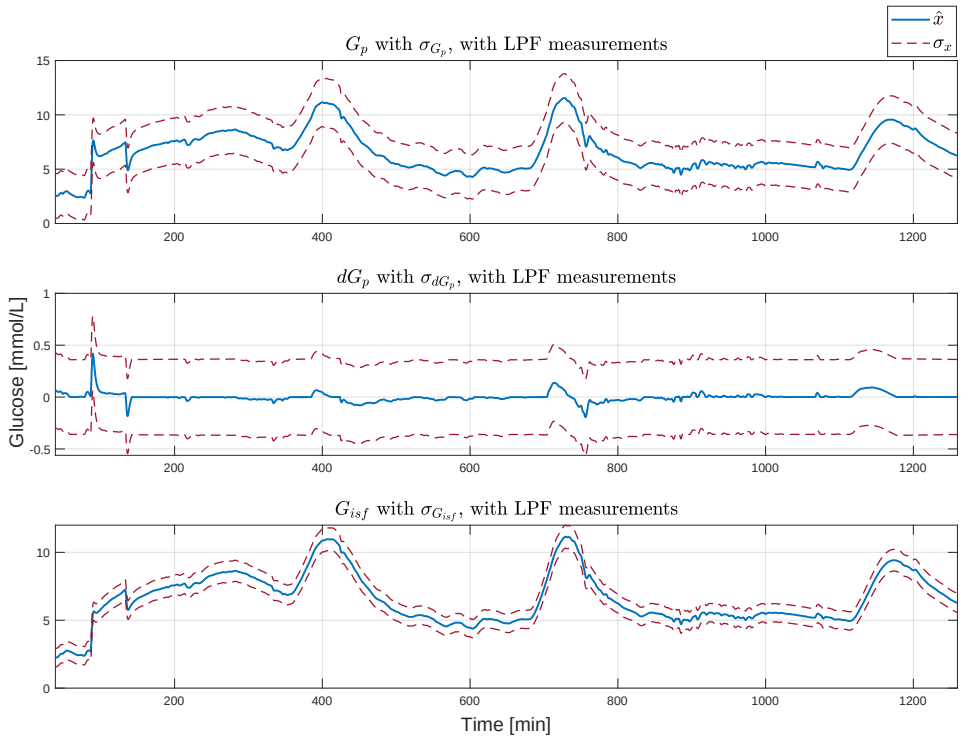

(b) M-robust KF estimate of BG level of LPF measurements, with SD.

Figure B.17: M-robust KF results for the Mar 1st, 2021 data set, displayed with SDs. $\hat{x}$ describes estimate x, while σ_x referrers to the standard deviation of estimate x.

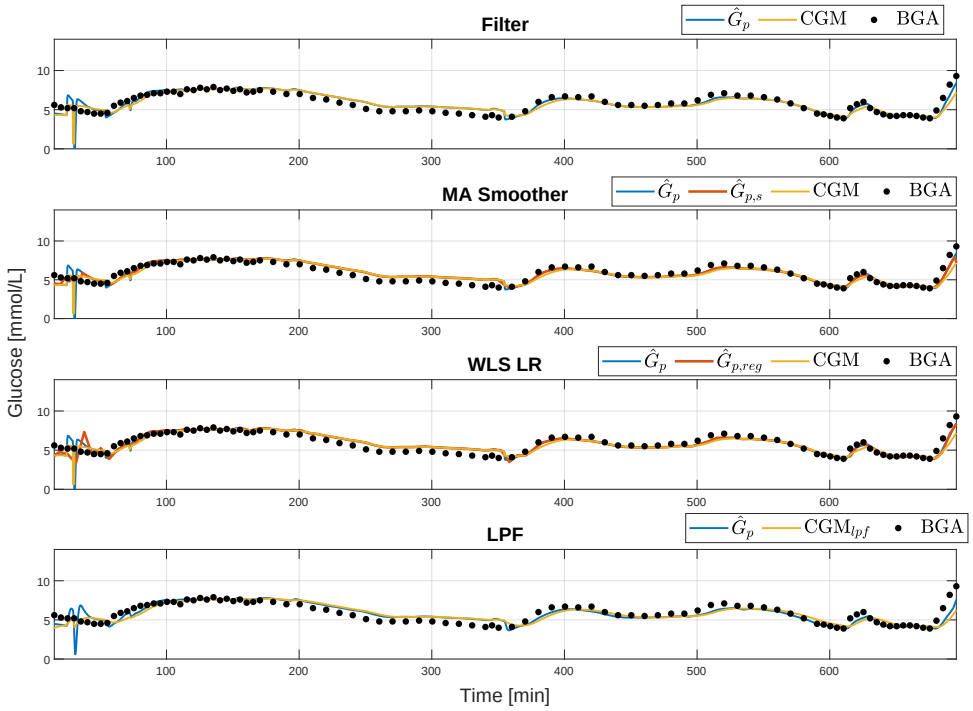

(a) M-robust KF estimate of BG level with enhancements.

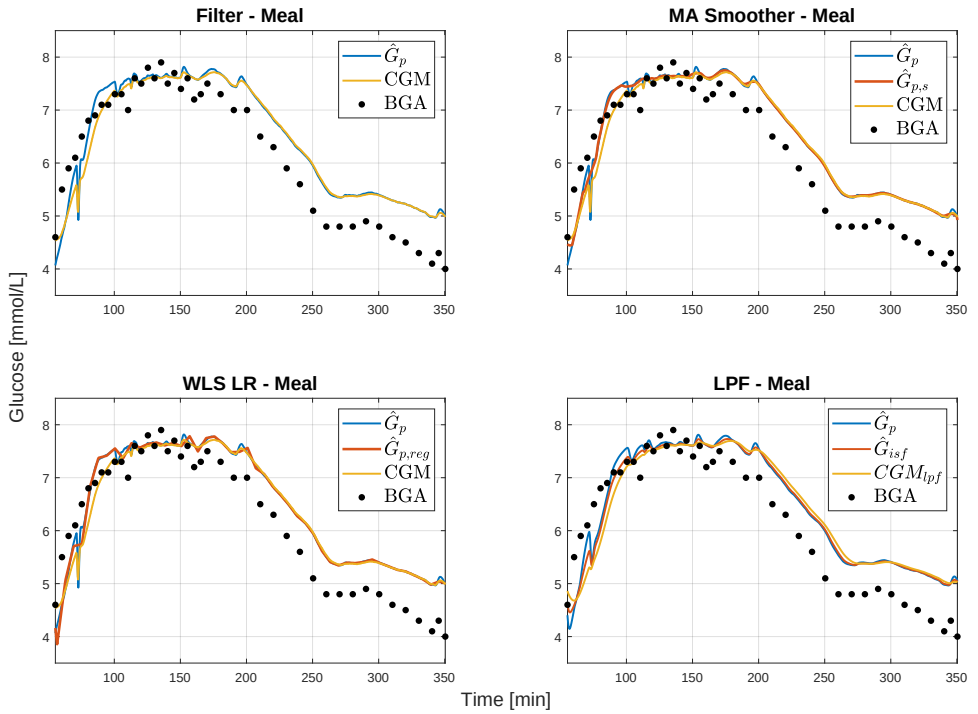

(b) M-robust KF estimate of BG level with enhancements, zoomed in on meal number two.

Figure B.18: M-robust KF results for the Mar 1st, 2021 data set.

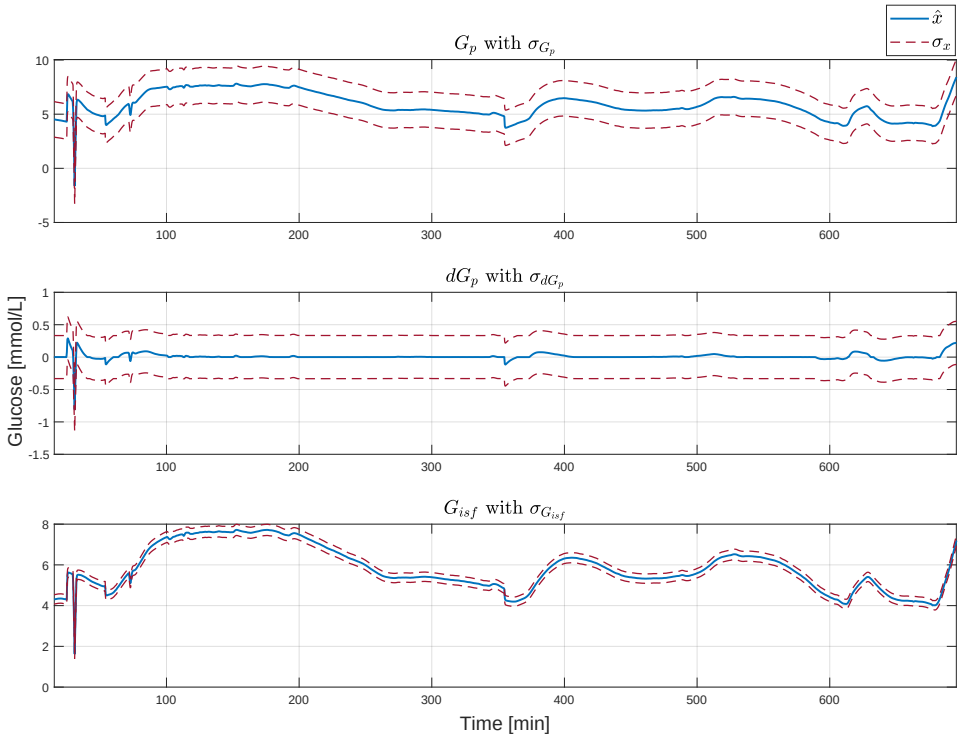

(a) M-robust KF estimate of BG level with SD.

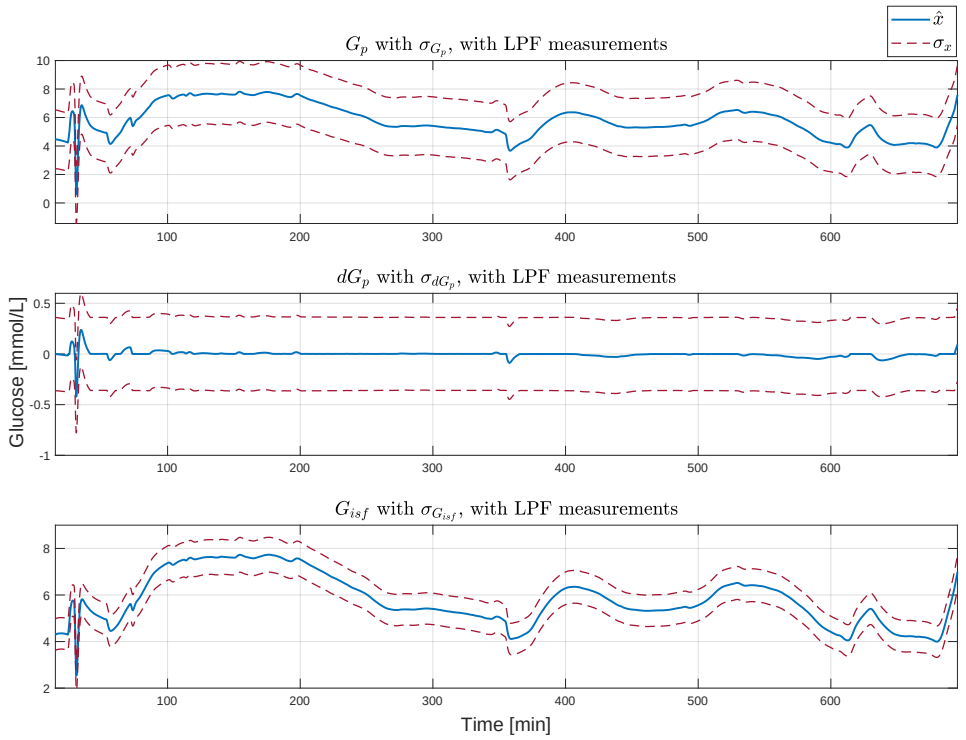

(b) M-robust KF estimate of BG level of LPF measurements, with SD.

Figure B.19: M-robust KF results for the Nov 20th, 2020 data set, displayed with SDs. $\hat{x}$ describes estimate x, while σ_x referrers to the standard deviation of estimate x.

Appendix C

Tuning Result

Tuning results for adjusting process noise covariance matrix Q, smoothing factor for LPF b and regression and moving average smoothing intervals N_{reg} and N_s, respectively, are displayed in this appendix, for Mar 5th, 2021 data set only. Results of regression and MA smoothing intervals, as well as LPF smoothing factor are only displayed for the KF estimate of G_p, seen as the observations are similar across different filters, while tuning of Q are shown for each individual filter and model, with the exception of KF and M-robust KF, where M-robust KF is left out due to similarities to KF.

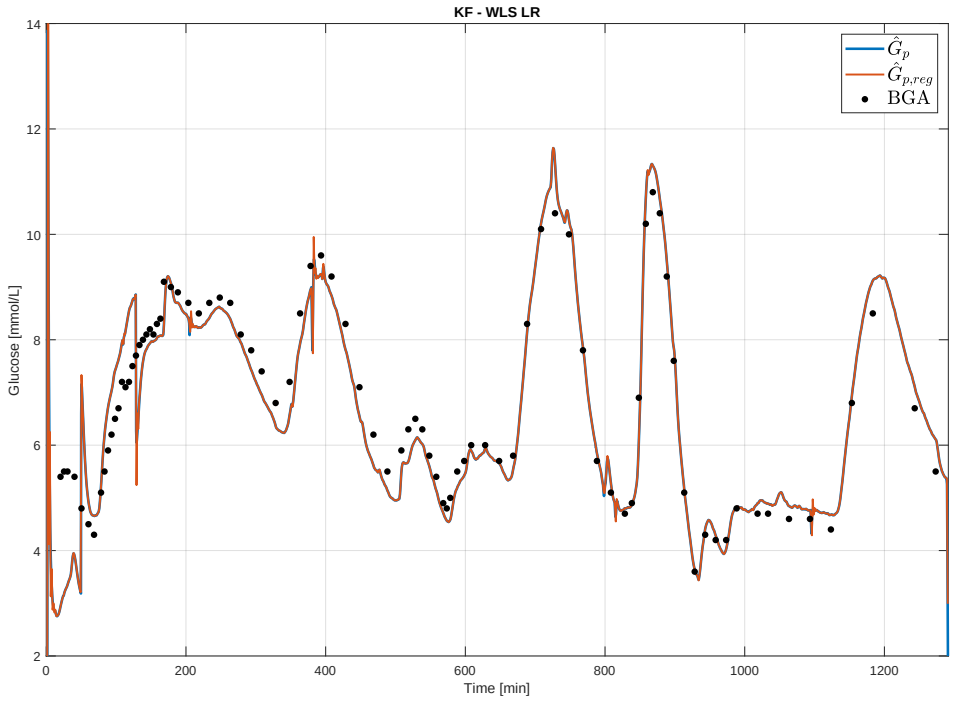

(a) $N_{reg} = 75$.

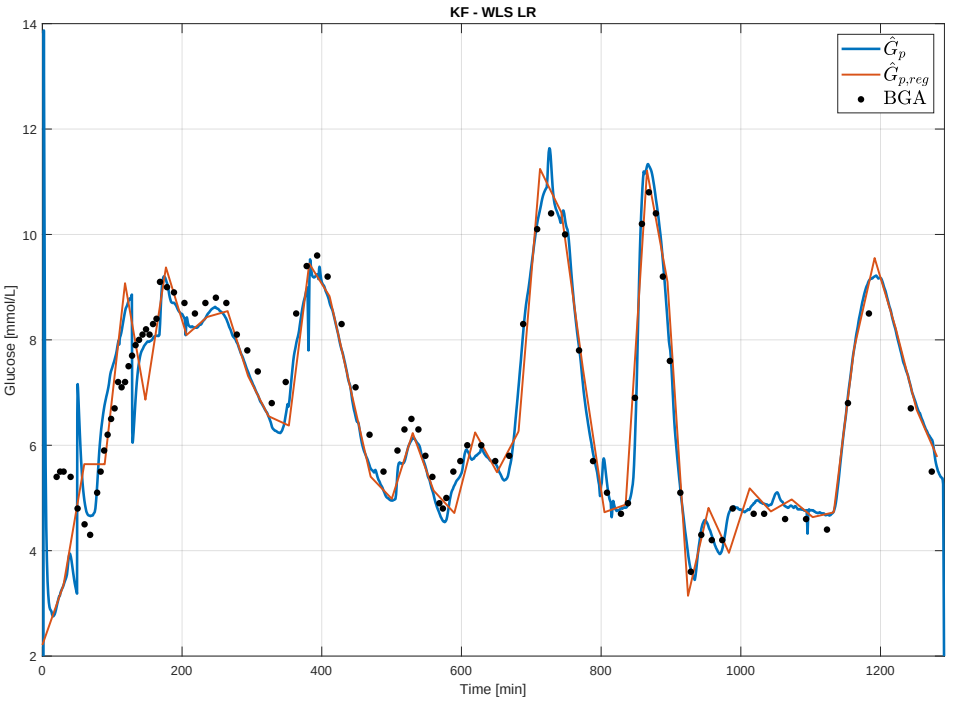

(b) $N_{reg} = 1750$.

Figure C.1: Tuning results for N_{reg}, where N_{reg} is given in number of iterations between every time filters regress the G_p estimate.

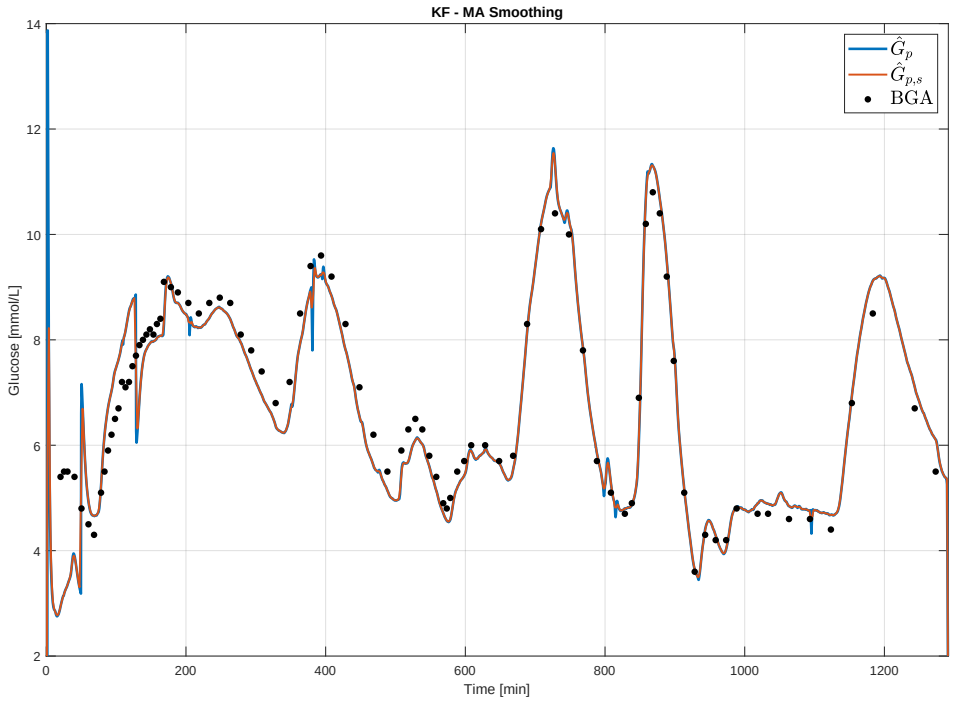

(a) $N_s = 250$.

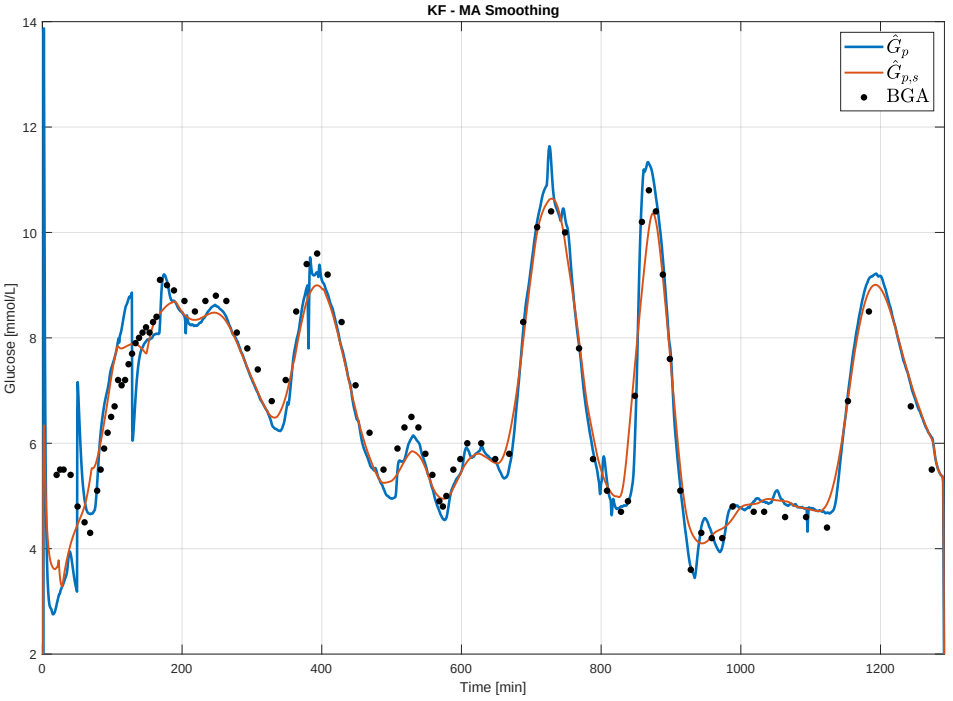

(b) $N_s = 2500$.

Figure C.2: Tuning results for N_s, where N_s is given in number of iterations between every time filters regress the G_p estimate.

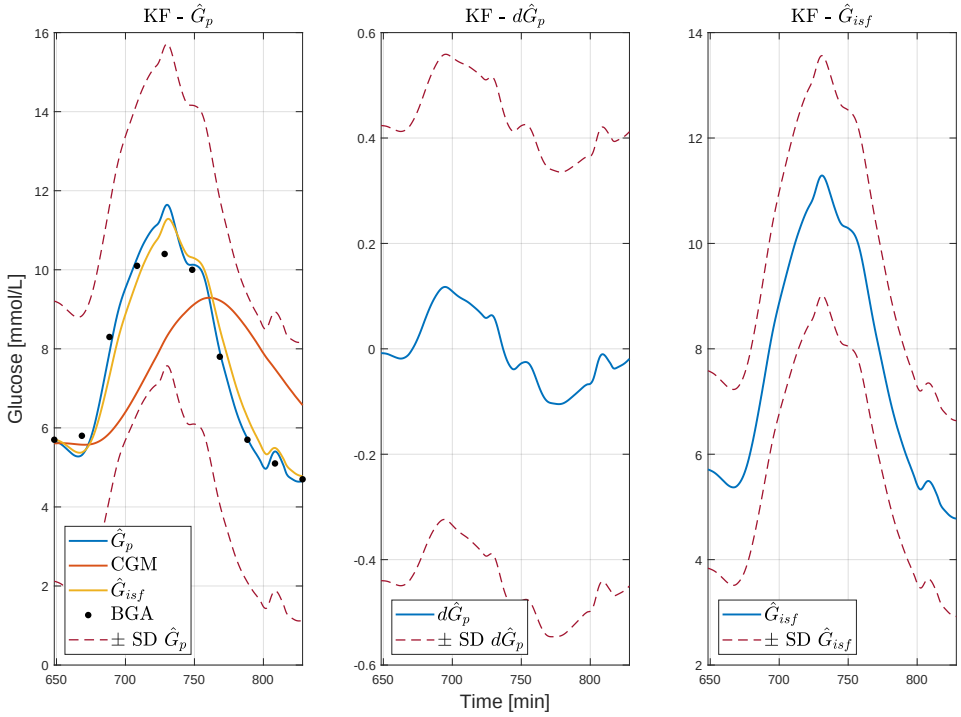

(a) $b = 0.0004$.

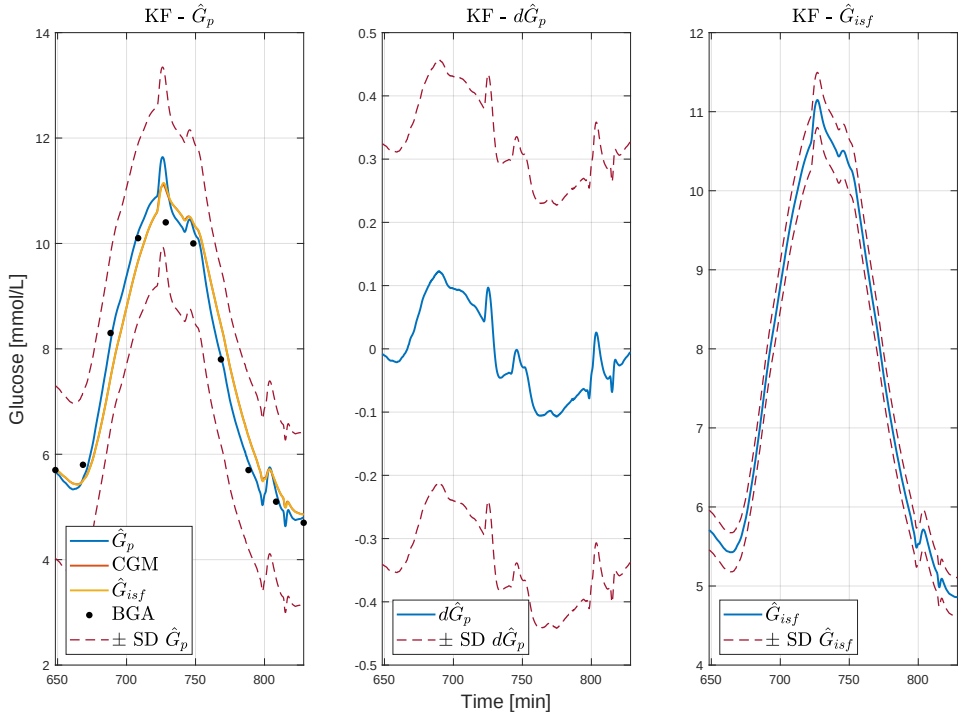

(b) $b = 0.4$.

Figure C.3: Tuning results for LPF smoothing factor b.

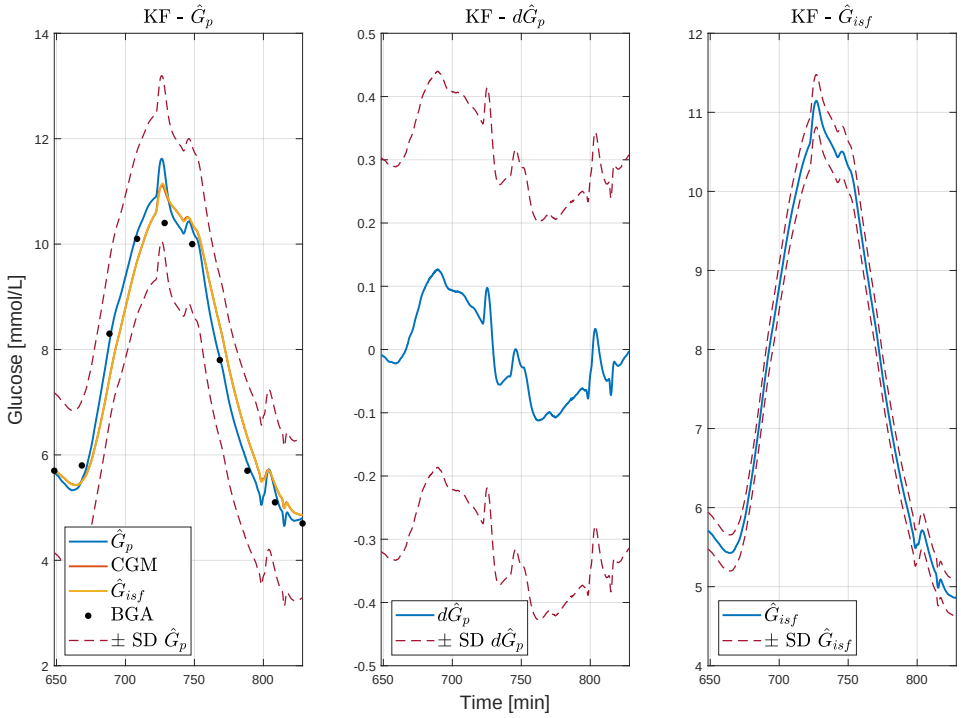

(a) $\sigma^2_{G_p} = 10^{-7}$ [mmol^2/L^2].

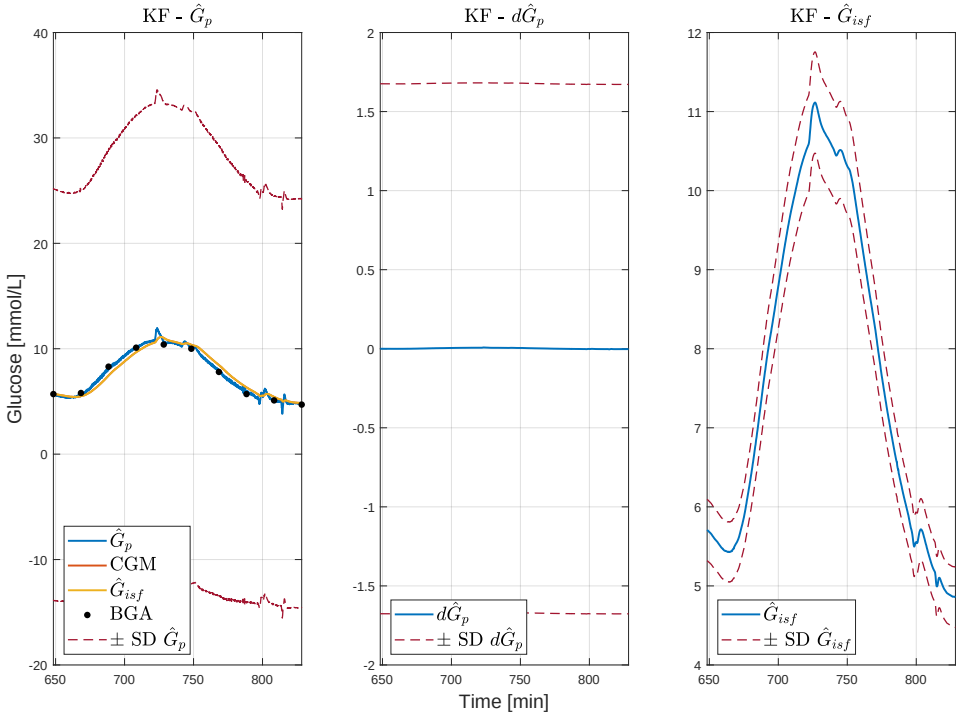

(b) $\sigma^2_{G_p} = 10$ [mmol^2/L^2].

Figure C.4: Tuning results for $\sigma^2_{G_p}$ for rate-only model.

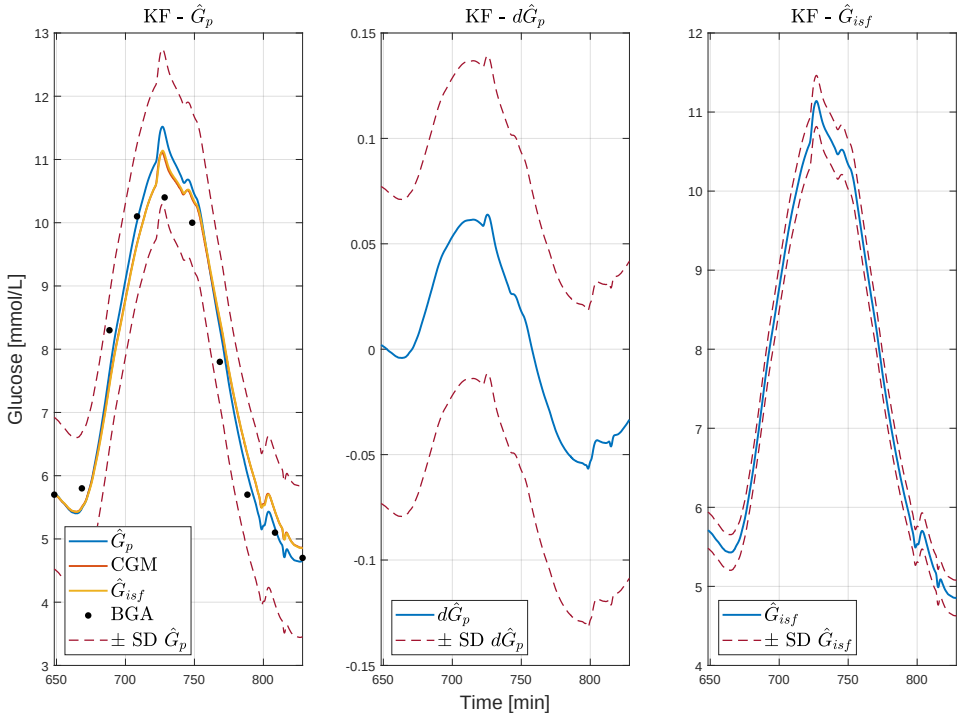

(a) $\sigma^2_{dG_p} = 7 \cdot 10^{-7}$ [mmol^2/L^2].

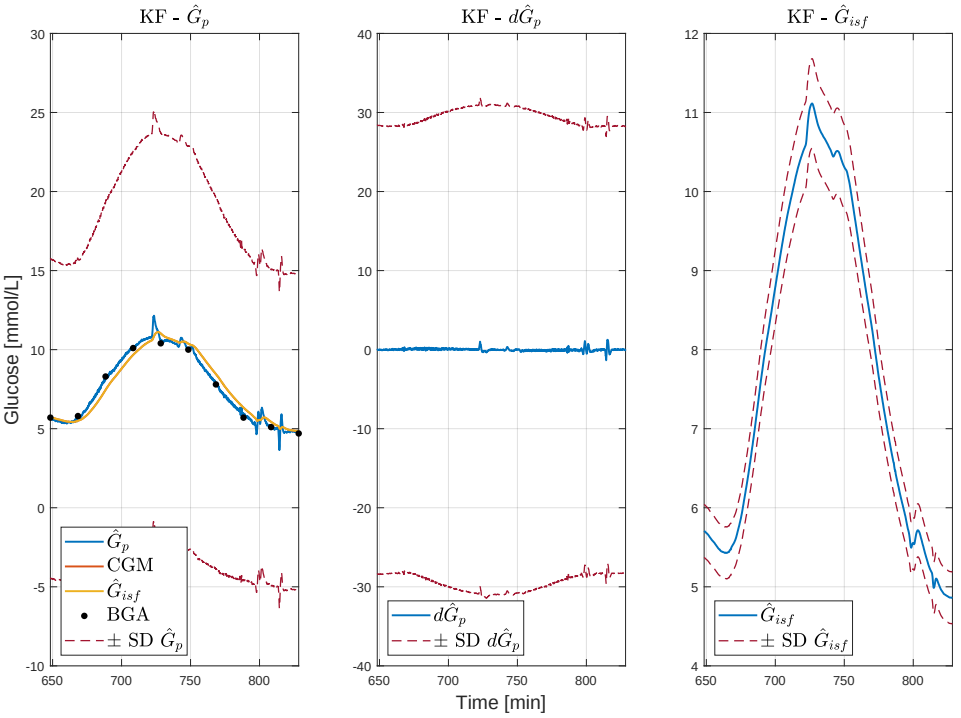

(b) $\sigma^2_{dG_p} = 7$ [mmol^2/L^2].

Figure C.5: Tuning results for $\sigma^2_{dG_p}$ for rate-only model.

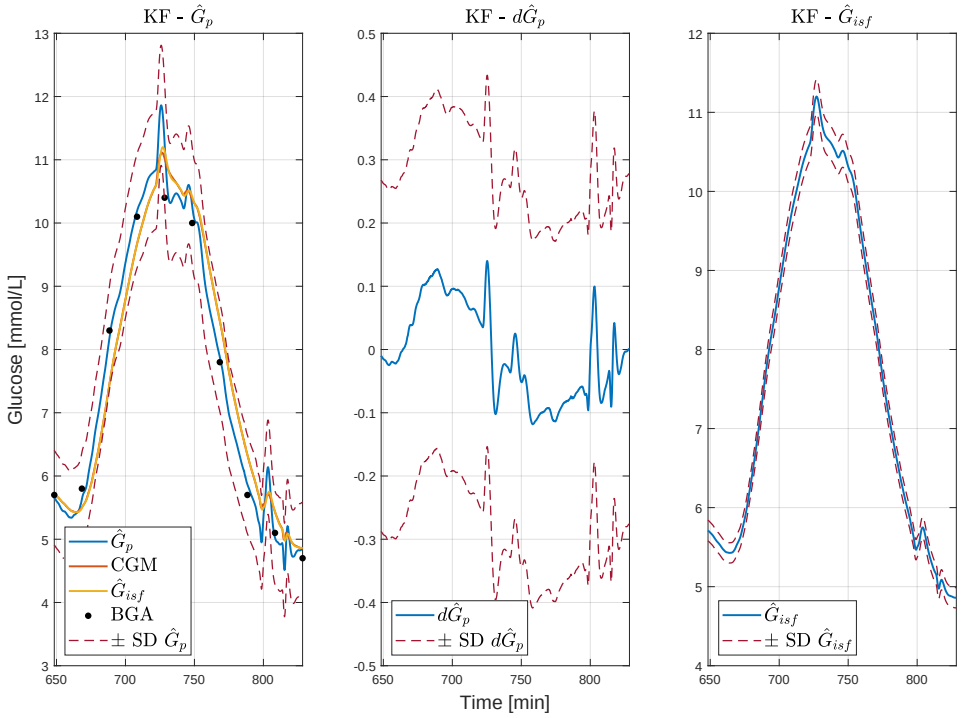

(a) $\sigma^2_{G_{isf}} = 10^{-7}$ [mmol^2/L^2].

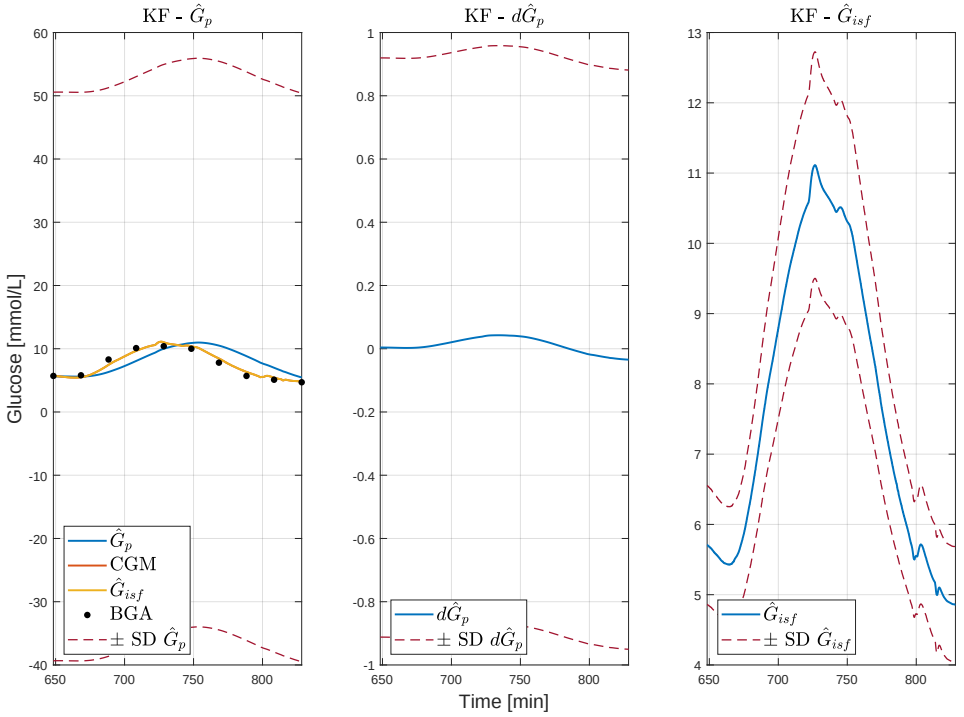

(b) $\sigma^2_{G_{isf}} = 10$ [mmol^2/L^2].

Figure C.6: Tuning results for $\sigma^2_{G_{isf}}$ for rate-only model.

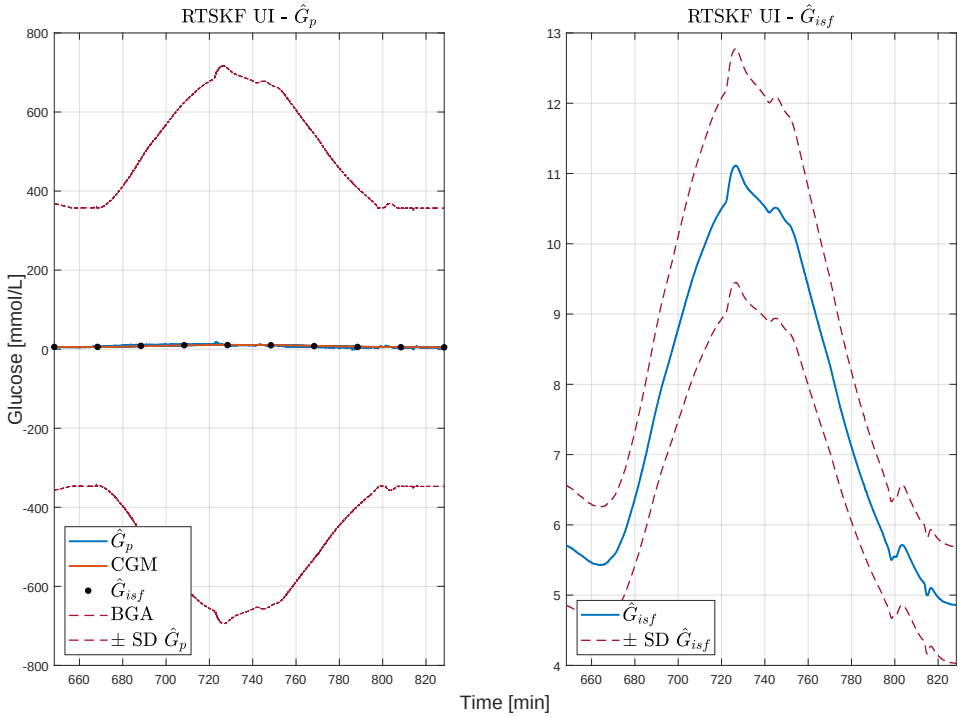

(a) $\sigma^2_{G_{isf}} = 10^{-7}$ [mmol^2/L^2].

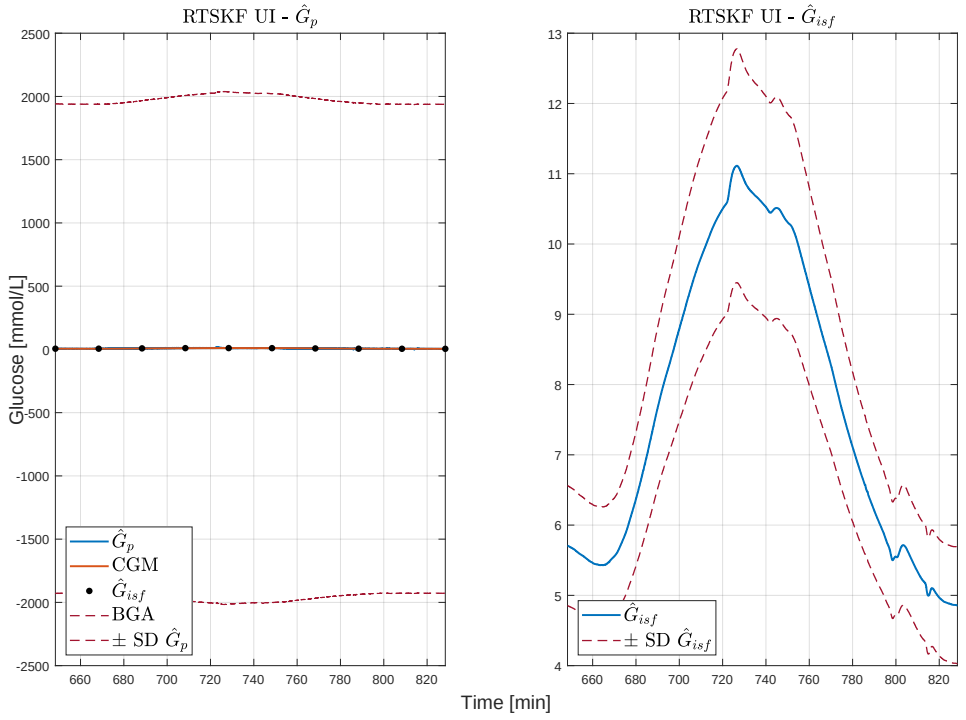

(b) $\sigma^2_{G_{isf}} = 10$ [mmol^2/L^2].

Figure C.7: Tuning results for $\sigma^2_{G_{isf}}$ for Steil-Rebrin model with BG level as unknown inputs, estimated with RTSKF-UI.

Appendix D

CDC Paper

Pending approval IEEE Conference on Decision and Control (CDC 2022) paper, delivered March 2022, see next page.

Blood Glucose Level Prediction Using Subcutaneous Sensors for in Vivo Study: Compensation for Measurement Method Slow Dynamics Using Kalman Filter Approach

Martha Halvorsen, Karim Davari Benam*, Hasti Khoshamadi*, Anders Lyngvi Fougner

***Abstract*— The continuous glucose monitoring (CGM) system is the most common system used by people with type 1 diabetes to monitor blood glucose levels. However, it measures glucose in interstitial fluid in subcutaneous tissue rather than directly in plasma. Measuring blood glucose level in this method has slow dynamics and introduce a time lag in capturing the blood glucose level. This can reduce the quality of blood glucose regulation and result in hypo- or hyperglycemia. In this paper, a linear Kalman filter is developed to predict blood glucose concentration using CGM data to compensate for that slow dynamics. To this end, an observable input-less model describing the glucose diffusion from plasma to interstitial fluid is utilized. Notably, this model is physiology-based, and its parameters can be obtained from the literature. The designed structure is evaluated on data from two animal experiments conducted in pigs. The data sets include CGM measurements every 1.2 seconds and sporadic blood sample analysis during experiments. Results show that the designed approach sufficiently can compensate for the slow dynamics of CGM measurements when compared to blood glucose samples, and the performance is measured using statistical accuracy scores. This compensation improves the decision-making of control algorithms for glucose regulation during rapid changes in glucose concentration, e.g., during meals and exercise.**

I. INTRODUCTION

Diabetes mellitus is a metabolic disorder or disease that affects approximately 537 million adults worldwide as of 2021 [1]. It is characterized by chronic hyperglycemia in response to ingestion of carbohydrates, fat, and protein, resulting from defects of insulin secretion, insulin action, or both [2]. In a healthy individual, glucose regulation is performed by two hormones, insulin, and glucagon, produced in the pancreas. Insulin secretion makes the glucose concentration in the blood decrease, while glucagon secretion increases the blood glucose (BG) concentration [2]. In type 1 diabetes mellitus (T1DM), the pancreas does not produce insulin due to the destruction of beta cells, which produce insulin in the pancreas [3]. Hence the insulin must be administered by an external source [2]. As a result, people with type 1 diabetes require daily insulin treatment, regular BG monitoring, and a healthy lifestyle to manage their condition effectively [4].

In 1999 diabetes technology made huge progress when the continuous glucose monitoring (CGM) system was approved by the Food and Drug Administration (FDA) and became commercially available [5]. The CGM sensor is placed in the subcutaneous tissue and measures glucose levels in the interstitial fluid in real-time [2]. The minimally invasive structure of the sensor system allows for continuous glucose measurements, eliminating the need for self-monitoring systems, e.g., finger prick [5]. In addition, continuous glucose measurements provide BG trends and fluctuations.

Despite the sensor's revolutionary qualities, it is not without problems. One of its disadvantages is that the sensor measures ISF glucose level rather than plasma glucose level. Due to plasma-to-ISF glucose dynamics, the CGM measurements are delayed compared to measurements taken directly from the blood during rapid changes in BG [6]. The plasma-to-ISF glucose dynamics refers to glucose diffusion across capillaries and through the interstitial space where the sensor is located [6]. Hence, during both BG rising and falling, the time of the diffusion process will result in the ISF glucose lagging behind the BG. The slow dynamics between these two compartments, together with sensor processing time, causes about, on average, a $4-10\,\mathrm{min}$ lag between the BG and the sensor readings [2].

Control algorithms, along with CGM sensors and infusion pumps, are employed in commercially available control devices (artificial pancreas) to regulate BG levels in patients with T1DM. Based on the CGM measurements, the control algorithm will automatically infuse the optimal amount of insulin, and glucagon, in a timely manner. Notably, the absorption and effect of hormones are not instantaneous. Hence, using CGM measurements can lead to a late response to BG level fluctuations which in turn cause severe low or high BG levels. Therefore, predicting the BG levels can help artificial pancreas systems to improve glycemic control.

There are several ways proposed in the literature for predicting or estimating the blood glucose level using CGM measurements. The deconvolution approach is employed to reconstruct the plasma glucose from ISF glucose measurements in [7]. However, it is concluded that perfect linearity and time invariance of the system is required for this method. In addition, various works have addressed the problem through the use of Kalman filtering. In [8], a physiological model is considered for the glucose diffusion from plasma

This research is funded by the Research Council of Norway (project no. 248872), and the Centre for Digital Life Norway. Inreda Diabetic (Goor, the Netherlands) provided transmitters, materials and hormones infusion systems (AP3) for animal experiments at no cost.

M. Halvorsen, K.D. Benam, H. Khoshamadi, and A.L. Fougner are with Department of Engineering Cybernetics, Faculty of Information Technology and Electrical Engineering, Norwegian University of Science and Technology (NTNU), O. S. Bragstads Plass 2D, 7034 Trondheim, Norway. marthalv@stud.ntnu.no, {karim.d.benam, hasti.khoshamadi, anders.fougner}@ntnu.no

*These authors contributed equally to this work

to ISF glucose dynamic; nevertheless, it is assumed that plasma glucose changes randomly in a step or rate fashion. Moreover, the superiority of the Kalman filter approach to the intuitive finite differences approach [9] is shown. In [10], the Kalman filter estimates plasma glucose and sensor gain from CGM and fingerstick measurements. In this approach, both plasma glucose level and sensor gain are modeled as ramp disturbances; however, the time lag between plasma and ISF glucose is neglected. A smoothing Kalman filter is used in [11] in an offline manner to interpolate BG measurements when blood samples are taken irregularly utilizing the CGM and fingerstick measurements. The smoothing Kalman filter is based on the central-remote rate model proposed for plasma glucose dynamics. Moreover, the plasma-to-ISF dynamic is also combined in the model.

In this paper, the Kalman filter, together with the input-less model introduced in [11] is utilized to estimate the BG level and compensate for the slow plasma-to-ISF dynamics. The proposed structure is tested on data from animal experiments, and the performance is analyzed using standard statistical methods. The paper is structured as follows. The data used in this paper is described in Section II. A brief description of the standard linear Kalman filter is given in Section III, a plasma-to-ISF glucose dynamics model is introduced in Section IV and evaluation tools and metrics for measuring filter performance are given in V. The results are presented in VI, and are discussed in VII, before a conclusion is provided in Section VIII.

II. Data

The data used for the simulations in this paper is collected through two animal experiments performed in the animal faculty of the University of Norwegian science and technology. These experiments were conducted on two anesthetized pigs whose endogenous insulin and glucagon secretions were suppressed using Octreotide (Sandostatin) with a rate of 5 µg/kg/h. In addition, intravenous glucose infusion was used to simulate different meals. In order to control the BG level, intraperitoneal insulin and glucagon administrations were used.

The CGM sensors used in these experiments were the Medtronic Enlite sensor (Northridge, Canada). These sensors were paired with custom transmitters from Inreda Diabetic (Goor, the Netherlands), providing measurements with a sampling rate of $1.2\,\mathrm{s}$. In order to measure the BG level directly, blood samples were taken sporadically, varying between every $5\,\mathrm{min}$-$1\,\mathrm{hour}$, and analyzed by ABL800 FLEX analyzer (Copenhagen, Denmark), which is a blood gas analyzer (BGA) system.

Data set 1 is the collected data from animal experiment 1 and consists of three meals, where the weight of the pig was $36\,\mathrm{kg}$, while data set 2 the collected data from animal experiment 2 and consists of four meals, where the weight of the pig was also $36\,\mathrm{kg}$. The CGM measurements are plotted together with the BGA measurements for data set 1 and for data set 2 in (1).

III. Kalman filter

The Kalman filter is a recursive filter that uses a time series of measurements in order to estimate the internal states of a linear dynamical system. Given an output signal y_k, any time-invariant discrete system can be assumed to be modelled as follows:

$$x_{k+1} = Fx_k + Bu_k + w_k \tag{1}$$
$$y_k = Hx_k + v_k \tag{2}$$

where $x_k \in \mathbb{R}^n$, $u_k \in \mathbb{R}^p$, and $y_k \in \mathbb{R}^m$ is the system state, system input and the system output vectors at time iteration k, respectively. Moreover, F is the state transition matrix, B is the input transition matrix, and H is the measurement matrix. Assume that the system matrices all have appropriate dimensions. The process and measurement noises are denoted by w_k and v_k which satisfy the following conditions:

$$\begin{aligned} w_k &\sim (0, Q) \\ v_k &\sim (0, R) \\ E[w_k w_j^T] &= Q\delta_{k-j} \\ E[v_k v_j^T] &= R\delta_{k-j} \\ E[v_k w_j^T] &= 0. \end{aligned} \tag{3}$$

where Q and R are covariance matrices of process and measurement noises respectively. In addition, δ_{k-j} is the Kronecker delta function which gives $\delta_{k-j} = 1$ if $k = j$, and $\delta_{k-j} = 0$ if $k \neq j$ [12].

The Kalman filter computes an estimate of the internal states, $\hat{x}$, as well the estimation error covariance matrix, P_k, for each time iteration k. P_k can be considered as a tool to evaluate of the quality the current estimate $\hat{x}_k$ quantitatively [13].

The estimation process is performed in two steps, a *prediction step*, and a *correction step*. In the prediction step the filter uses the model from (1) to predict the states one iteration ahead of time. The resulting estimate is known as the *a priori estimate*, and will be denoted as $\bar{x}_{k+1}$ and $\bar{P}_{k+1}$. In the following correction step the *a priori estimate* is used in combination with the measurement y_k to update and improve the *a posteriori estimate*, which is denoted $\hat{x}_{k+1}$ and $\hat{P}_{k+1}$.

Hence the Kalman filter equations are given by the followings [12]:

Prediction:

$$\begin{aligned} \bar{x}_{k+1} &= F\hat{x}_k + Bu_k \\ \bar{P}_{k+1} &= FP_kF^T + Q \end{aligned}$$

Correction: (4)

$$\begin{aligned} K_k &= \bar{P}_{k+1}H^T(H\bar{P}_{k+1}H^T + R)^{-1} \\ \hat{x}_{k+1} &= \bar{x}_{k+1} + K_k(y_k - H\bar{x}_{k+1}) \\ P_{k+1} &= (I - K_kH)\bar{P}_{k+1}. \end{aligned}$$

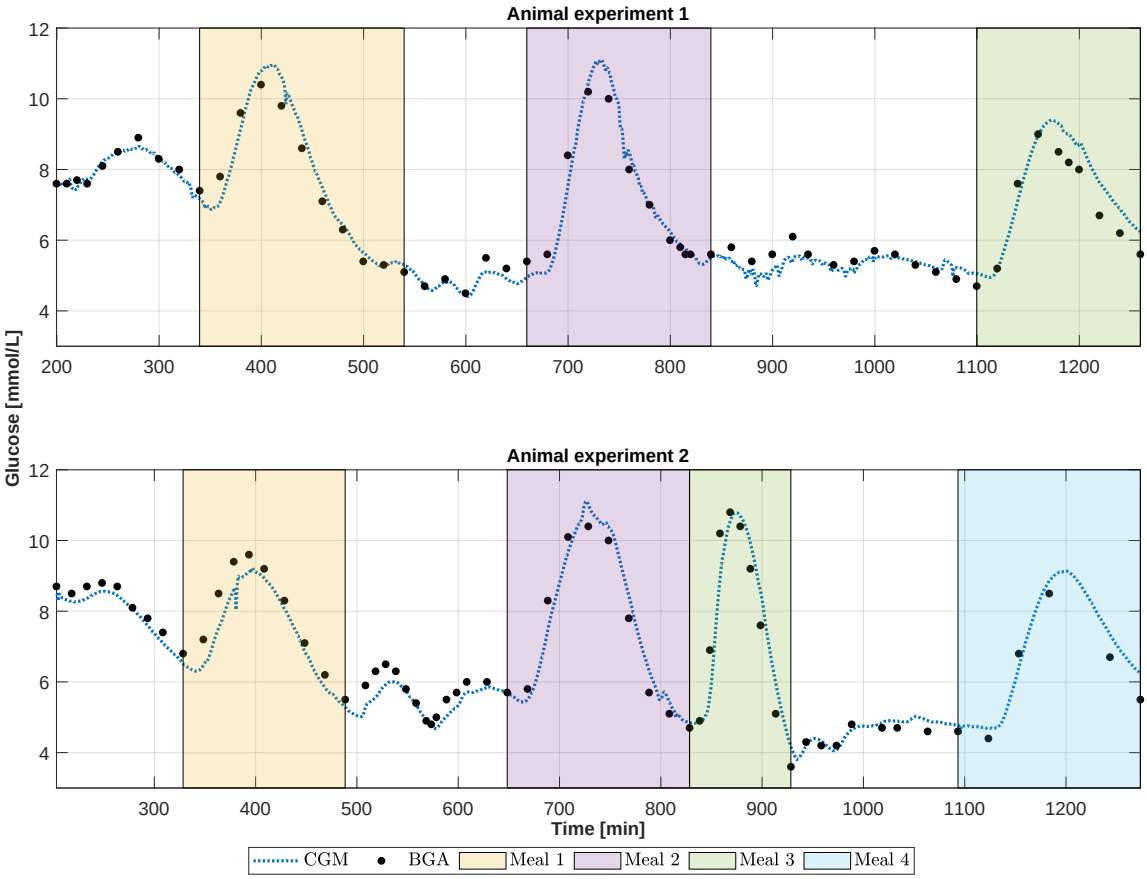

Fig. 1: Continuous glucose monitoring (CGM) and blood gas analyzer (BGA) measurements sectioned by color into specific meal times. The top row describes the data set from animal experiment 1, with three observed meal times, while the bottom row describes the data set from animal experiment 2, with four observed meal times.

where K_k is the Kalman gain matrix at time iteration k. The dynamical system given by (1) and (2) must be fully observable for the Kalman filter to obtain optimal estimates of all internal states. When a system is fully observable, the observability given by (5) is full rank.

$$O = \begin{bmatrix} H \\ HF \\ \vdots \\ HF^{n-1} \end{bmatrix} \tag{5}$$

IV. Mathematical Model

Using a Kalman filter requires a mathematical, dynamic model describing the system. Models describing the glucose dynamics are not limited in the literature, and they range from minimal [14] to quite complex [15]. Models like these describe the glucose dynamics where insulin and meals are inputs of the system. Using such models requires precise information about inputs and parameters, which is not always available or bears the quality needed. In this paper, the introduced model in [11] which combines the ISF glucose dynamics with a plasma glucose dynamical model is used. The combined model makes it possible to have plasma glucose as a state of the system, which is observable with CGM measurement. Notably, insulin and meals are treated as unknown system disturbances in this model.

A. Plasma-ISF Glucose Dynamics

The Steil-Rebrin model is a model describing the ISF glucose dynamics, using a two compartmental structure as follows [9], [16] :

$$\frac{dG_{isf}}{dt}(t) = -(k_{02} + k_{12})G_{isf}(t) + k_{21}\frac{V_1}{V_2}G_p(t). \tag{6}$$

where k_{02} is the glucose uptake rate of subcutaneous tissue from ISF, k_{12} and k_{21} are diffusion rates between plasma and ISF compartments, V_1 and V_2 are volumes of the plasma and ISF glucose compartments, respectively [12]. G_{isf} describes the glucose concentration in ISF, and G_p describes the glucose concentration in plasma. The relationship between the plasma glucose concentration and the ISF glucose concentration can be further simplified:

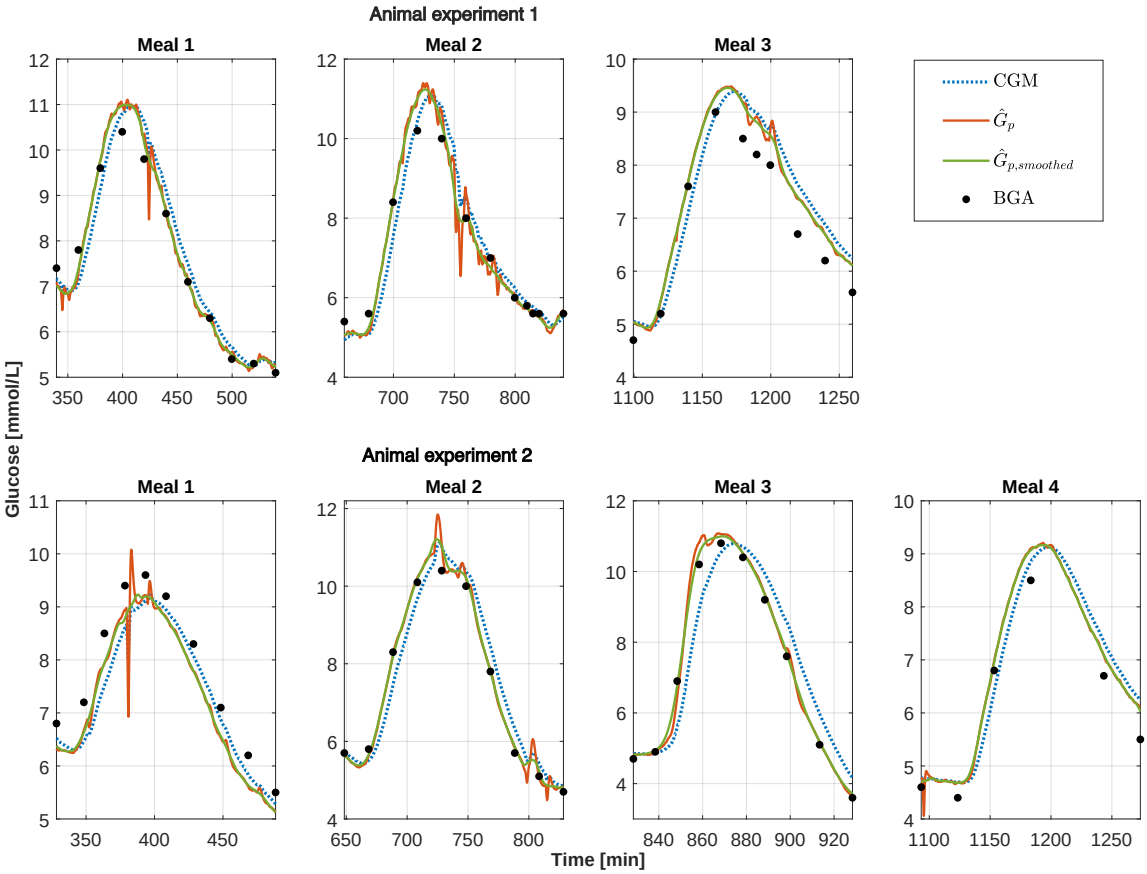

Fig. 2: Kalman filter estimate, $\hat{G}_p$, plotted together with the moving average smoothed Kalman filter estimate, $\hat{G}_{p,smoothed}$, where Continuous glucose monitoring (CGM) measurements and blood gas analyzer (BGA) measurements are shown for comparison. The top row is the result from data set 1, while the bottom row is the result from data set 2.

$$\frac{dG_{isf}}{dt}(t) = -\frac{1}{T_{isf}}G_{isf}(t) + \frac{g}{T_{isf}}G_p(t), \tag{7}$$

where T_{isf} is the diffusion time constant, and g is a steady-state gain. These parameters are defined as follows:

$$T_{isf} \triangleq \frac{1}{k_{02}+k_{12}} \tag{8}$$

$$g \triangleq \left(k_{21}\frac{V_1}{V_2}\right)T_{isf} \tag{9}$$

Notably, in the steady state, $g = G_{isf}/G_p$. Physiologically, for a given change in plasma glucose concentration, the same long-term change in the ISF glucose concentration is expected, and thus $g = 1$ [7], [12].

B. Central-Remote Rate Model

The plasma glucose model is divided into a central compartment, C_c, and a remote compartment, C_r. Insulin or meals going into the system will first affect the central compartment before it diffuses over to the remote compartment by a first-order delay [11], where it finally causes changes in the plasma glucose concentration, G_p. The state-space equations are as followings:

$$\begin{aligned}\frac{dG_p}{dt}(t) &= C_r(t)\\ \frac{dC_c}{dt}(t) &= -\frac{1}{T_d}C_c(t)\\ \frac{dC_r}{dt}(t) &= \frac{1}{T_d}(C_c(t) - C_r(t)),\end{aligned} \tag{10}$$

where T_d is a time constant, describing the diffusion rate between the central and remote compartments [11].

C. Combined Model

The models from (IV-A) and (IV-B) are combined to create a fully observable system in which the plasma glucose concentration is part of the state vector. At the same time, it also provides an insight into plasma glucose dynamics. The

TABLE I: Mean absolute error (MAE) and mean absolute percentage error (MAPE) scores for the continuous glucose monitoring (CGM) measurements, the Kalman filter blood glucose estimate, $\hat{G}_p$ and for the moving average smoothed Kalman filter estimate, $\hat{G}_{p,smoothed}$, where blood gas analyzer (BGA) is considered as the reference blood glucose level.

		MAE [mmol/L]			MAPE [%]		
		CGM	$\hat{G}_p$	$\hat{G}_{p,smoothed}$	CGM	$\hat{G}_p$	$\hat{G}_{p,smoothed}$
Data set 1	Meal 1	0.38	0.24	0.21	4.82	2.99	2.61
	Meal 2	0.34	0.31	0.20	4.68	4.17	2.69
	Meal 3	0.55	0.47	0.45	8.02	6.90	6.60
	All	0.32	0.30	0.25	4.68	4.36	3.72
Data set 2	Meal 1	0.46	0.48	0.50	5.78	6.47	6.55
	Meal 2	0.43	0.16	0.17	5.86	2.03	2.22
	Meal 3	0.65	0.21	0.13	9.53	2.71	1.86
	Meal 4	0.44	0.37	0.34	7.30	6.12	5.55
	All	0.40	0.28	0.27	5.84	4.11	3.98

state-space form of this combined model is given by:

$$\begin{bmatrix} \dot{G}_{p,k} \\ \dot{C}_{c,k} \\ \dot{C}_{r,k} \\ \dot{G}_{isf,k} \end{bmatrix} = \begin{bmatrix} 0 & 0 & 1 & 0 \\ 0 & -\frac{1}{T_d} & 0 & 0 \\ 0 & \frac{1}{T_d} & -\frac{1}{T_d} & 0 \\ \frac{1}{T_{isf}} & 0 & 0 & -\frac{1}{Tisf} \end{bmatrix} \begin{bmatrix} G_{p,k} \\ C_{c,k} \\ C_{r,k} \\ G_{isf,k} \end{bmatrix} + w_k$$
$$y_k = \begin{bmatrix} 0 & 0 & 0 & 1 \end{bmatrix} \begin{bmatrix} G_{p,k} \\ C_{c,k} \\ C_{r,k} \\ G_{isf,k} \end{bmatrix} + v_k, \tag{11}$$

where the dot notation is equivalent to the time-derivative notation, i.e $\dot{x} = \frac{dx(t)}{dt}$.

V. Metrics

To evaluate the performance of the filter more in detail, the mean absolute error (MAE) and mean absolute percentage error (MAPE) are used, which are defined as below:

$$\text{MAE} = \frac{1}{n}\sum_{i=1}^{n}|e_i|, \tag{12}$$

$$\text{MAPE} = \frac{1}{n}\sum_{i=1}^{n}\frac{|e_i|}{y_i}100\%, \tag{13}$$

with

$$e_i = y_i - \hat{y}_i, \tag{14}$$

where y_i and $\hat{y}_i$ are the real value and the estimate of that, respectively, and n is the total number of samples. The more accurate the method, the smaller the resulting values for MAE and MAPE.

In the calculation of MAE and MAPE, the CGM measurements, the Kalman filter estimate ($\hat{G}_p$), and the smoothed estimates ($\hat{G}_{p,smoothed}$) are compared with the BGA measurement as the reference value. As the BGA samples were taken sporadically while CGM sensor readings and the estimates via Kalman filter are available every $1.2\,\text{sec}$, the error is calculated based on BGA samples and their closest corresponding samples in CGM readings or Kalman filter estimates.

VI. Results

In order to predict the BG level using the CGM measurements, a Kalman filter is utilized. This filter is designed based on the model given in (11). In this model, T_d is set to $10\,\text{min}$ as in [11], and T_{isf} is set to $7\,\text{min}$, as the middle point of what has been reported in the literature $(4-10\,\text{min})$ [2]. The process noise covariance Q and the measurement noise covariance R are given in (15) and (16), respectively.

$$Q = \begin{bmatrix} 0.01 & 0 & 0 & 0 \\ 0 & 0.01 & 0 & 0 \\ 0 & 0 & 0.01 & 0 \\ 0 & 0 & 0 & 0.01 \end{bmatrix} \tag{15}$$

$$R = 2 \tag{16}$$

The Kalman filter estimates, as well as CGM measurements and BGA samples for each of the two animal experiments, are shown in fig. 2. This figure describes specifically the meals throughout the experiments, which are recognized by rise and fall in the blood glucose concentration. As is shown in fig. 2, the Kalman filter successfully reconstructed the BG level using the CGM measurements and compensated for what can be interpreted as the time lag due to the glucose diffusion process between plasma and interstitial compartments. The Kalman filter is observed to be oversensitive to small changes in the CGM measurements, hence a moving average smoother is employed to smooth the estimates. Using a moving average function in Matlab with a span of 1000 samples does not make a significant delay in the estimates, but it results in smoothed estimates. The only drawback is the requirement of having enough CGM samples to start the smoother, which is equal to having $20\,\text{min}$ of CGM readings.

In table I, the evaluation scores are calculated for every meal registered in each data set, as well as for the whole time window, with the exception of the calibration interval, from about $0-200\,\text{min}$. As demonstrated in this table, there is a clear trend where the Kalman filter outperforms the CGM system due to the prediction, and the moving average filtering improves the performance of the Kalman filter. Meal 1 in

data set 2 is an exception to this trend, showing the best score for MAE and MAPE in the CGM measurements. As shown in Meal 1, data set 2, in fig. 2, approximately no time lag exists between CGM and BGA measurements when glucose is decreasing, implying that the poor performance of the Kalman filter in this meal is more related to the sensor itself rather than the Kalman filter. The importance of smoothing can be observed in meal 2 of data set 1, where the CGM and the Kalman filter performances do not differ to a high degree, while the smoothed Kalman filter estimate has a significantly lower score for both MAE and MAPE, see table I, and follows the slope of the BGA precisely, see fig. 2.

Predictions achieved by the Kalman filter and the smoothed Kalman filter bear more resemblance to the BGA measurements compared to the CGM readings, and for most of the meals the estimates can be seen eliminating what can be interpreted as the slower dynamic of CGM. This is especially evident in Meal 1, Meal 2 and on glucose increase in Meal 3, for data set 1, and Meal 2, Meal 3, and on glucose increase in Meal 4, in data set 2, see fig. 2.

VII. DISCUSSION

The advantage of the proposed structure is that it is general and easy applicable. The parameters of the model is adjusted according to the literature. Hence, given any CGM measurements, the proposed method with the same parameters should be able to predict the BG level without the identification procedure. However, performance degradation might be expected if the CGM sampling rate increases. Only two data sets have been used in the simulations for this method, and in order to achieve more reliable results the method should be tested on more data sets with varying CGM sensors, and CGM sampling rates. This is saved for future work.

VIII. CONCLUSIONS

The glucose diffusion process from plasma to interstitial fluid causes a time lag between BG levels and CGM measurements as the CGM sensor measures glucose in the subcutaneous tissue. The Kalman filter with an input-less model of the glucose dynamics has been used to estimate the BG level based on the CGM measurement. In addition, the Kalman filter estimates were smoothed in order to reduce the Kalman filter sensitivity to the disturbances of CGM readings. Considering the BGA values as the reference, the performance of the CGM sensor, Kalman filter, and moving average smoothed Kalman filter were assessed. Results showed that estimates obtained from both the Kalman filter and moving average smoothed Kalman filter resembled the BGA measurements to a higher degree, than the CGM measurements.

IX. ACKNOWLEDGMENTS

The animal experiments were carried out at the Comparative medicine core facility in the Norwegian University of Science and Technology (NTNU). The study was partly funded by The Norwegian Research Council (with project no. 248872) through the Center for Digital Life Norway. The transmitters and the hormones infusion system are provided by Inreda Diabetic company (Goor, the Netherlands) for this study at no cost. The authors would like to thank Marte Kierulf Åm, Oddveig Lyng, and Patrick Christian Bösch for their contribution to the data collection.

REFERENCES

[1] IDF Diabetes Atlas, "Diabetes around the world in 2021," https://diabetesatlas.org/ (accessed: 22.03.2022), 2021.

[2] A. Cinar and K. Turksoy, *Advances in Artificial Pancreas Systems, Adaptive and Multivariable Predictive Control*. Gewerbestrasse 11, 6330 Cham, Switzerland: Springer International Publishing AG, 2018.

[3] Centers for Diseases Control and Preventing, "What is type 1 diabetes?" https://www.cdc.gov/diabetes/basics/what-is-type-1-diabetes.html (accessed: 22.03.2022), 2022.

[4] International Diabetes Fedartion, "Type 1 diabetes," https://idf.org/aboutdiabetes/type-1-diabetes.html (accessed: 22.03.2022), 2020.

[5] G. Cappon, M. Vettoretti, G. Sparacino, and A. Facchinetti, "Continuous glucose monitoring sensors for diabetes management: A review of technologies and applications," *Diabetes and Metabolism Journal*, vol. 43, no. 4, pp. 383–397, 2019.

[6] G. Schmelzeisen-Redeker, M. Schoemaker, H. Kirchsteiger, G. Freckmann, L. Heinemann, and L. del Re, "Time delay of cgm sensors: Relevance, causes, and countermeasures," *Journal of Diabetes Science and Technology*, vol. 9, no. 5, pp. 1006–1015, 2015.

[7] C. C. Andrea Facchinetti, Giovanni Sparacino, "Reconstruction of glucose in plasma from interstitial fluid continuous glucose monitoring data: Role of sensor calibration," *IEEE Transactions on Biomedical Engineering*, vol. 1, no. 3, pp. 671–623, 2007.

[8] B. Bequette, "Optimal estimation applications to continuous glucose monitoring," in *Proceedings of the 2004 American Control Conference*, vol. 1, 2004, pp. 958–962 vol.1.

[9] K. Rebrin, G. M. Steil, W. P. van Antwerp, and J. J. Mastrototaro, "Subcutaneous glucose predicts plasma glucose independent of insulin: implications for continuous monitoring," *American Journal of Physiology-Endocrinology and Metabolism*, vol. 277, no. 3, pp. E561–E571, 1999.

[10] M. Kuure-Kinsey, C. C. Palerm, and B. W. Bequette, "A dual-rate kalman filter for continuous glucose monitoring," in *2006 International Conference of the IEEE Engineering in Medicine and Biology Society*, 2006, pp. 63–66.

[11] O. M. Staal, S. Salid, A. Fougner, and O. Stavdahl, "Kalman smoothing for objective and automatic preprocessing of glucose data," *IEEE Journal of Biomedical and Health Informatics*, vol. 23, no. 1, pp. 218–226, 2019.

[12] D. Simon, *Optimal Estimation*. John Wiley & Sons, Inc., Hoboken, 2006.

[13] F. Auger, M. Hilairet, J. M. Guerrero, E. Monmasson, T. Orlowska-Kowalska, and S. Katsura, "Industrial applications of the kalman filter: A review," *IEEE Transactions on Industrial Electronics*, vol. 60, no. 12, pp. 5458–5471, 2013.

[14] C. Claudio, M. Chiara, Dalla, T. Gianna, B. Rita, V. Adrian, and R. Rizza, "The oral minimal model method," *Diabetes*, vol. 63, no. 4, p. 1203–1213, 2014.

[15] C. D. Man, F. Micheletto, D. Lv, M. Breton, B. Kovatchev, and C. Cobelli, "The uva/padova type 1 diabetes simulator: New features," *Journal of Diabetes Science and Technology*, vol. 8, no. 1, pp. 26–34, 2014.

[16] T. Koutny, "Blood glucose level reconstruction as a function of transcapillary glucose transport," *Computers in Biology and Medicine*, vol. 53, pp. 171–178, 2014.

Martha Halvorsen

Robust Estimation of Blood Glucose Level Based on Subcutaneous Sensors and Analysis of Blood Samples

NTNU
Norwegian University of
Science and Technology